A STUDY OF THE EFFECTS OF ENVIRONMENTAL CHANGES ON THE STRESS-STRAIN PROPERTIES OF KAOLINITE

by

ANWAR E. Z. WISSA
B.A., Oxford University
1957

Submitted in partial fulfillment of the
requirements for the degree of
MASTER OF SCIENCE
at the
MASSACHUSETTS INSTITUTE OF TECHNOLOGY
June 1961

Signature of Author . . . . . .
Department of Civil and Sanitary Engineering
May 20, 1961

Certified by . . . . . .
Thesis Supervisor

Accepted by . . . . . .
Chairman, Departmental Committee
on Graduate Students

ABSTRACT

A STUDY OF THE EFFECTS OF ENVIRONMENTAL CHANGES ON THE STRESS-STRAIN PROPERTIES OF KAOLINITE

by

ANWAR E. Z. WISSA

Submitted to the Department of Civil and Sanitary Engineering on May 20, 1961 in partial fulfillment of the requirements for the degree of Master of Science.

The results of a series of triaxial compression tests on an artificially sedimented Sodium Kaolinite have been presented and it has been shown that a comprehensive mechanistic picture of the behavior of the clay can be obtained by considering structure to be a combination of fabric and interparticle bonds. These bonds may include a brittle "cementing" effect produced by aging after consolidation. The cementing effect is apparently destroyed if the soil is consolidated further after aging.

The triaxial compression tests also show that if the environment is changed after consolidation, without an alteration in the fabric (produced by the diffusion of NaCl into the pore-water), then:

1) The environmental change has no effect on the undrained strength of the soil at maximum deviator stress.

2) The change of environment does alter the undrained strength at the maximum principal stress ratio. In Kaolinite NaCl reduces the undrained strength.

3) At any one void ratio the effects of aging (cementation) after consolidation do not show up in the shear strengths at maximum deviator stress nor at maximum obliquity.

4) The drained friction angle at maximum deviator stress is a property of the "structure" prior to shear and is not affected by the environment during shear. The more the cementing during aging the lower the friction angle will be.

5) The drained angle of friction at maximum principal effective stress ratio is governed by the environment during shear and is not affected by the cementation that existed prior to shear. In the case of Kaolinite, NaCl reduced the drained friction angle at the maximum principal stress ratio.

Finally it is shown that Sedimentation Tests and Atterberg Limits (especially the liquid limit) are helpful in predicting the effect of a change in environment on the strength parameters at maximum principal effective stress ratio.

Thesis Supervisor: T. William Lambe

Title: Professor of Soil Engineering

ACKNOWLEDGEMENTS

The author wishes to express his sincere gratitude to his thesis supervisor, Professor T. W. Lambe, for his guidance and advice during the research program.

The author is greatly indebted to Dr. R. T. Martin and Mr. C. C. Ladd for their invaluable suggestions and assistance on the interpretation of the test results.

Special thanks are due to Messrs. W. T. Jackson Jr., R. S. Ladd, D. J. Leary and J. B. York for their assistance in performing part of the experiments, to Mr. Carl Stahle, Division Mechanic, for his skill in making special apparatus, and to Miss N. Blanchard for her patience in drafting the figures.

Thanks are due to Mr. F. V. Lawrence Jr. for proofreading the manuscript, and Mrs. G. Rand for typing the final manuscript.

The author gratefully acknowledges the Waterways Experiment Station of the Corps of Engineers and National Science Foundation for their financial support which made this work possible.

TABLE OF CONTENTS

TABLE OF CONTENTS (Continued)

LIST OF FIGURES (Continued)

LIST OF TABLES

NOMENCLATURE

A = Skempton pore-pressure coefficient (A-Factor)

B = Skempton pore-pressure coefficient (B-Factor)

c = shear intercept of drained strength envelopes

c_e = Hvorslev "true" cohesion

c_u = shear intercept of undrained strength envelopes

E = initial Modulus of Elasticity

e = Void Ratio

e_f = Void Ratio at failure

L.L = Liquid Limit

p = consolidation pressure ($\bar{\sigma}_c$)

P.L = Plastic Limit

P.I = Plasticity Index

S_u = undrained Shear Strength

u = pore-pressure

ω = water-content

Δu = excess pore-pressure

σ_1 = Major principal total stress

$\bar{\sigma}_1$ = Major principal effective stress

σ_3 = Minor principal total stress

$\bar{\sigma}_3$ = Minor principal effective stress

$(\sigma_1-\sigma_3)$ = Deviator stress

$\frac{1}{2}(\sigma_1-\sigma_3)$ = shear stress

$\frac{1}{2}(\bar{\sigma}_1+\bar{\sigma}_3)$ = Average principal effective stress

NOMENCLATURE (Continued)

$\bar{\sigma}_1/\bar{\sigma}_3$	=	Principal effective stress ratio or obliquity
$\bar{\sigma}_c$	=	consolidation pressure (p)
$\bar{\sigma}_e$	=	Hvorslev equivalent consolidation pressure
$\bar{\sigma}_f$	=	the effective normal stress on the failure plane
$\bar{\sigma}_{ff}$	=	the effective normal stress on the failure plane at failure ($\bar{\sigma}_1/\bar{\sigma}_3$ max)
τ_f	=	shear stress
τ_{ff}	=	shear stress at failure ($\bar{\sigma}_1/\bar{\sigma}_3$ max)
ϕ_e	=	Hvorslev "true" angle of internal friction
ϕ_u	=	undrained friction angle
$\bar{\phi}$	=	drained angle of friction
ϵ	=	strain
$\tan\theta$	=	slope of undrained envelope
$\tan\alpha$	=	slope of drained envelope
γ_d	=	final average dry densities for sedimentation tests

I. INTRODUCTION

The work presented in this thesis is part of a program initiated at the Massachusetts Institute of Technology by Professor T. William Lambe to investigate the effect of environment on the shear strength of clays.

Three clays are being used in this investigation, a montmorillonitic clay (Vicksburg Buckshot clay), an illitic clay (Boston Blue clay), and a pure Kaolinite obtained from the Georgia Kaolin Company.

Originally this thesis was to cover the effects of salt flocculation (NaCl) and dispersion (NaOH) on the shear strength of Kaolinite. However, only the effect of salt has been completed to date due to experimental difficulties which have been encountered in diffusing NaOH through the consolidated samples. The author expects to have the effects of NaOH by the end of 1961.

In the last two decades a considerable amount of research has been conducted on Kaolinite. Thiessen (24)* in 1942 showed by means of electron photomicrographs that negatively charged gold colloid particles were absorbed only along the edge of the kaolin plates. This strong evidence of positive charge edges did not influence the

---

* Numbers in ( ) refer to references listed at the end of this thesis.

majority of soil researchers until Schofield and Samson (21) published their paper in 1954. The existence of positive charge edges is now generally accepted. Martin (17), substantiated by Cashen (7), has proved the negative charge on the faces of Kaolin particles must be due to isomorphous substitution since there still exists a cation exchange capacity at pH 3. To the author's knowledge no work has been done to explain the positive charge on the edges, but it is very likely a surface effect which is polarizable.

The crystal structure of Kaolinite, and of the other common clay minerals, is well described by Grim (10) in Clay Mineralogy, 1953.

Brindley (5), Grim (10), Kahn (12), and many others have determined particle size and shape for the clay minerals and there is good agreement between the various investigators.

From a consideration of particle size, shape, surface charge density, and the relative stacking of the particles it can be shown that Kaolinite behavior may be considerably governed by its positively charged edges so that any observed effects of environments on illite or montmorillonite will not necessarily be the same for Kaolinite. For example, Bjerrum and Rosenqvist (3) have shown that for an illitic clay, salt will increase the undrained strength, and work presented here shows the reverse to be true for Kaolinite.

During the last ten years, Lambe (14)(15) has demonstrated the importance of structure and mineralogical composite in the behavior of inorganic soils. Lambe's latest paper (16), titled "A Mechanistic Picture of Shear Strength in Clay," has been a considerable help in developing the mechanistic model used in this thesis.

The main work presented is an attempt to show the effect of salt and aging on the strength of Kaolinite having initially the same structure* and orientation. Identical samples were triaxially consolidated and the environment then changed by means of diffusion, in order to minimize any change in particle orientation prior to shearing. Pore-pressure measurements were taken during shear so as to obtain both the undrained and drained strength envelopes. The Hvorslev strength parameters (11) were also obtained for the Kaolinite samples before any change of environment.

Sediment Densities, Atterberg Limits, and Shrinkage Limits supplemented the main tests in the hope of better explaining the triaxial test results.

---

* By structure is meant both orientation (fabric) and linkage (bond) between particles.

II. PREPARATION OF THE CLAY SLURRY

The untreated material used in these tests is an ultra fine, acid-washed, dry powdered, Kaolinite obtained from the Georgia Kaolin Company with the trade name of Hydrite-UF. The manufacturer's (8) particle size distribution is given in Figure 1, and the untreated Kaolin has a pH of 4.2 to 5.2 in a 20% aqueous slurry. The liquid limit of the clay is 95%, plastic limit 39%, and plasticity ~~limit~~ index 57%. The specific gravity is 2.62.

The Kaolinite used for the triaxial tests was sodium homoionized by mixing in a 1N NaCl solution at a clay-fluid ratio of 45. The salt was then extracted by successive washing with demineralized water until the salt concentration was 0.005N and pH 6.7 $\pm$ 0.2. Experimental details are given in Appendix A.

This method of treatment was considered sufficient for homoionization even though most of the amorphous surface alumina was not removed. It is possible to remove this alumina by successive washing of the clay with a 1N NaCl pH 3 as shown by Figure 2. This was not done because such a type of homoionized Kaolinite would, within a period of weeks, produce fresh amorphous alumina.

The liquid limit of the salt-washed slurry was 105% and plasticity index 58%. The Atterberg limits of the

treated clay did not change with time, nor, as will be seen later, did the shear strength.

Figure 3 shows that the amount of alumina extracted in three washings was greater for both the oven-dried and wet treated soil than for the untreated soil. This does not necessarily mean that the treated soil ended up with more extractable alumina; it merely shows that the alumina was more easily extractable. Further tests are at the moment being carried out to determine the effect of aging on the extractable alumina for both treated and untreated Kaolinite.

The treated slurry at a water content of 550% was then sedimented through 10 cm of 0.005N NaCl into the large consolidometer described in Appendix B and slowly consolidated to approximately 1.5 Kg/cm^2.

The consolidated soil was then extruded, cut into blocks, and stored in a water-repellant oil until used. This method of storage has proved satisfactory since no detectable change in water content occurred during the period of storage which, for some blocks of soil, was well over a year.

Eighteen 1.4" diameter triaxial samples were obtained from the batch consolidated in the large consolidometer. The variation in water content, throughout the batch, was small due to the low wall friction of the

consolidometer (the consolidometer has teflon-coated walls).

A new method for producing single, 1.4" diameter, saturated triaxial samples is described in Appendix B. This method is being used to produce triaxial samples sedimented in various environments. The method is advantageous when only a few samples with a given pore fluid are needed.

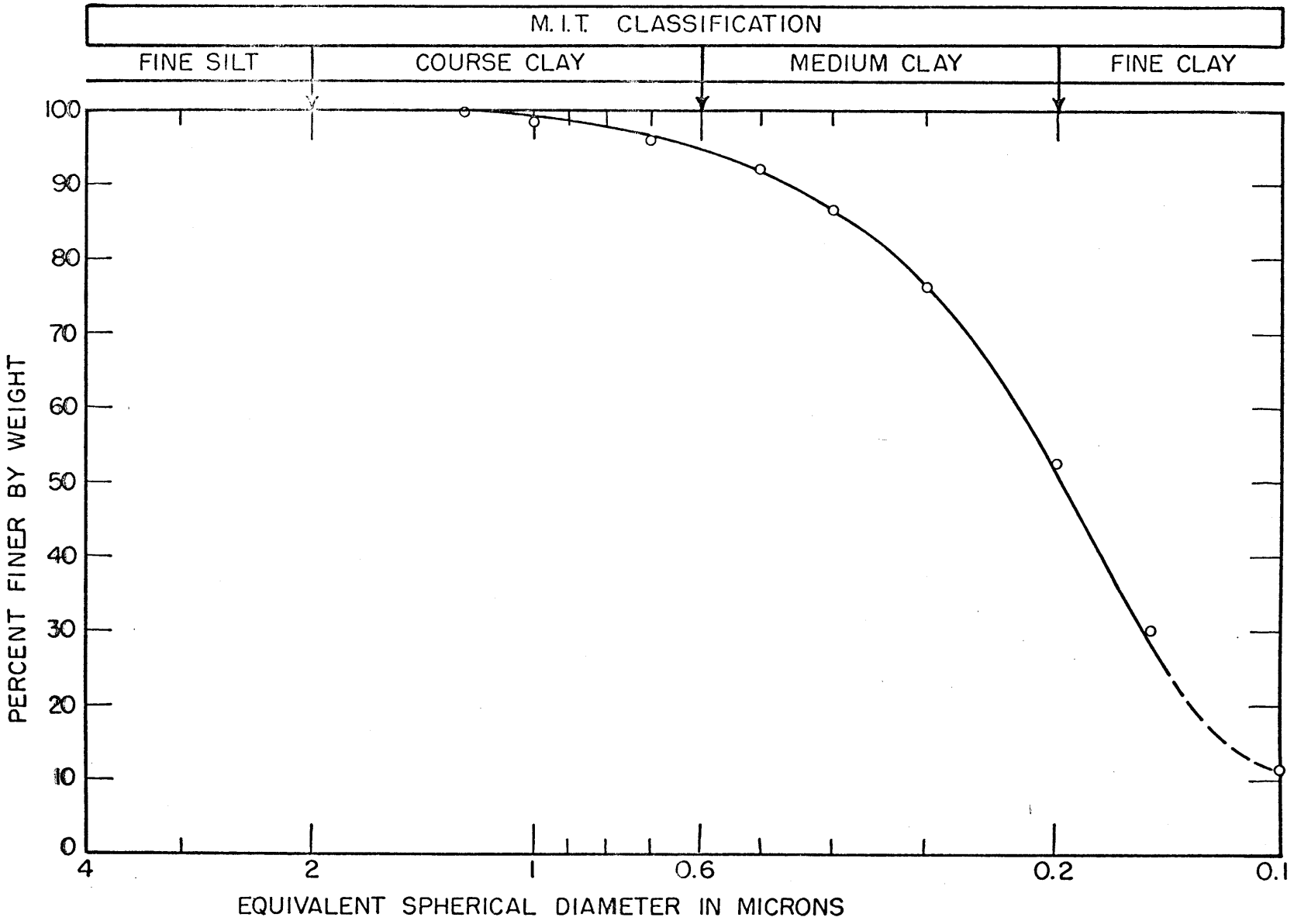

FIGURE I PARTICLE SIZE DISTRIBUTION OF THE ULTRA FINE KAOLINITE

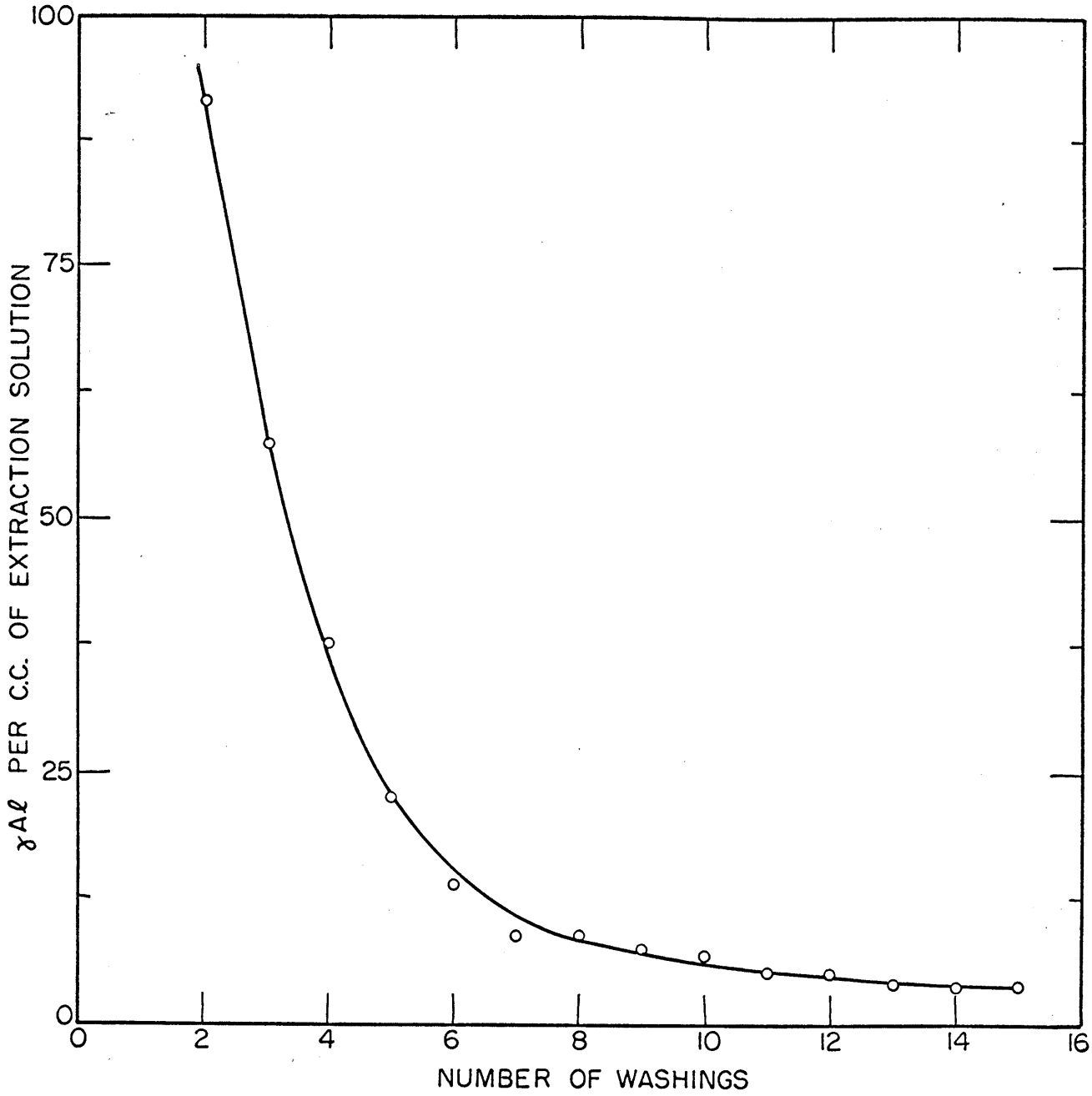

FIGURE 2 RATE OF ALUMINUM EXTRACTION WITH WASHINGS OF 1 N. NaCl pH 3

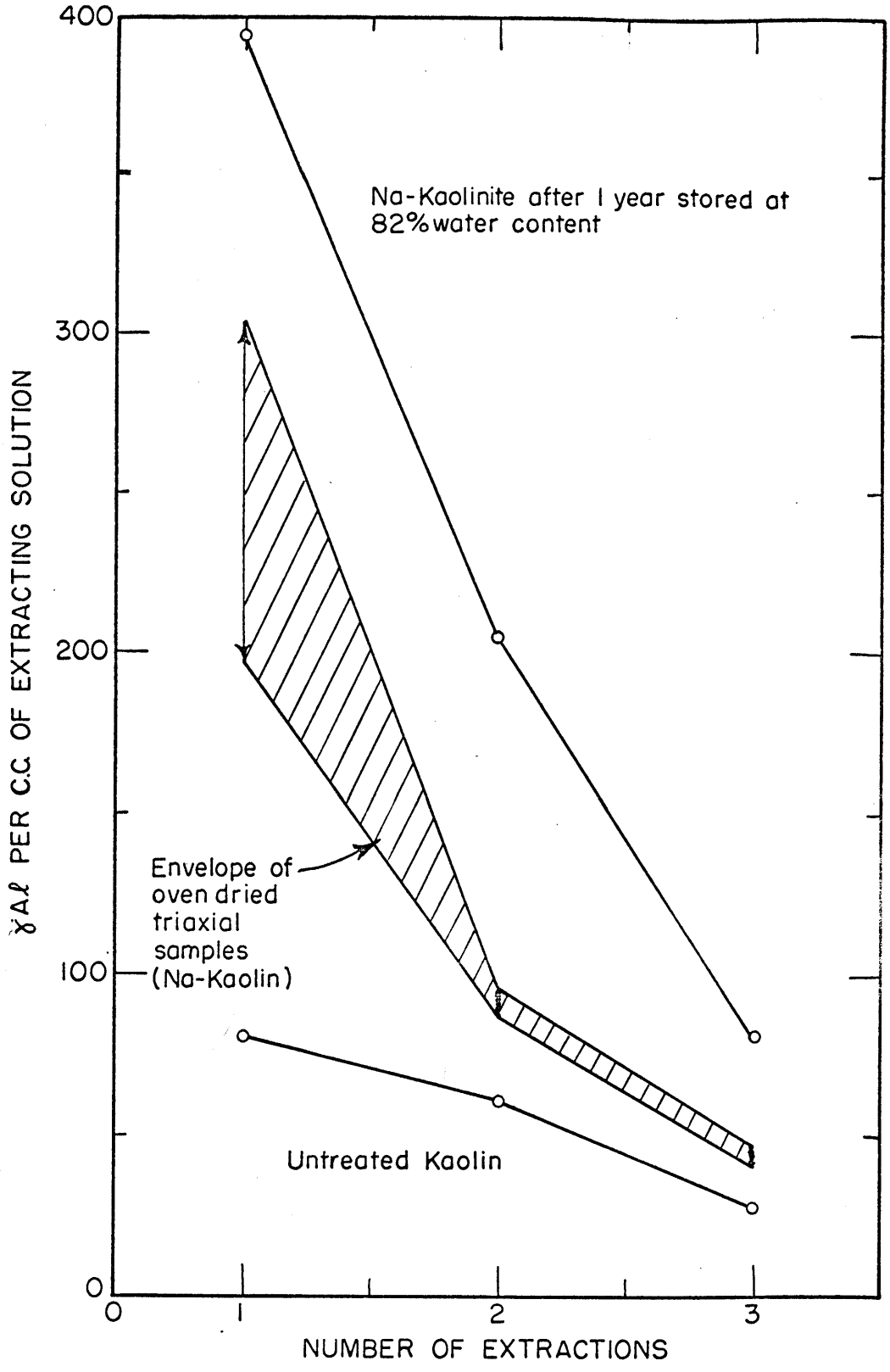

FIGURE 3 EFFECT OF AGING ON EXTRACTABLE SURFACE ALUMINA

III. SEDIMENTATION DENSITIES

3.1 Discussion of the Validity of Sedimentation Test Results in Explaining Environmental Effects on the Shear Strength of Consolidated Sedimented Clays

Bolger (4) has done some work on the rheology of kaolin suspensions and explains his findings by means of a model. The model he proposes is of use in trying to evaluate the engineering significance of final sediment densities obtained from sedimentation tests and, therefore, is presented here.

The Bolger Model

The model is based on the premise that in a flocculated clay suspension the basic "flow units" in sedimentation are not the primary particles but are, rather, small clusters of particles (plus enclosed water) which are called flocs (Figure 4b). In a dispersed suspension, however, the primary particle is the basic unit. In sediments, the shape of these flocs are most likely spherical so as to resist surface forces during agitation. The internal orientation of primary particles within a floc will depend on the forces between the individual particles. The size of floc will depend not only on the interparticle forces but also on the method and duration of agitation, and on the clay-liquid ratio during mixing, i.e. the size of floc will increase as the clay concentration increases

or as the shear due to mixing decreases. At low shear rates the flocs tend to group into clusters of flocs called aggregates. The aggregates may join together to form extended networks which extend to the walls of the container during sedimentation and give the suspension its plastic and structural properties (Figure 4a). Comparatively few "floc-floc" bonds hold the aggregates together, and these aggregates are weak compared to the flocs and may grow by collisions or be broken down by surface shear during gravity settling.

His model explains the different stages of sedimentation, but only the final sediment density model shall be explained here. This model consists of two layers (Figure 4c):

1) An upper layer of loosely packed flocs (which is of no interest in soil mechanics).

2) A lower layer of closely packed flocs produced by the weight of the overlaying, loosely packed flocs. The density of this lower layer is uniform since the individual flocs are fairly strong compared to the weight of overburden.

In all practical soil engineering problems the weight of overburden is much larger than in sedimentation tests. This might suggest that sedimentation tests are not representative of the actual particle orientation. Olsen (18)

uses a similar floc model, utilizing the concept of clusters to explain hydraulic flow through saturated clays at consolidation pressures up to 1/2 T/ft^2.

The author finds that Olsen's "cluster" and Bolger's "floc" are the same except that consolidation causes a distortion of the "floc" accompanied by a small amount of volume decrease. This distortion will cause some reorientation of the individual particles within the floc. Anisotropic consolidation (which occurs in nature) will cause more distortion, i.e. a higher degree of floc surface parallelism, than would isotropic consolidation. The sketch in Figure 5c shows the author's idea of the effect of consolidation. The outer disturbed surfaces will cause a continuous matrix, around the flocs, having a more oriented fabric.

In conclusion it may be said that final sediment density is a useful means of qualitatively comparing the effects of environment on the fabric of consolidated sedimented clays (even though in the case of flocculated clays there is some distortion during consolidation) provided the following factors are considered and taken into account in such tests:

1) The fundamental unit controlling the final sediment density is the floc which is produced during initial mixing.

2) The individual floc density is determined by the interparticle forces. The average floc size does not only depend on the interparticle forces but also on the method of mixing of the slurry and its clay liquid ratio. Therefore in comparing results the clay liquid ratio and method of mixing should be kept constant.

3) The time of mixing should be sufficient to produce a stable average floc size.

4) The geometry of the sedimentation containers should be kept constant, i.e. both the initial slurry height and the diameter of container should not vary.

5) The final sediment height should be large so as to minimize the effect of its loose upper layer in computing average densities.

6) For laboratory comparisons relatively low clay-liquid ratios should be used (2% by weight).

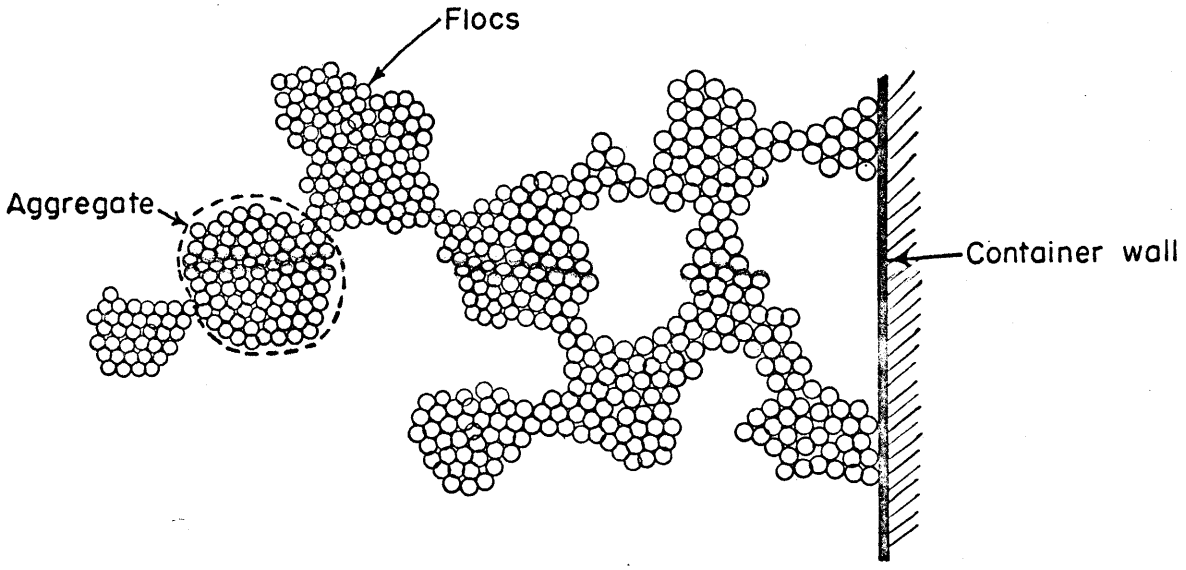

FIGURE 4a THE FLOC AGGREGATE STRUCTURAL MODEL AFTER BOLGER

FIGURE 4b TYPES OF KAOLIN FLOCS AFTER BOLGER

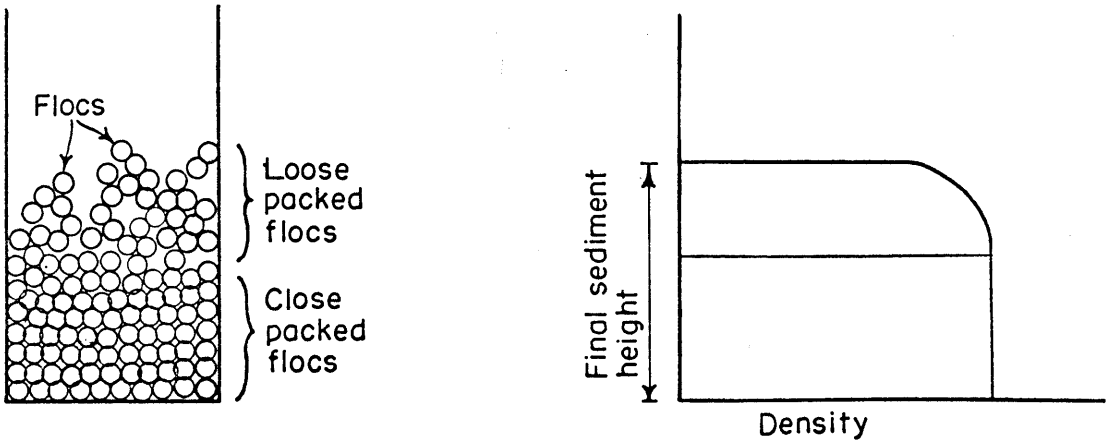

FIGURE 4c DENSITY PROFILE AND PACKING ARRANGEMENT AFTER BOLGER

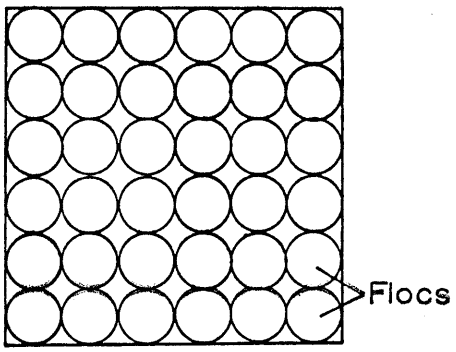

Low Consolidation

(a) BOLGER MODEL

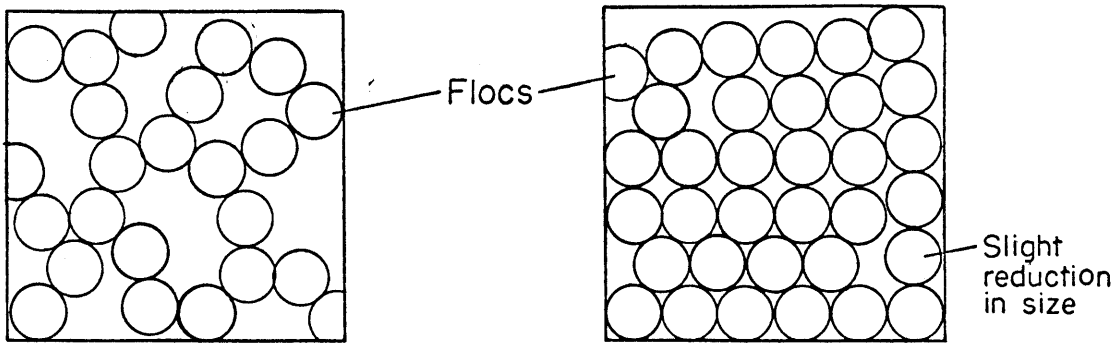

Low Consolidation

High Consolidation (assumed)

(b) OLSON MODEL

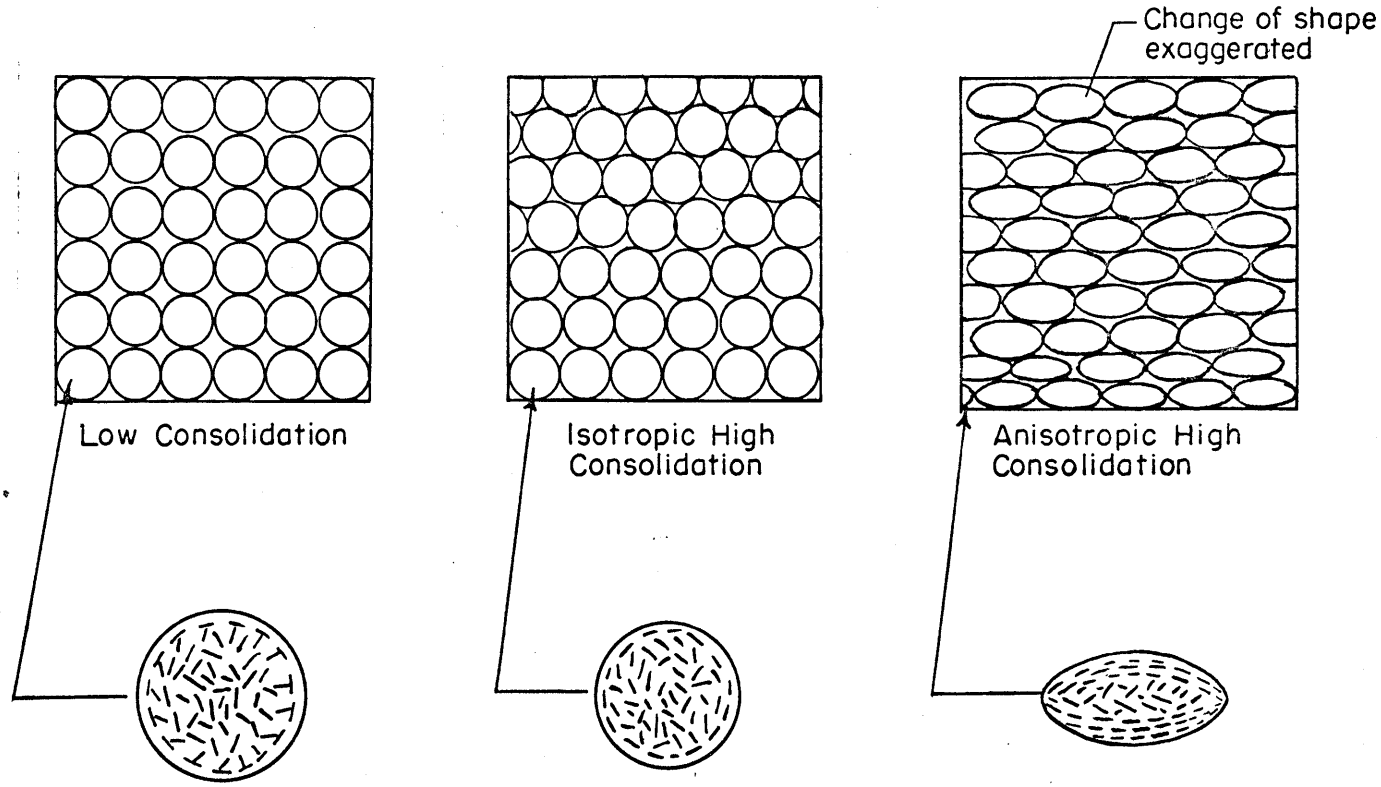

Enlarged Floc Showing Particle Orientation (water flocculation)

(c) AUTHOR'S MODEL

FIGURE 5 VARIOUS FLOC MODELS

3.2 Effect of Salinity on the Sediment Density of Kaolin

The results of Sedimentation Tests* show that Kaolinite had the lowest final sediment density in salt-free water and that the sediment density increased slightly with increased salinity (Figure 6), i.e. a reduction in degree of flocculation with increased salinity. The observed effect was small but it is believed that if the clay in these tests had been sodium homoionized, like the clay used in making the triaxial test samples, the change in density with salinity would have been more pronounced. The reasons for this belief are twofold:

1) It was observed that in distilled water the Al-Kaolinite had a lower sediment density than the Na-Kaolinite, i.e. it was less flocculated. The sediment density of Na-Kaolinite in water was 0.06 gm/cc compared to 0.10 gm/cc for the untreated Al-Kaolinite. Even though the two test procedures were by no means identical this large difference cannot be due solely to differences in test procedure. The main reason is that Al-Kaolin has Al ions adsorbed in the negatively charged particle's face with a larger neutralizing effect than Na in the Na-Kaolin.

---

* General procedure is given in Appendix D.

Green (9) shows that Ca-Kaolin has a lower sediment density than Na-Kaolin which agrees with the foregoing.

2) The addition of NaCl to the Al-Kaolin would mainly reduce the positive charge on the edges of the particle by means of the Cl ion but have little effect on the negative faces, since the adsorbed Aluminum has already reduced the effective charge spacing. In the case of Na-Kaolin, however, the addition of NaCl will reduce both the negative and positive charges on the clay particles, thus having a larger effect than on Al-Kaolin. It should be noted that the charge on the negative faces is due to isomorphous substitution, but the positive charge on the edges is due to dissociation and is a surface effect that can be polarized.

The conclusions from these tests are:

1) Kaolinite is more flocculated in water than in sodium chloride.

2) The degree of flocculation decreases with increasing salinity.

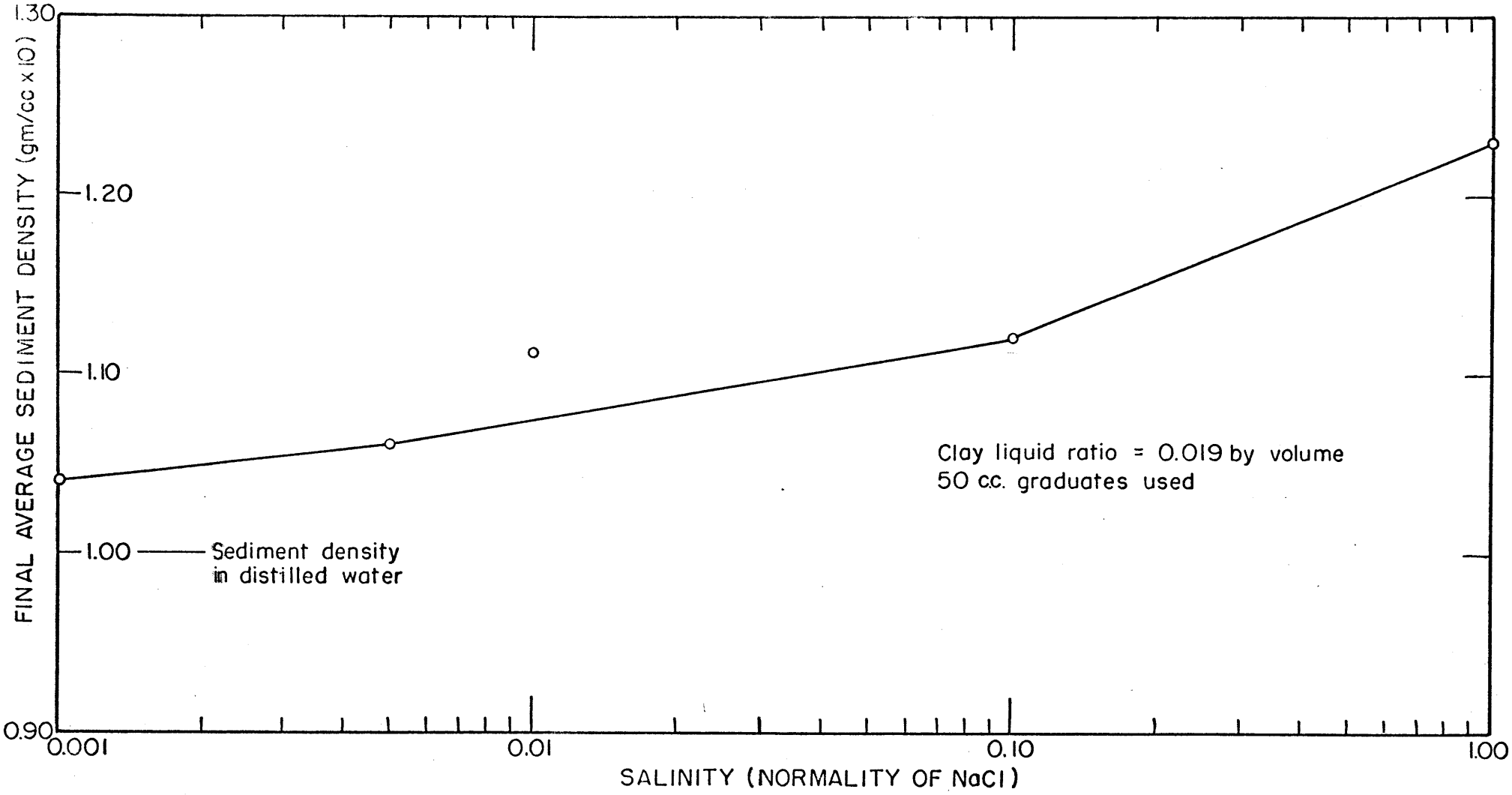

FIGURE 6 EFFECT OF NaCl ON THE FINAL SEDIMENT DENSITY OF UNTREATED KAOLIN AT 20° C

IV. THE ATTERBERG LIMITS

4.1 Procedure

Plastic limits, liquid limits, and shrinkage limits were run on the untreated Kaolinite remoulded in aqueous solutions of NaCl and NaOH of various concentrations. The procedure followed is described in Chapter 3 of "Soil Testing for Engineers" (13).

In running the liquid limits, no drying of the soil was allowed since this would have changed the salt concentration. A fresh mixture of clay and solution was used for each fluid content. The mixtures were equilibrated for four days in sealed glass jars before running the liquid limits.

For the plastic limits, the soil was either dried from the liquid limit or dry soil was mixed with the soil at the liquid limit, until the plastic limit was reached. It was found that the plastic limit was not sensitive to changes in salt concentration which occur upon drying from the liquid limit to the plastic limit provided the plastic limit is defined as the percentage of pore fluid volume in cc to the weight of dry soil in grams (i.e. "fluid content").

A method for correcting the water content obtained from oven drying to the "fluid content" (with NaCl as the pore fluid) is given in Appendix A. A similar method was used for NaOH.

Shrinkage limits were run on soil pats made up at the liquid limit and on the triaxial samples after testing. All samples were allowed to dry very slowly to avoid cracking.

4.2 Liquid and Plastic Limits

The results are plotted on a Casagrande type Plasticity Chart (Figure 7). There is considerable scatter in the results on such a plot; however, only the 1.0N and 0.5N NaOH mixtures and the untreated Kaolin lay slightly above the A-line in the region for clays of high plasticity. The NaCl, treated clay, and low concentration NaOH samples were close to the A-line in the region of inorganic silts of high plasticity. The plastic limit for all the NaCl lay between 37% and 41% while the liquid limits varied considerably. The average liquid limit for 1.0N NaCl was 72% and 87% for 0.005N NaCl. The limits of the treated clay showed no variation with aging as is seen by the following table:

Elapsed Time After Treatment (0.005N NaCl pH 6.7)	Liquid Limit	Plastic Limit	Plasticity Index
2 Months	105%	47%	58%
10 Months	106%	50%	56%
16 Months	106%	49%	57%

The effect of NaOH on the liquid limit and the plastic limit is shown in Figure D-1 of Appendix D.

It should be noted that the limits as presented here have been corrected for the effects of the various pore fluids and computed on the basis of the equivalent weight of dry, salt-free soil. Graphs are given in Figure C-1 to simplify the calculations involved in correcting for NaCl solutions.

4.3 Shrinkage Limits

The results of shrinkage limits are tabulated below, after being corrected for the weight of salt in the dried samples. No correction was made for the volume of salt because salt crystals could not be seen under a powerful microscope and therefore were assumed to have a negligible effect on the shrinkage of the soil.

EFFECT OF ENVIRONMENT ON THE SHRINKAGE LIMITS OF THE REMOULDED PATS

Environment	Shrinkage Limit
0.005N NaCl	46 ± 0.5%
1.0N NaCl	44 ± 1.0%
0.1N NaOH	37 ± 0.5%
1.0N NaOH	36 ± 0.6%

SHRINKAGE LIMITS OF THE UNDISTURBED TRIAXIAL SAMPLES

Environment	Shrinkage Limit		
	Sample Top	Sample Middle	Sample Bottom
0.005N NaCl no aging	45.2 ± 0.2%	44.9 ± 0.1%	45.3 ± 0.1%
0.005N NaCl (water diffusion)	46.5 ± 0.5%	46.0 ± 0.5%	46.0 ± 0.2%
0.7N NaCl (salt diffusion)	45 ± 1%	43 ± 1%	45 ± 1%

EFFECT OF CONSOLIDATION PRESSURE ON THE SHRINKAGE LIMITS

	Shrinkage Limit*			
	0.005N NaCl	1.0N NaCl	0.005N NaCl Diffusion	1.0N NaCl Diffusion
Remoulded Pats	46 ± 0.5%	44 ± 1.0%	-	-
Triaxial Samples $\bar{\sigma}_c$ = 3.19 kg/cm^2	45.1 ± 0.1%	-	45.8 ± 0.5%	42.8±1.0%
Triaxial Samples $\bar{\sigma}_c$ = 6.35 kg/cm^2	45.1 ± 0.3%	-	46.5 ± 0.5%	43.1±1.0%

* Average values for the whole triaxial sample.

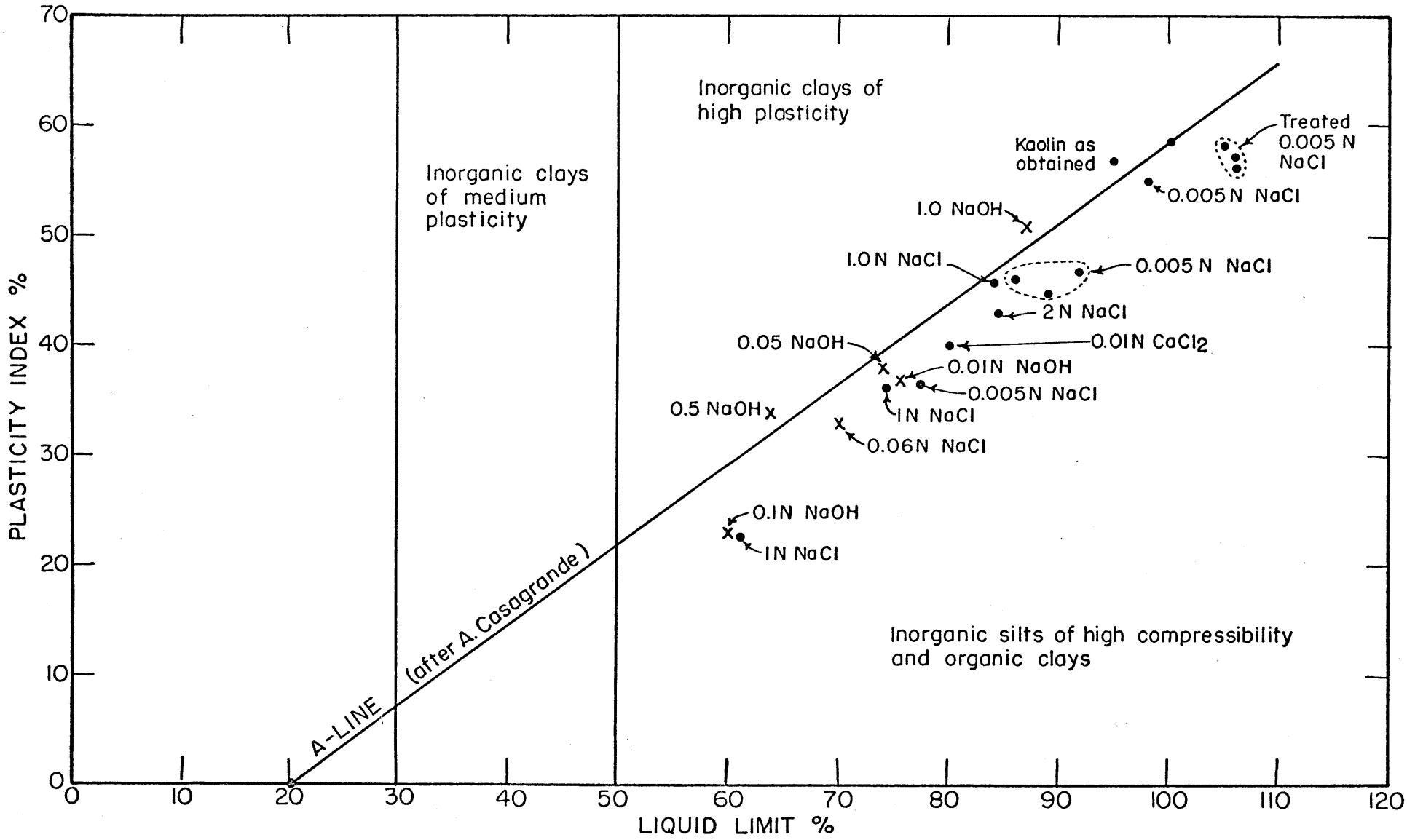

FIGURE 7 PLASTICITY CHART (after A. Casagrande)

4.4 Discussion of the Effects of Environment on the Atterberg Limits of Kaolinite

A. Casagrande (6) has done a considerable amount of work on the use of the Atterberg limits and indices in the investigations of plastic characteristics of any given clay. Taylor (23) gives a very good physical picture of the significance of the various limits and indices from which the following conclusions have been drawn for any given soil:

1) The higher the liquid limit the more flocculated is the soil.

2) The more flocculated the structure the higher the shrinkage limit.

Summarizing the results it can be concluded that:

1) The treated soil was the most flocculated and the degree of flocculation did not change with aging after homoionization.

2) The degree of flocculation decreased as the pore fluid salinity increased.

3) The particle orientation in the triaxial samples was not considerably altered during diffusion.

4) The plastic limit is not sensitive to variations in the pore-fluid salinity and decreases only under extreme dispersing conditions.

5) The shrinkage limit is not sensitive to consolidation pressure.

It is of interest to note that the shrinkage limit of the ends of the triaxial samples was usually higher than in the center. The reduction in shrinkage limit in the center is very likely due to the reduction in degree of flocculation in the failure zone which occurs at large strains. Also, the final water-content was lower in the center. The higher water-content at the ends is due to the end restraints on the samples during consolidation in the triaxial cells and the flow of water into the ends of the samples from the porous stones while they are being dismantled.

V. THE TRIAXIAL COMPRESSION TESTS

5.1 Procedure

These tests may be divided into two groups:

1) Short-term tests which consisted of running triaxial tests on the soil immediately after triaxial consolidation.

2) Long-term tests or diffusion tests in which the triaxially consolidated samples were submitted to diffusion for periods of three months prior to shearing.

The blocks of clay which had been stored in oil were gently wiped and trimmed, in a humid room, to a 1.4" diameter cylinder 3.15" long, with a thin wire saw as described by Lambe (13), page 115.

Three representative water contents were taken from the trimmings. The samples were then weighed and their circumferences measured with a thin strip of paper. The average circumference of the samples was 4.42" with a maximum variation of ±0.04". The maximum variation in weight of the samples was ±0.8%. The initial void ratio varied from 2.09 to 2.17.

The trimmed samples were then placed in triaxial cells which had been completely deaired and whose drainage

lines had been filled with deaired 0.005N NaCl aqueous solution. The samples were capped with two 150 KV porous discs 1.4" diameter and 0.2" thick which were saturated with the dilute salt solution by boiling under vacuum for at least half an hour. Saturated discs of filter paper were placed between the sample and stones to prevent the erosion of clay into them. In all tests both top and bottom stones were used, even though top drainage was allowed only with the diffusion samples. This was done in order to keep the friction on the ends of the samples the same and to get good final water content comparisons, since the fluid in the stones is sucked into the ends of the sample while it is being dismantled at the end of the test.

Eight 1/4" thick saturated filter strips* were equally spaced down the sides of the samples. The function of the filter strips was to accelerate consolidation, diffusion, and pore-pressure response during shearing - Bishop and Henkel (2).

Each sample was enclosed by rolling up, from the base, two rubber prophylactics with a film of silicon grease between them. The membranes were sealed to the base and top cap by means of neoprene O-rings. Rolling the membranes up from the bottom minimized the amount of air entrapped between the membranes and the sample.

* Whatman's No. 54 filter paper was used which does not soften in water.

For short-term tests, no top drainage was allowed and the top loading caps had 3/4" long collars which were guided by the loading pistons to prevent the samples from tilting during consolidation and shear. A stainless-steel ball was placed between the top cap and loading piston to assure good seating between them during shear. Weep-holes were drilled through the collar walls of the top caps to prevent the development of pressure in the collars while the load piston was being inserted.

The top caps for the diffusion samples were also of the guided type but had a 3 mm O.D., 1 mm I.D. flexible polyethylene drainage tube connected through them to the top porous stone. The seal between the drainage line and top stone was a small O-ring and plug as shown in Figure C-1. The tube was spiralled down to the top drainage connection in the base of the cell so as to minimize its force on the cap during compression of the sample. (The polyethylene tubing was softened in boiling water, coiled, and then allowed to cool in the desired shape.)

The cells were then closed and filled to 1/4" from the top with freshly deaired water. The top 1/4" was filled with a light oil so as to decrease leakage around the loading piston during consolidation. For the long-term tests, it was felt that not sufficient oil could be safely stored in the cells without running the risk of getting oil

on the membranes (which are quickly attacked by petroleum oils). To overcome this, the cell pressures were applied through a vent in the top of the cells in such a way that any leakage of oil was automatically replaced by oil externally stored under the cell pressure, in lucite containers (see Figure 8).

A cell pressure of 2.11 kg/cm^2 was then applied to all samples, and the samples were left to consolidate for two days. The pressure was then raised to 3.17 kg/cm^2 and the samples allowed to consolidate again. The samples which were to be tested at 6.35 kg/cm^2 were consolidated to this pressure after primary consolidation at 3.17 kg/cm^2 was complete. The overconsolidated samples were rebounded from 6.35 kg/cm^2 to the desired overconsolidation ratio, in several increments of decreasing pressure.

Burette readings of sample volume changes were taken throughout the period of consolidation (and rebound, in the case of the overconsolidated samples). The above techniques were common to both the short-term and diffusion tests; however, thereafter the tests differed as follows:

a) The Short-Term Tests (Tests Nos. 5 to 10 in Table I)

The short-term samples were then ready for triaxial testing. A well deaired mercury null indicator* for

---

* The two types were used and are described in References 1 and 2.

measuring pore pressures was connected under water to the bottom drainage line of the cell to make sure no air got trapped in the lines while the connection was being made. The pore-pressure response of the sample was then determined, i.e. the pore-pressure measured by the null indicator five minutes after the cell pressure was raised by 0.7 kg/cm^2. If the system is saturated then the pore measured should be equal to the increment of cell pressure, and 100% response is obtained. In other words, the Skempton B-Factor (22) was determined after 5 minutes for $\Delta\sigma_3$ = 0.7 kg/cm^2. In most of these tests the B-Factor so determined was about 0.90 which was not satisfactory so 2 kg/cm^2 back-pressure was applied to the system in order to dissolve the air entrapped in the system. This was done by increasing simultaneously the cell pressure and the pore-pressure by 2 kg/cm^2. The samples were then allowed to equilibrate for 24 hours under these conditions, after which time the B-Factor was found to range between 0.97 and 1.0. Therefore, no further back-pressuring was required.

The cells were placed in load frames, and the samples submitted to triaxial compression with pore-pressure measurements, as described in Bishop and Henkel, Part III (2). The tests were strain controlled using a sensitive proving ring (sensitivity 0.18 in./kg). The rate of feed of the load frame was 1% strain in 4 hours which gave 10%

strain in about 50 hours. It should be noted that a feed of 1% in four hours is not the actual straining rate of the sample since the proving ring is very flexible. The actual rate of strain was about seven hours for the first 1% and gradually increased as the rate of the proving ring deflection decreased. If the deviator stress started to drop, the rate of straining was more than 1% in four hours.

The method of loading, using a flexible proving ring and a constant rate of feed, has considerable merit when running tests with pore-pressure measurements. At the beginning of a test, the pore-pressure is increasing rapidly with strain, and, therefore, the slower the rate of strain the more accurate are the pore-pressures which are measured at the base of the sample. As the sample approaches failure, however, there is very little change in pore-pressure with strain, and the increase in strain rate does not impair the pore-pressure measurements.

Failure was defined as the condition when the principal effective stress ratio had reached a constant value.

The samples were then unloaded and dismantled. They were weighed, any failure planes noted, and all dimensions measured. The samples were then sliced into six equal discs, and their water contents determined. These water content samples were allowed to dry gradually at room temperature before finally drying in an oven at 110°C to prevent

cracking. The samples were then used to obtain shrinkage limits as described by Lambe (13), page 25.

The photograph in Figure 9b shows one of these samples being tested triaxially with pore pressure measurements.

b) The Long-Term Diffusion Tests (Tests Nos. 1 to 4 in Table I)

After consolidation, the long-term test samples were subjected to diffusion by means of a small seepage head of two metres of water. This was done to keep a fresh solution flowing through the stones and filter strips, thus accelerating diffusion into the samples. Two samples were diffused with 1N NaCl and two with 0.005N NaCl for a period of about three months. The diffusion arrangement is shown in Figure 8. The deaired solution flowed in through the bottom drainage line and out through the top drainage for the purpose of getting rid of any entrapped air. Burettes were arranged in such a manner so as to be able to measure the flow in and out of the samples. In all samples, the flow "in" was about 10% greater than the flow "out". The reason for this apparent discrepancy was that the flow "in" was measured by means of a burette placed at the beginning of the diffusion line, which was 4 metres of thin walled nylon tubing, and sufficent flow was occurring through the walls of these nylon tubes to account for the difference. About

one and one-half void volumes flowed through the samples during diffusion which is flow of a little under 1 cc per day.

After three months had elapsed, diffusion was stopped and the samples were allowed to equilibrate for a week with only the top drainage line open. The two water diffusion samples (0.005N NaCl) were then tested in exactly the same manner described for the short-term tests, except that no back pressure was required since they were completely saturated.

The testing of the two salt samples was unavoidably delayed for two months. Both drainage valves were therefore closed to stop any further secondary consolidation. Before testing at the end of the two months, large excess pore-pressures were found to exist in both samples. The excess pore-pressures were allowed to dissipate before testing, and a corresponding flow out of the samples of 0.6 cc was observed. The samples were then tested in the same manner as the others except that the null indicators were filled with 1N NaCl. It is not known whether the excess pore-pressures were due to secondary consolidation or diffusion of cell water through the membranes. Tests are now being run to determine the reasons for this excess pore-pressure by eliminating any possible flow through the membranes using a mercury jacket which is described in

Appendix C. The photographs in Figure 10 show the mercury jacket in use.

The final salt concentrations of the salt diffusion samples were determined from the oven-dried samples by means of a conductivity bridge (R.C. type). The results were erratic throughout the depth of the samples and were very likely due to movement of salt during the period of drying. However, the average salinity of the pore fluid was 0.7N and varied between 0.6N and 0.8N throughout the samples (see Appendix A).

Aluminum determinations were also run on the oven-dried samples, and the results are shown by the shaded area in Figure 3. A colorimetric method was used and is described in Appendix A.

It is worth mentioning that in the case of the unsuccessful NaOH samples, the flow of solution up the filter strips stopped after about a week. This is very likely due to the clogging up of the filter strips with dispersed clay.

The triaxial test results are given in Table I and the stress-strain curves in Figures 11 through 14.

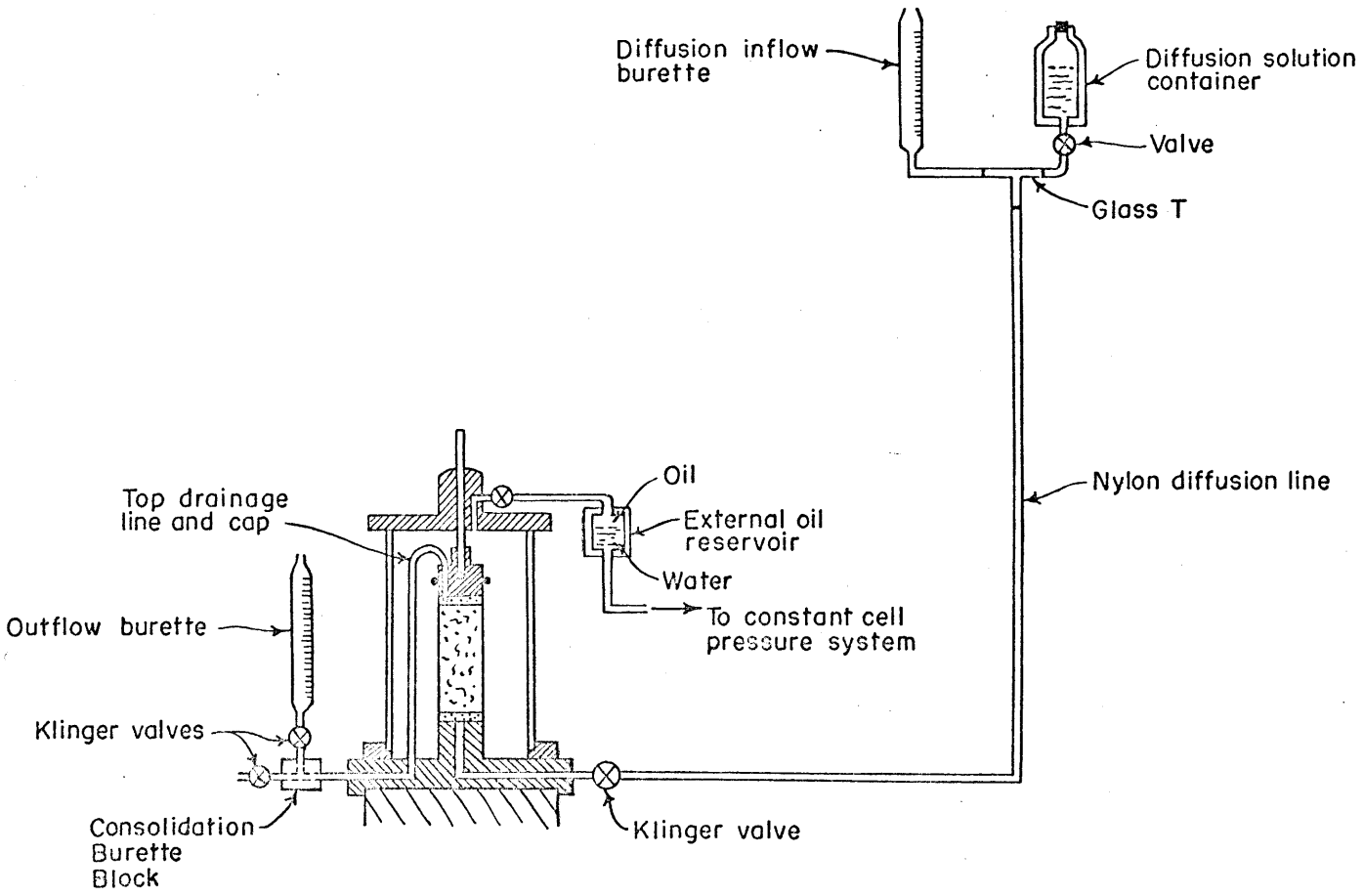

FIGURE 8 THE LAYOUT FOR THE DIFFUSION TESTS

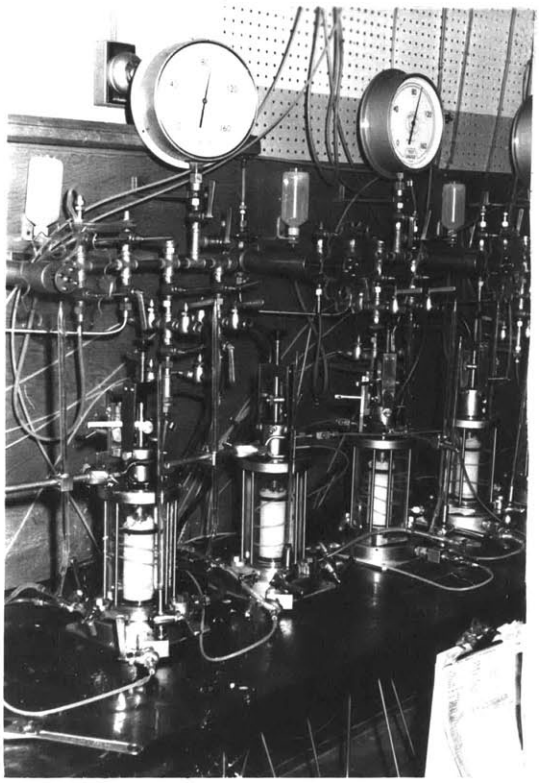

FIGURE 9a

PHOTOGRAPH OF THE TRIAXIAL SAMPLES DURING DIFFUSION

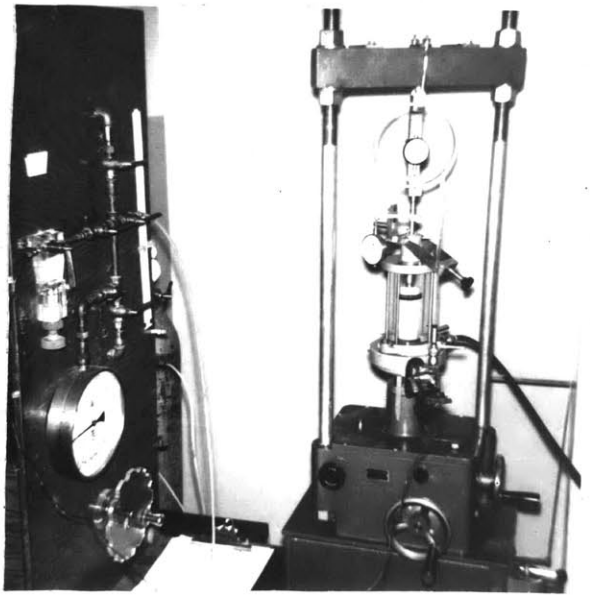

FIGURE 9b

THE TRIAXIAL COMPRESSION TEST WITH PORE PRESSURE MEASUREMENTS

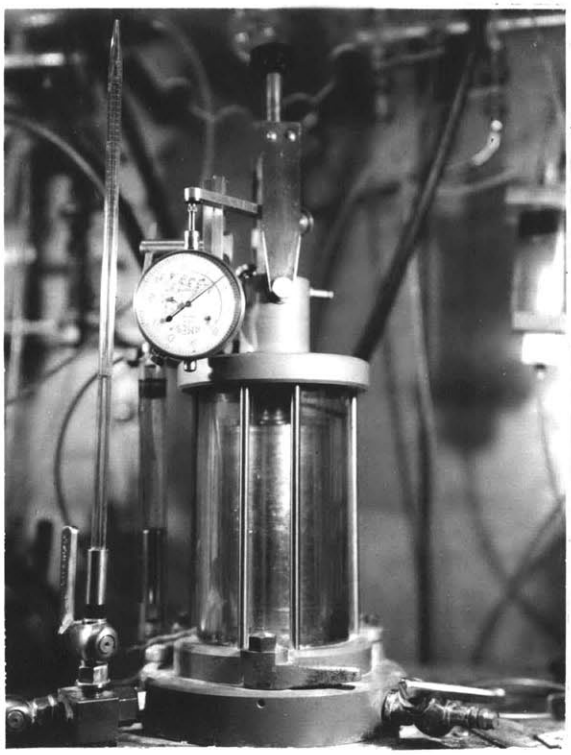

FIGURE 10a

CLOSE UP VIEW OF MERCURY JACKET ASSEMBLY SHOWING EXTERNAL MERCURY RESERVOIR

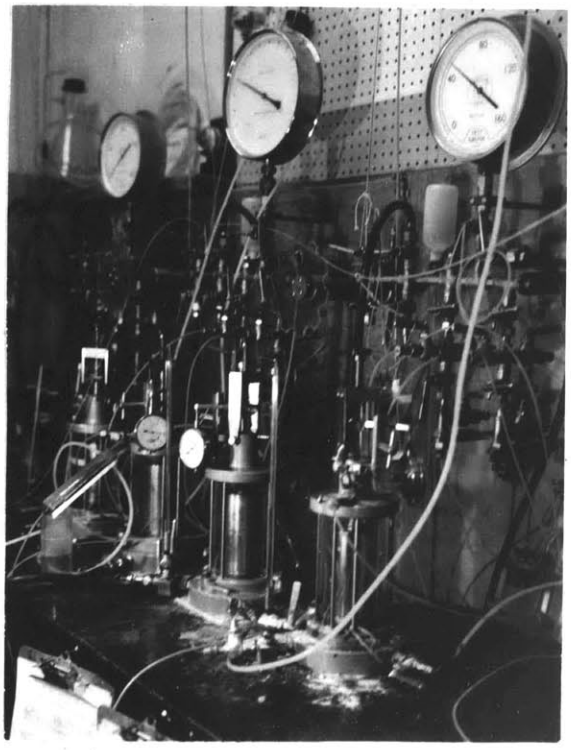

FIGURE 10b

DIFFUSION SAMPLES WITH MERCURY JACKETS

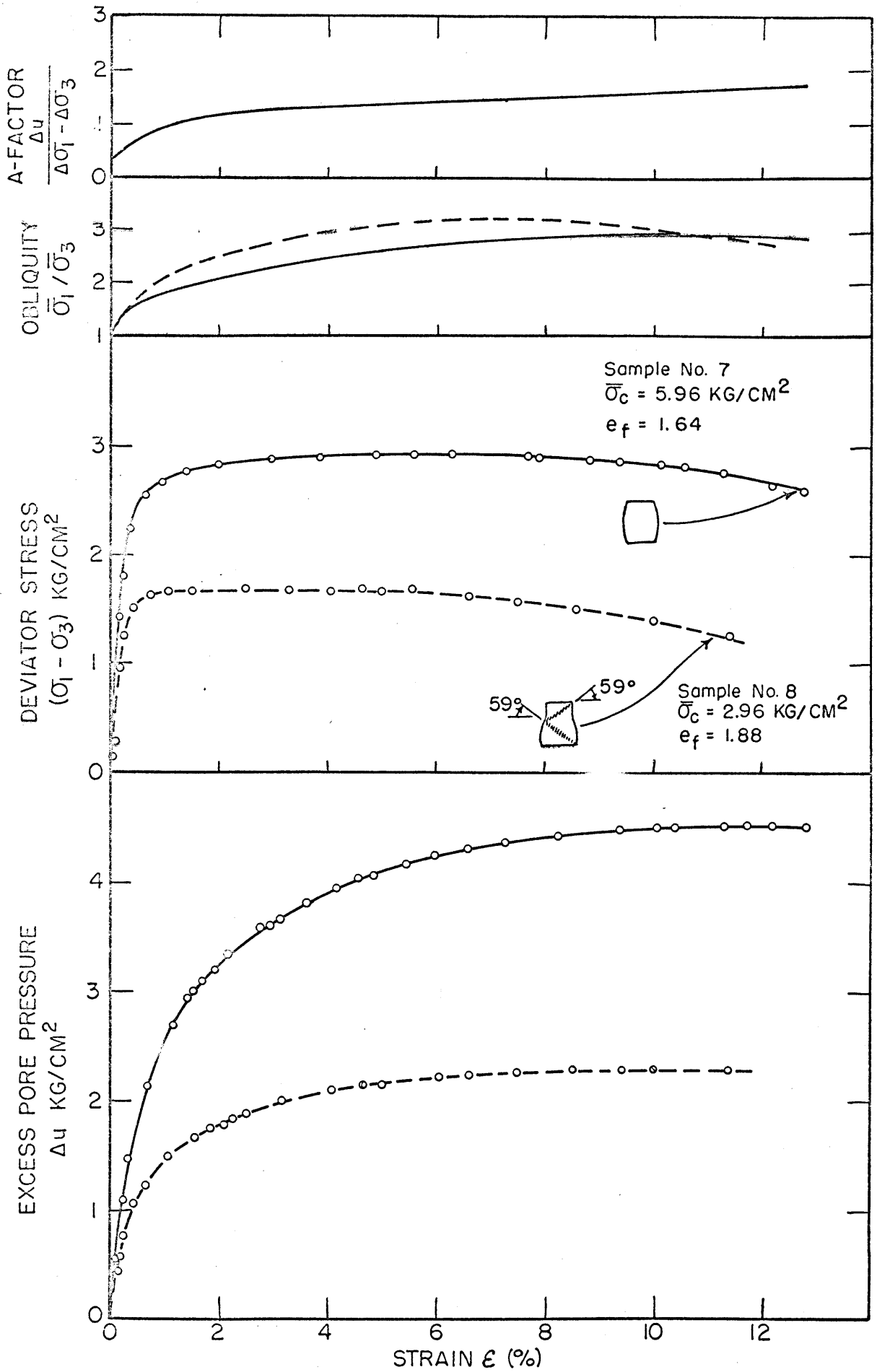

FIGURE 11 STRESS-STRAIN CURVES FOR NORMALLY CONSOLIDATED SAMPLES

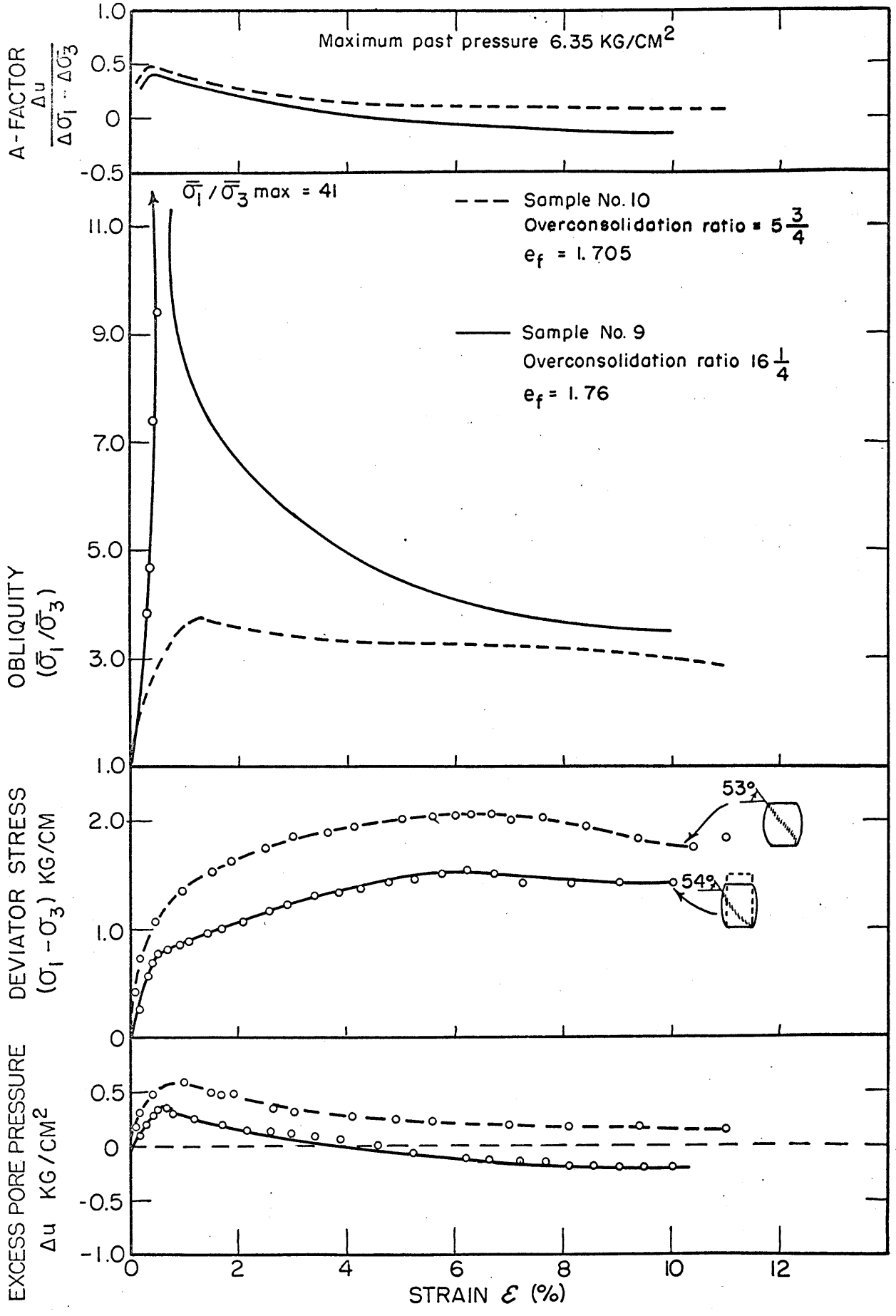

IGURE 12 STRESS-STRAIN CURVES FOR OVERCONSOLIDATED SAMPLES

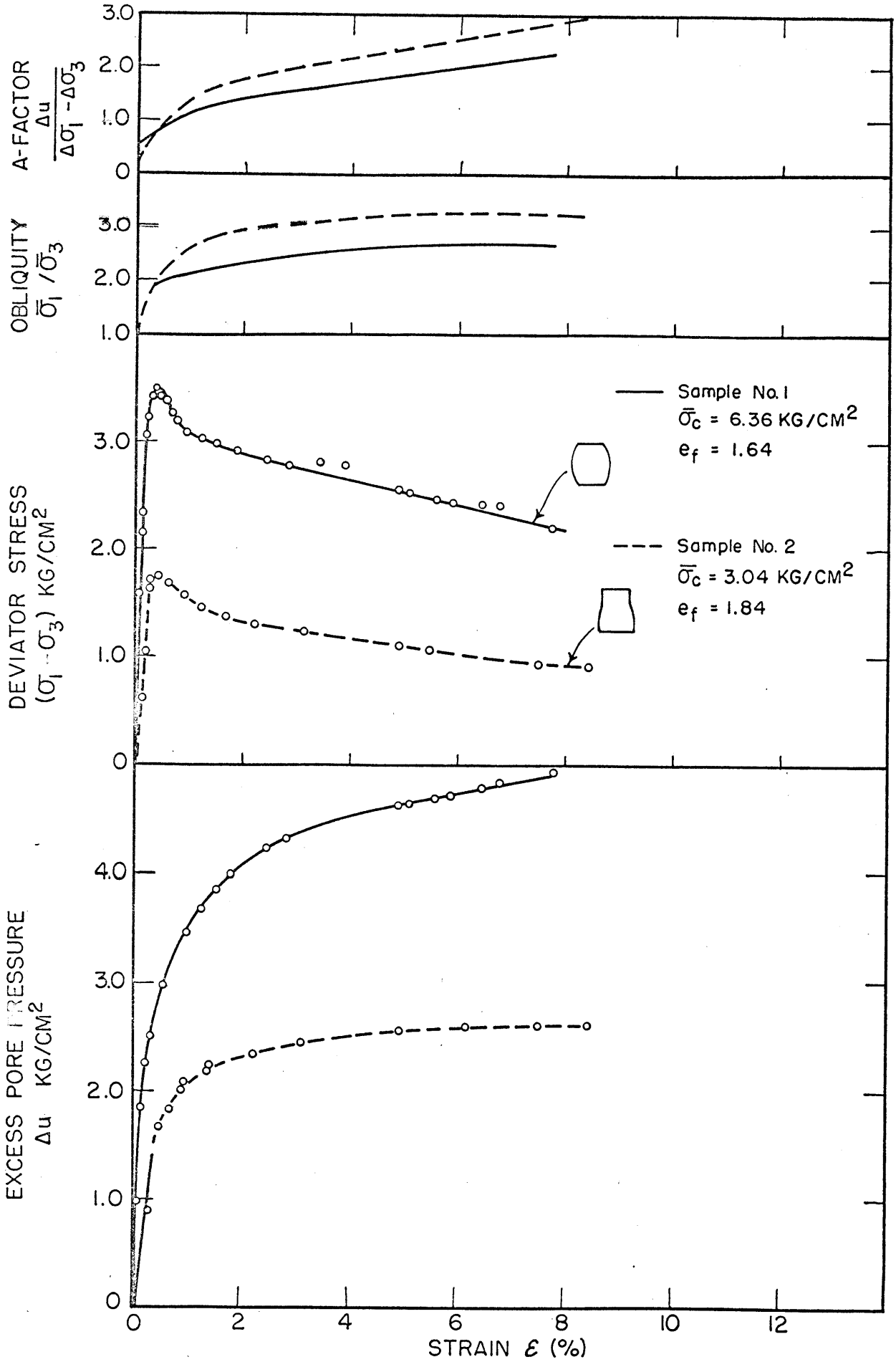

FIGURE 13 STRESS-STRAIN CURVES FOR SALT DIFFUSION SAMPLES

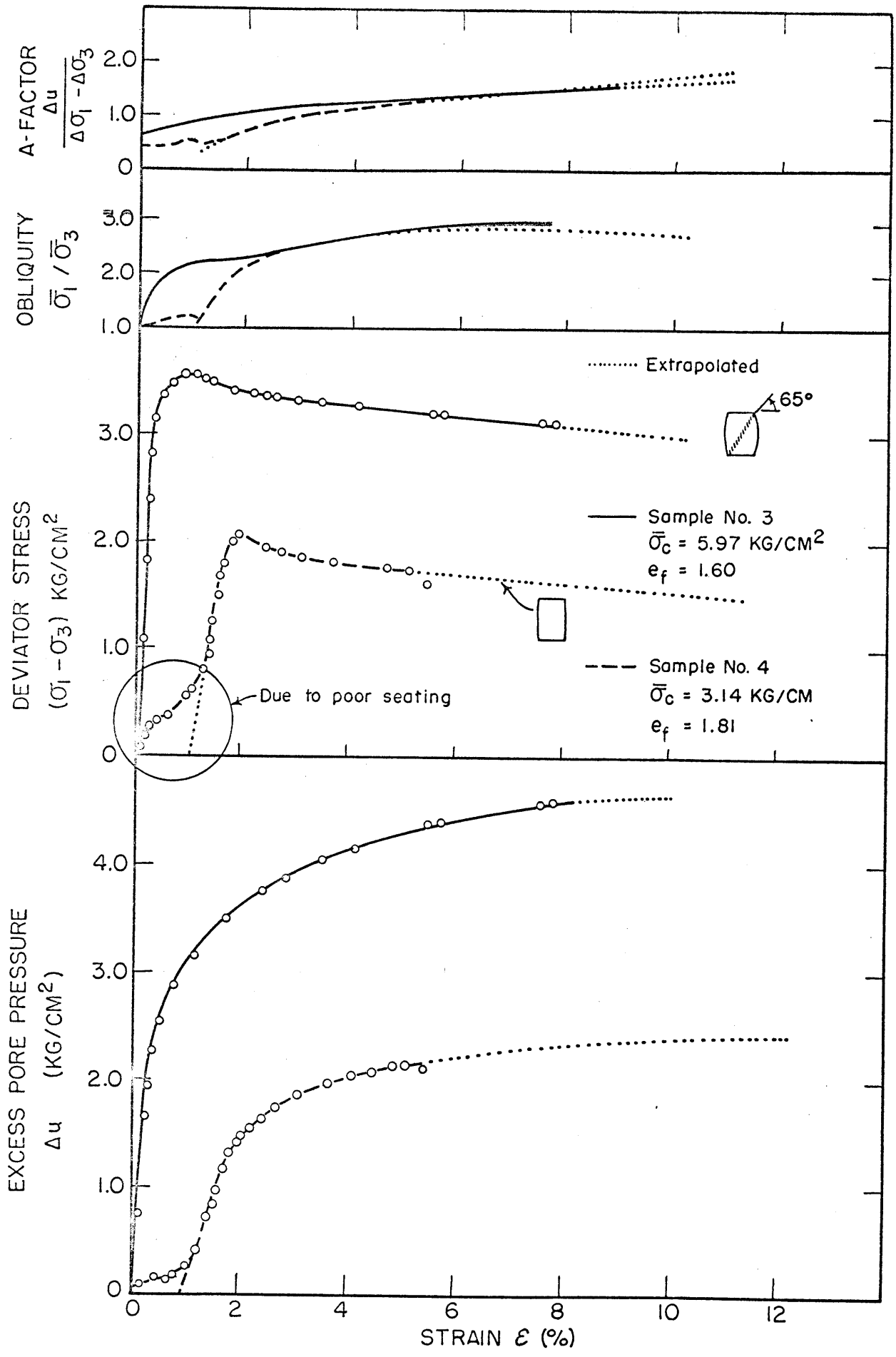

FIGURE 14 STRESS-STRAIN CURVES FOR WATER DIFFUSION SAMPLES

TABLE I - SUMMARY OF TRIAXIAL COMPRESSION TEST RESULTS

ne Elapsed After ionization Before Shearing	Time Elapsed After Triaxial Consolidation Before Shearing	Initial Void Ratio	Maximum Past Pressure kg/cm²	Consolidation Pressure Prior to Shearing kg/cm²	Final Void Ratio e_f	Initial Modulus of Elasticity kg/cm²	Conditions at Maximum Deviator Stress				Conditions at Maximum Principa		
							Strain %	Deviator Stress $(\sigma_1-\sigma_3)$ kg/cm²	Excess Pore-Pressure $\Delta\mu$ kg/cm²	Principal Effective Stress Ratio	Skempton A-Factor	Strain %	Deviator Stress $(\sigma_1-\sigma_3)$ kg/cm²	Excess Pore-Pressure $\Delta\mu$ kg/cm²
) months	5 1/2 months(a)	2.17	6.32	6.28	1.64	1500	0.39	3.49	2.59	1.95	0.74	6.8	2.40	4.85
) months	5 1/2 months(a)	2.16	3.16	3.04	1.84	550	0.40	1.75	1.54	2.16	2.37	8.3	0.93	2.62
7 months	3 months	2.16	6.35	5.97	1.60	1000	0.90	3.57	3.00	2.12	0.84	7.75	3.10	4.59
1/2 months	2 1/2 months	2.15	3.19	3.14	1.80	300(b)	0.95	2.05	1.42	2.19	0.69	4.1(c)	1.74	2.16
4 months	-	2.17	6.35	6.35	1.62	1350	3.09	3.45	3.86	2.35	1.12	8.3	3.38	4.64
5 months	-	2.16	3.19	3.19	1.88	400	3.05	1.79	2.20	2.80	1.23	7.6	1.68	2.52
2 months	-	2.12	6.35	5.96	1.64	750	6.00	2.92	4.23	2.68	1.45	9.4	2.84	4.50
2 months	-	2.09	3.19	2.96	1.88	420	6.03	1.65	2.20	3.17	1.33	7.2	1.58	2.26
2 months	-	2.11	6.35	0.39	1.76	175	6.20	1.54	-0.10	4.21	-0.06	10.0(d)	1.43	-0.18
2 months	-	2.15	6.35	1.10	1.705	325	6.00	2.07	0.20	3.30	0.10	11.0(d)	1.86	0.17

e from the same batch of soil
1960.

allowed for 2 months before shear-
iod pore-pressures developed in
owed to dissipate immediately prior
No. 1 had 2.95 kg/cm² excess pore-
red 0.48 cc volume decrease for
ure. Sample No. 2 had 1.85 kg/cm²
dissipation.

ating effects (see stress-strain

reach maximum $(\bar{\sigma}_1/\bar{\sigma}_3)$ and strain
ting effect.

samples $(\bar{\sigma}_1/\bar{\sigma}_3)$ has no signifi-
nt final obliquity conditions have

5.2 Discussion of the Triaxial Compression Test Results

5.2.1 Limitations in the Use of Void Ratios in Explaining Strength Data

The void ratio (e) is defined as the ratio of the volume of voids (which is the volume of fluid only in the case of saturated soils) to the volume of dry soil. It is by no means a fundamental property of soils since the void ratio depends on the environmental and stress histories of the soil. Strength will be a unique function of void ratio only if these conditions are identical.

According to a hypothesis put forward by Hvorslev (11) the shearing strength τ_{ff} of a saturated clay may be expressed as:

$$\tau_{ff} = c_e + \bar{\sigma}_{ff} \tan \phi_e$$

where c_e = true cohesion and is a function of water content (or void raio) only.

$\bar{\sigma}_{ff}$ = the effective normal stress on the failure plane at failure.

ϕ_e = the true angle on internal function.

It has also been shown by Hvorslev that the true cohesion at any water content, ω, is directly proportional to the equivalent consolidation pressure, $\bar{\sigma}_e$, and in a triaxial test it is taken as the all-round consolidation pressure which produces this particular water content, w, in a normally consolidated sample.

Figure 15 is a dimensionless plot to determine the Hvorslev strength parameters. The equivalent consolidation pressures $\bar{\sigma}_e$ used are those for the virgin compression curve shown in Figure 16.

To obtain Hvorslev's "True" angle of internal friction and "True" cohesion from such a plot, it is necessary to convert the angle and intercept obtained from this plot by using the following equations given by Bishop and Henkel (2):

$$\tan \theta = \frac{\sin \phi_e}{1 - \sin \phi_e}$$

and

$$a = \frac{c_e \cos \phi_e}{\bar{\sigma}_e (1 - \sin \phi_e)}$$

where $\tan \theta$ = the slope of the line in Figure 15.

a = the intercept of the line in Figure 15.

and ϕ_e = Hvorslev true angle of internal friction.

c_e = Hvorslev true cohesion and is a function of void ratio only.

$\bar{\sigma}_e$ = equivalent consolidation pressure.

Substituting in the above equations, the Hvorslev shear strength parameters for the plain samples are:

$$\frac{c_e}{\bar{\sigma}_e} = 0.035 \quad \text{and} \quad \phi_e = 22.6^\circ$$

No values have been obtained for the diffusion samples since insufficient tests were run.

Figure 16 gives the e-log p curves for all the samples tested. The virgin curve for the plain samples was obtained from the burette reading at the end of primary consolidation. The points shown in this figure represent conditions at failure. This accounts for the scatter from the virgin compression line.

The diffusion sample's e-log p lines were drawn parallel to the virgin compression line. It is worth noticing that the salt samples had less secondary consolidation than the water diffusion samples, but not sufficient tests were run to draw definite conclusions.

Figure 17 gives a plot of void ratio versus maximum shear stress and shear stress at maximum principal effective stress ratio for all the samples triaxially tested. These differ slightly in their stress history as follows:

1) Little or no secondary consolidation occurred with the plain water samples prior to shearing.

2) Secondary consolidation occurred for two months in the aged water samples during diffusion.

3) For the salt samples, no drainage was permitted for two months after diffusion during which time large positive pore-pressures developed in the samples. These pore-pressures were dissipated prior to shearing.

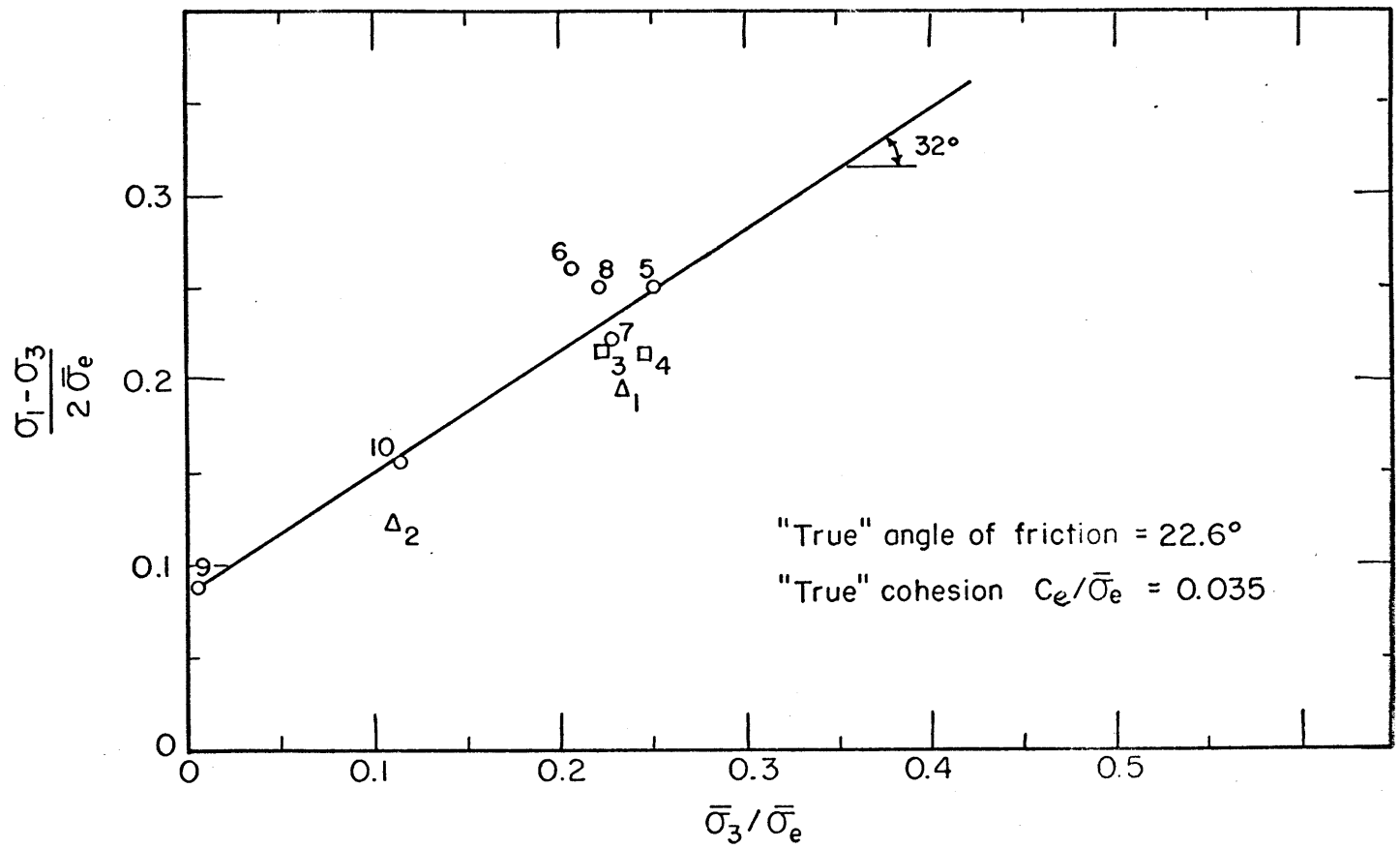

FIGURE 15 HVORSLEV PLOT AT MAXIMUM PRINCIPAL EFFECTIVE STRESS RATIO

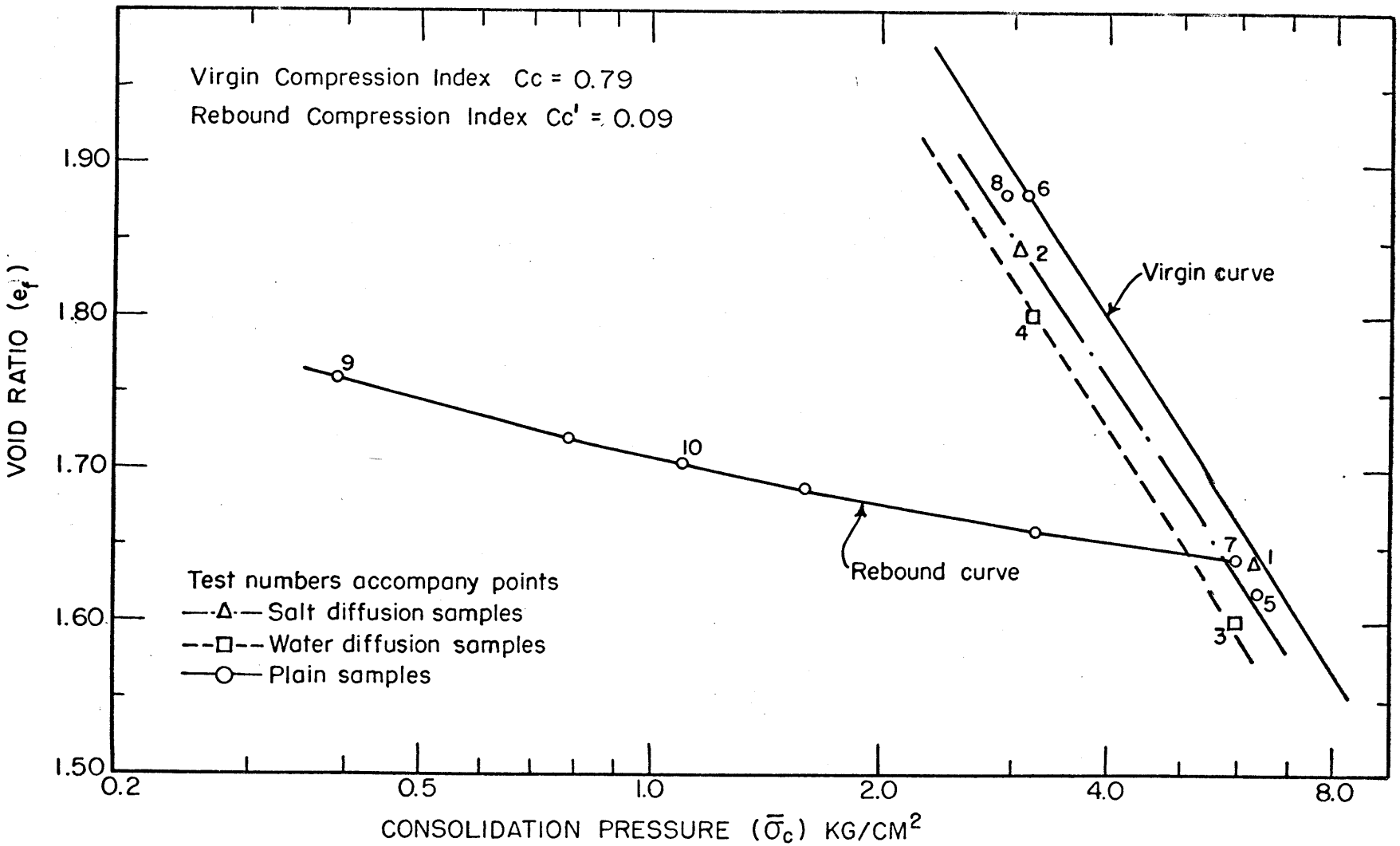

FIGURE 16 VOID RATIO vs CONSOLIDATION PRESSURE

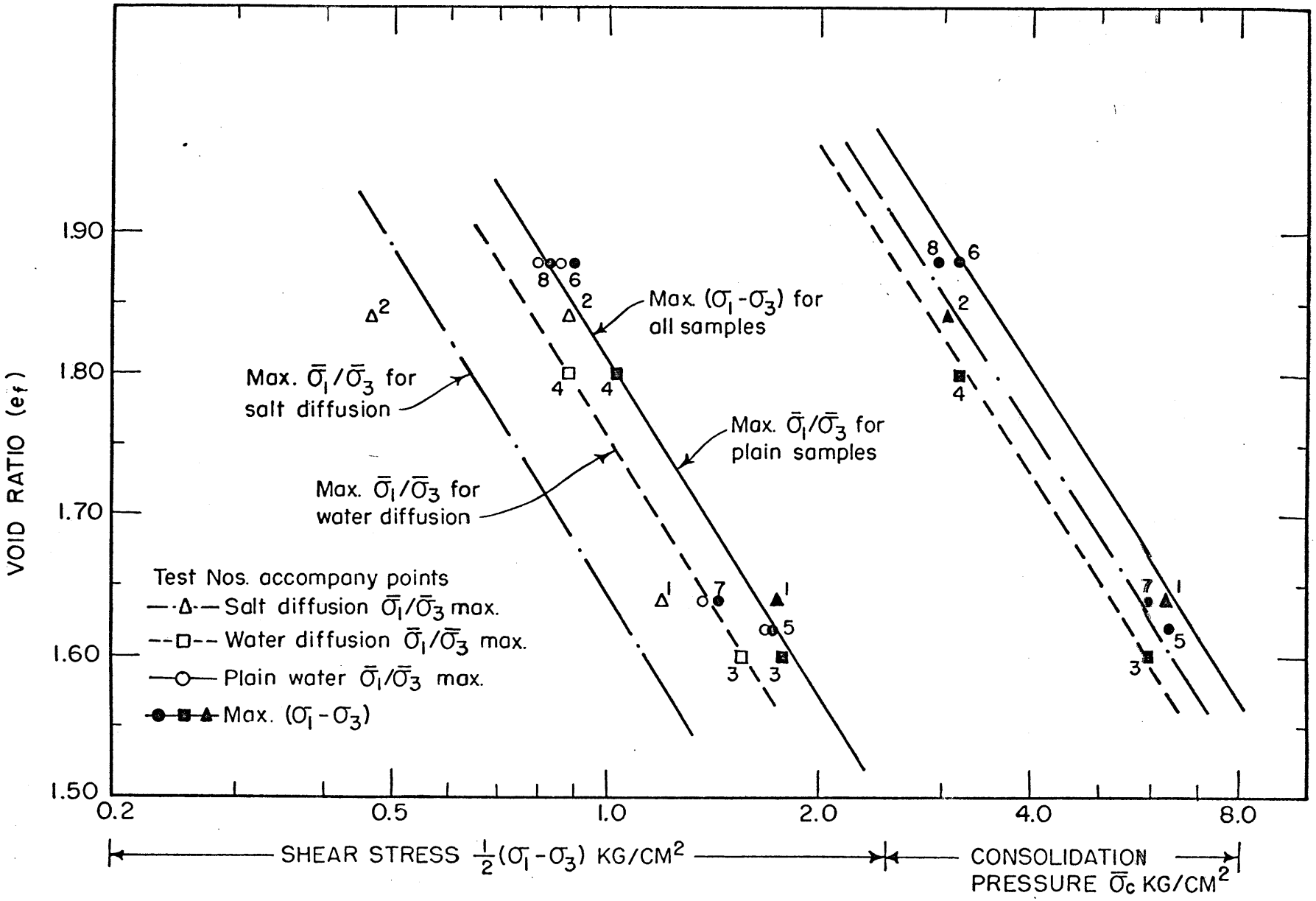

FIGURE 17 SHEAR STRENGTH vs VOID RATIO

Due to the limited number of tests the best strength lines have been drawn parallel to the virgin compression e-log p line as suggested by Rutledge (20) and therefore do not pass through all points.

There seems to be a unique relationship between void ratio and maximum shear stress for all the normally consolidated samples. The scatter in data can easily be due to slight variations in stress history.

On the other hand at maximum effective stress ratio for any given void ratio, the plain water sample is strongest, followed by the aged water. The weakest is the salt diffused sample.

5.2.2 The Undrained Shear Strength

If the undrained shear strength is defined as the shear stress at maximum deviator stress (Figure 18) as is usually the case, then all samples have the same strength:

$$S_u = 0.12 \text{ kg/cm}^2 + \bar{\sigma}_c \tan 14.5^\circ$$

where S_u is the undrained shear strength on the failure plane in kg/cm^2

$\bar{\sigma}_c$ = the consolidation pressure in kg/cm^2

The intercept of 0.12 kg/cm^2 is believed to be solely due to the restraints imposed by the rubber membranes and filter strips on the samples. If this is the case, then

$$S_u = \bar{\sigma}_c \tan 14.5^\circ$$

Note all strength plots are for maximum shear stress, $\frac{1}{2}(\sigma_1 - \sigma_3)$, and the shear stress on the failure plane is obtained by the simple relation:

$$\tan \theta = \sin \phi$$

where $\tan \theta$ = the slope of the line given in these plots.

ϕ = the friction angle for shear on the failure plane.

If the undrained shear strength is defined by maximum obliquity (Figure 19), then the salt diffusion samples are considerably weaker.

For the plain and diffusion water samples:

$$S_u = 0.15 \text{ kg/cm}^2 + \bar{\sigma}_c \tan 14^\circ$$

For the salt diffusion samples:

$$S_u = 0.15 \text{ kg/cm}^2 + \bar{\sigma}_c \tan 10^\circ$$

Again, if the intercept is due to membrane and filter strips (note it is slightly higher here than at maximum deviator stress since larger deformations have occurred), then for all the water samples:

$$S_u = \bar{\sigma}_c \tan 14^\circ$$

and for all salt diffusion samples:

$$S_u = \bar{\sigma}_c \tan 10^\circ$$

The undrained shear strength at maximum obliquity is of no practical importance but shows that salt reduces the undrained strength only after considerable shearing has occurred.

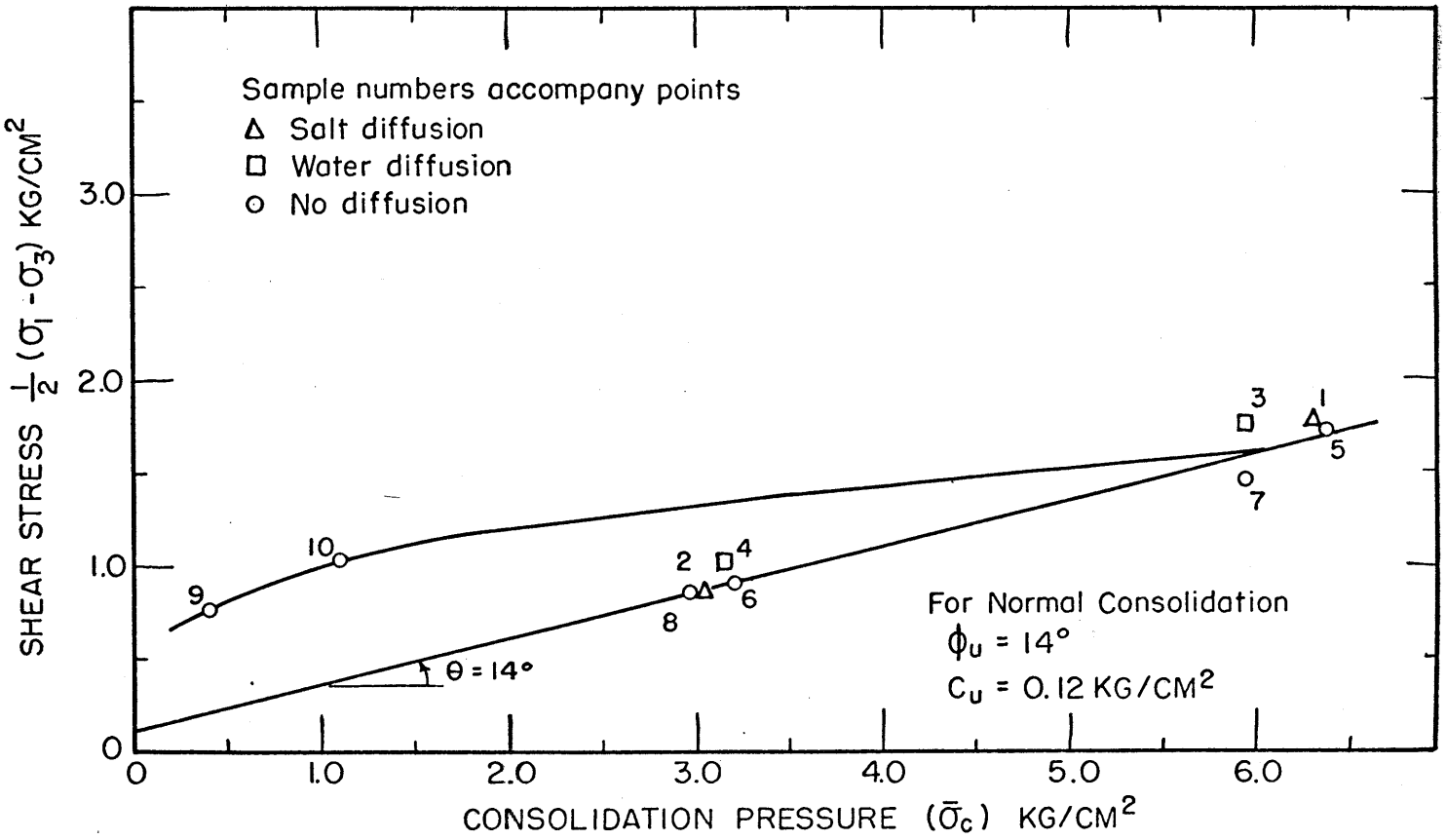

FIGURE 18 MAXIMUM SHEAR STRESS vs CONSOLIDATION PRESSURE

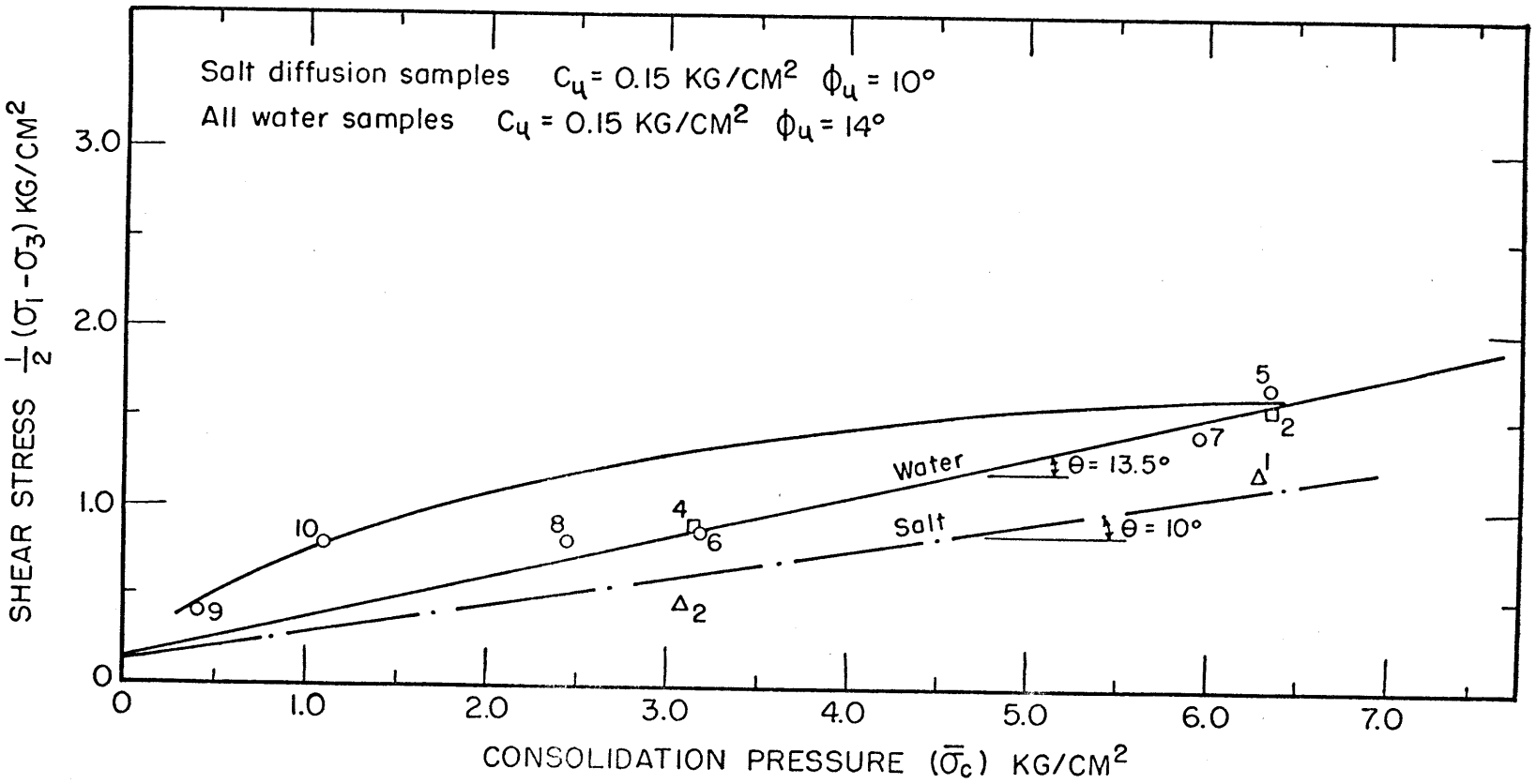

FIGURE 19 SHEAR STRESS AT MAXIMUM $\bar{\sigma}_1/\bar{\sigma}_3$ vs CONSOLIDATION PRESSURE

5.2.3 The Triaxial Stress-Strain Characteristics
A Mechanistic Picture to Explain the Triaxial Test

In Fundamentals of Soil Mechanics (pages 342-343) Taylor (23) states that due to the nonuniform stress and strain conditions in triaxial tests progressive failure occurs. "Therefore bulging occurs at the center of the sample and this in itself proves that conditions are not uniform." In fact, these nonuniform stress and strain conditions also exist in most cases of consolidation and shear, taking place in the field as well as in the laboratory.

The stress-strain characteristics of fine-grained soils can be explained with the use of a simple mechanistic picture in which progressive action is considered as a continual "breaking" and "making" of interparticle contracts (bonds).

The net effect of the breaking and making of bonds will determine the amount of load carried by the soil structure. (Structure refers to the interparticle bond strength as well as the relative particle orientation or fabric.)

In a triaxial test, the portion of the total load carried by the structure will show up as the deviator stress, while the pore-pressure is a measure of the pore fluid contribution to the total load.

It is important to note that the strength of the bonds which are broken and made during shear depends on the ambient environmental conditions, but the original bonds existing prior to shear exhibit characteristics dictated by the environment during consolidation and by the stress history of the soil. These original bonds usually include a "cementing" component of strength which has been produced by aging. This "cementing" effect gives the soil its brittle structure and is very sensitive to disturbance of the soil fabric. For example, a soil consolidated anisotropically will lose its initial brittle structure if reconsolidated isotropically, but the "cementing" will rebuild with time.

The bond strength may, therefore, be divided into two separate components: 1) Fabric which is controlled solely by interparticle electrical forces, 2) A cementing component which has a complex reversible nature.

5.2.4 Pore-Pressures During Shear

In 1954 Skempton (22) proposed the following equation for the pore-pressure change during undrained shear:

$$\Delta u = B[\Delta\sigma_3 + A(\Delta\sigma_1 - \Delta\sigma_3)]$$

This expression can be seen to be a function of changes in principal major and minor total stresses and where A and B are pore-pressure coefficients.

He showed that the coefficient B is very close to 1 for saturated soil and for all practical purposes, may be taken as unity.

In all the triaxial tests presented here, B was essentially 1.0 ($B = \frac{\Delta u}{\Delta \sigma_3}$ prior to shearing and therefore is the pore-pressure response which was never less than 0.97 as previously mentioned).

The triaxial tests were run at constant cell pressure; therefore, $\Delta \sigma_3 = 0$, and the Skempton equation becomes:

$$\Delta u = A(\Delta \sigma_1 - \Delta \sigma_3)$$

or the A-Factor equals the change in pore-pressure divided by the corresponding change in deviator stress. Thus, the A-Factor is a measure of the amount of deviator stress carried as excess pore-pressure and is a measure of structural collapse.

The excess pore-pressure (Δu) and A-Factor as a function of strain are plotted in Figures 11 through 14. The effect of environment can be clearly seen in Figures 20 and 21.

The excess pore-pressures at failure ($\bar{\sigma}_1 / \bar{\sigma}_3$ max.) for any one consolidation pressure are not very different - the salt diffusion samples having the highest. There seems to be very little difference between the water samples, with the water diffusion samples possibly being slightly higher.

The A-Factors, on the other hand, which are also a function of deviator stress, ranged between 2.4 and 3.0 for the salt samples and was 1.5 for the plane and water diffusion samples.

Summing up, this means that there is a greater structural collapse during shear in the case of the salt diffusion samples than for the water samples in which aging has a negligible effect.

5.2.5 Initial Modulus of Elasticity (E)

The initial modulus of elasticity is defined here as the initial slope of the stress-strain curves. If all samples had initially the same structure and fabric, then their initial moduli of elasticity should have been the same. (By fabric is meant the relative orientation of the particles, while structure includes the linkage between particles.)

Samples having the same fabric would not have the same modulus of elasticity if the bond between particles, i.e. structure, is different. The bond strength increases with consolidation pressure and with degree of "cementing" due to aging. Disturbances such as reconsolidation (especially from an anisotropic state to an isotropic state) will cause considerable breakdown of the cementation which had developed during aging (the cementing will rebuild with time).

Peck and Uyanik (19) show how sensitive the modulus of elasticity is to disturbance and give this as the reason for the poor prediction of initial settlements in structures in which the modulus of elasticity obtained from laboratory samples is used in the computations.

The values of E for the triaxial tests are given in Table I.

For the higher consolidation pressure, E varied between 1500 kg/cm^2 and 750 kg/cm^2. For the lower consolidation pressure, it varied between 550 kg/cm^2 and 400 kg/cm^2. In the overconsolidation sample, E decreased as the overconsolidation ratio increased.

No conclusion can be drawn from the initial moduli of elasticity, since slight disturbances due to seating and reconsolidation caused variations of as much as a factor of 2 in the values of E. The modulus of elasticity did, however, increase with consolidation pressure for all normally consolidated samples and decreased as the overconsolidation ratio increased.

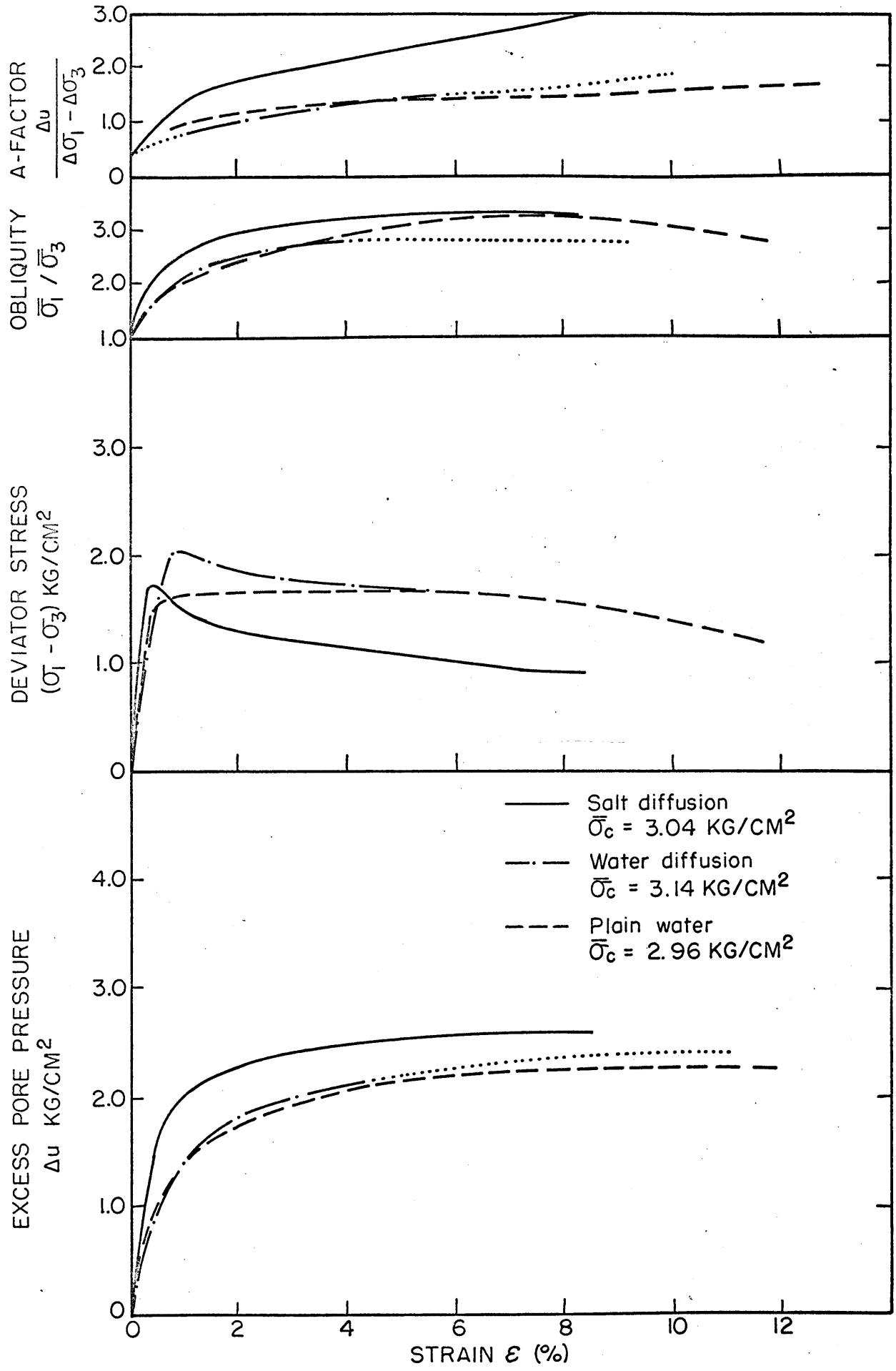

FIGURE 20 EFFECT OF ENVIRONMENT ON THE STRESS-STRAIN CURVES

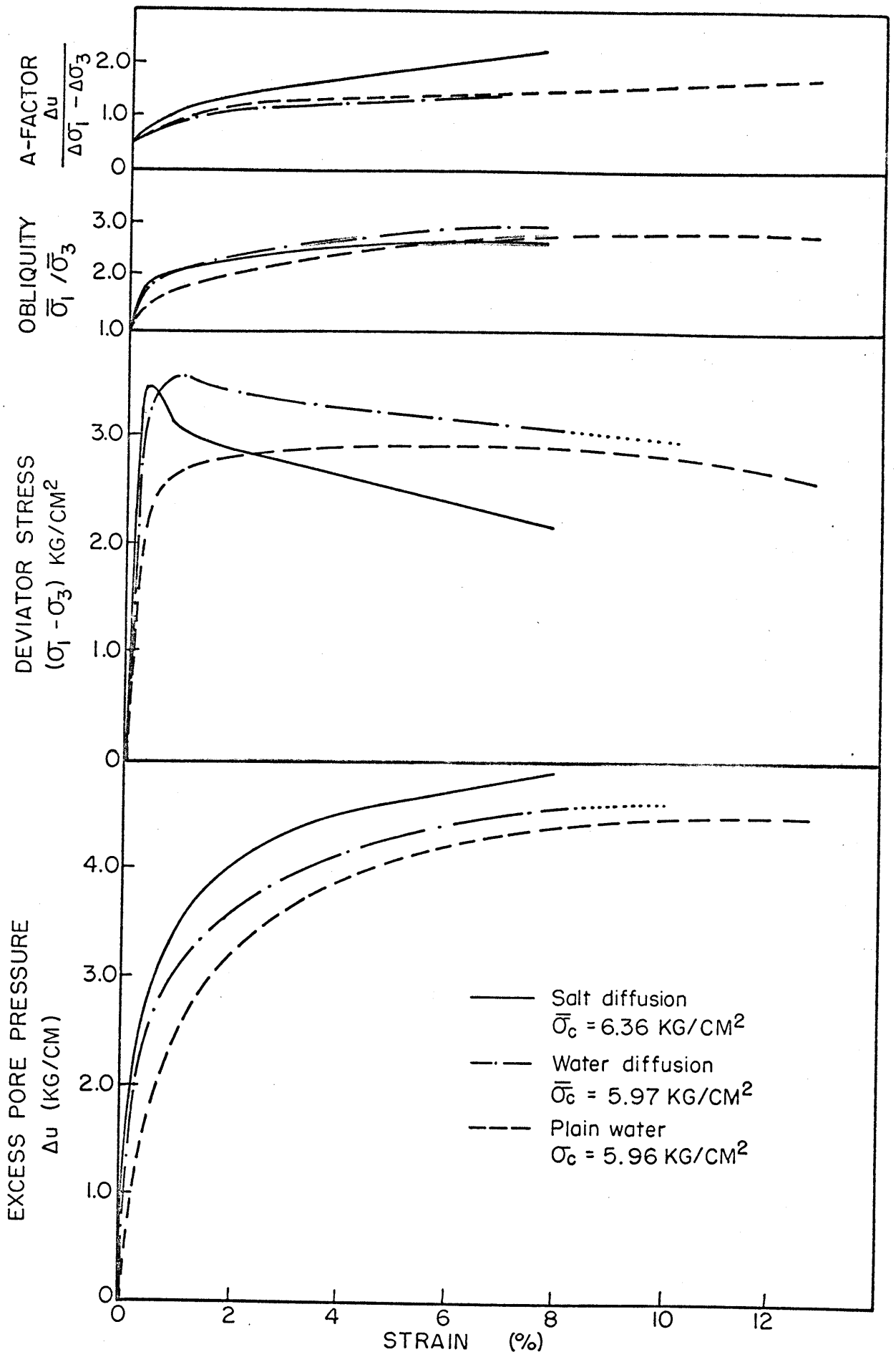

FIGURE 21 EFFECT OF ENVIRONMENT ON THE STRESS-STRAIN CURVES

5.2.6 The Deviator Stress

During the early stages of straining in a triaxial compression test, the deviator stress increases very rapidly since hardly any progressive action is taking place at these low strains. The original clay structure is carrying the deviator load with little "breaking" and "making" of bonds. As the strain increases more progressive action takes place accompanied by more and more "breaking" and "making" of bonds, until a time is reached when no original bonds remain. Only the new bonds which have developed will carry the deviator load. The strength of the newly formed bonds are governed by the environment existing during shear.

The deviator stress and excess pore-pressure will reach a relatively constant value when the rate of "breaking" of these newly formed bonds is equal to the rate of "making." On further straining there may be a reorientation of particles in the shear zone which would account for a further lowering of the deviator stress. This will occur only at large strains. Figure 22, which was obtained by Quigley (25), shows this effect, by means of X-Ray diffraction, on one of the overconsolidated samples which had a clearly visible failure plane and had been strained to 10% with the deviator stress flattening off at about 6% strain. The zone of shear was about 3 mm thick; however, the visibly apparent thickness was 2 mm. There was considerable

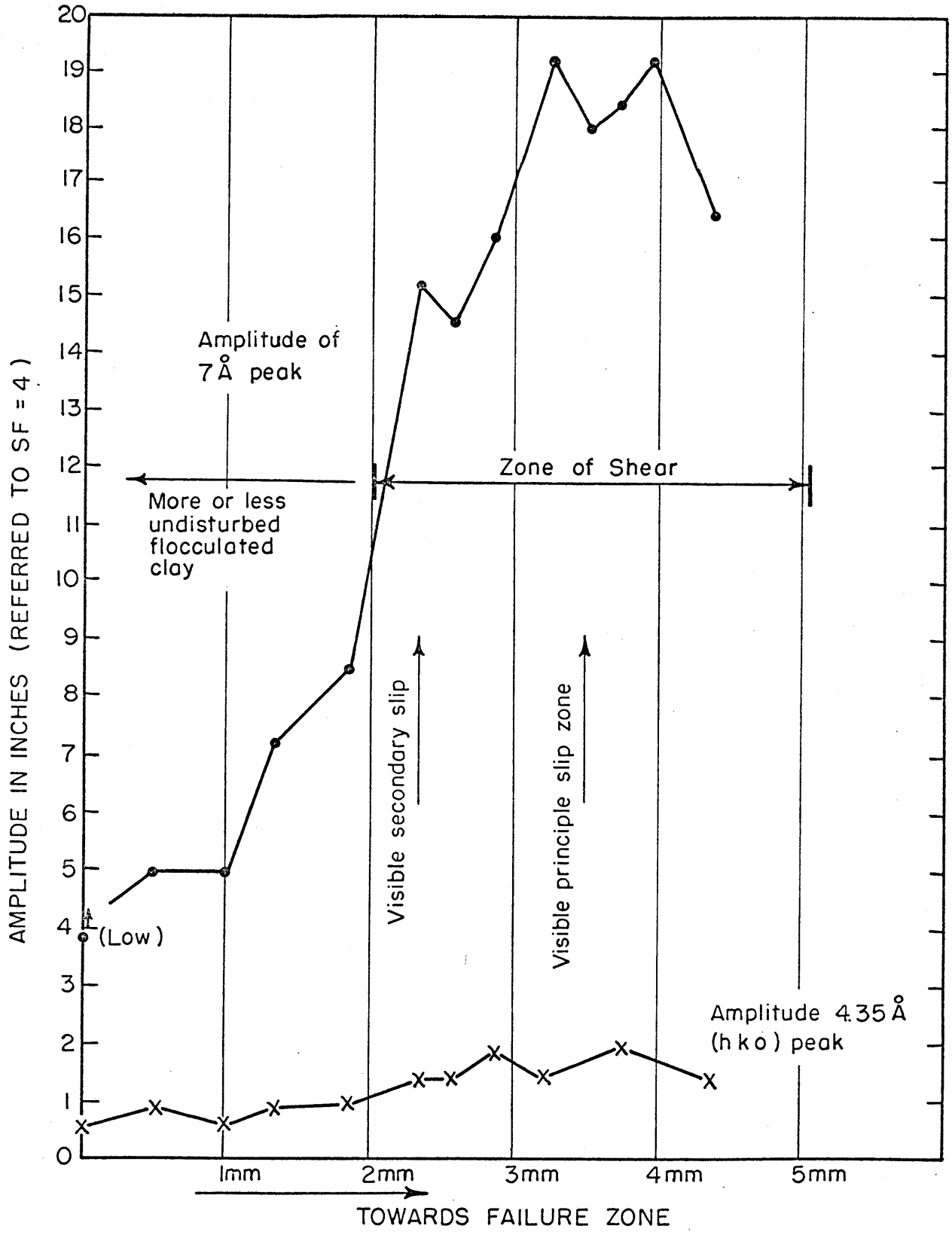

FIGURE 22 CHANGE IN PARTICLE ORIENTATION AS A RESULT OF SHEARING ACTION (after Quigley)

particle orientation produced in the shear zone as shown by a large increase in intensity of the (001), 7.2Å Kaolinite, peak. There was also some increase in intensity of the (hko), 4.35Å peak, but this is very likely due to an increase in Kaolinite density within the failure zone during drying, since the X-Rays were run on the oven-dried sample.

In the case of the normally consolidated plain water samples, the initial bonds which existed prior to shear are similar to the final bonds which have been produced during shearing. The deviator stress reaches a constant value as soon as the rate of "making" and "breaking" of bonds has reached a constant value.

The initial bonds in the water diffusion samples include the "cementing" action due to aging which is destroyed once the bond is broken. The new bonds which are formed are weaker than the original bonds and are the same as the ones for the plain water samples. This explains the peak in the deviator stress curve which occurs at a low strain (1.0%) after which time there is not a sufficient number of old bonds to carry the load, and load falls off until it is completely carried by the newly formed bonds which are the same as those that exist in the plain water samples. The deviator stress, therefore, reaches the same value as for the plan water samples as can be seen in Figures 20 and 21.

The process is similar in the salt diffusion samples to that in the water diffusion samples, but superimposed on the effect of initially cemented bonds is the effect of the NaCl on the bonds being formed during shear. This tends to further reduce the bond strength, and when all the original bonds have been broken in the failure zone, the new bonds, which are making and breaking, are considerably weaker than those produced in the water samples. This is confirmed by the deviator stress reaching a lower constant value for the salt diffusion sample than for the water samples (Figures 20 and 21). The reduction in bond strength, with NaCl as the environment, is confirmed by the results of both sedimentation tests and Atterberg limits.

5.2.7 The Effective Stress Envelopes

The effective stress envelopes at maximum deviator stress are shown in Figure 23. This plot shows mainly the effect of cementation due to aging on the soil structure at maximum deviator stress (i.e. where the initial structure is still predominant). The plain water samples have the highest friction angle ($\bar{\phi} = 24.5°$) since most of the friction has been mobilized by the time the maximum deviator stress has occurred ($\epsilon = 6\%$). On the other hand, in the diffusion samples, the cemented bonds are still predominant and therefore less friction has been mobilized.

The friction angles for the water diffusion and salt diffusion samples are 19.5° and 16.5°, respectively. The lower friction angle for the salt diffusion samples is believed to be due to a larger cementing action that occurred, because they were aged for a longer period of time.

It can be seen from Figure 24 that any cementation which occurred prior to triaxial consolidation is completely destroyed after this consolidation, since Samples Nos. 5 and 6 were isotropically consolidated and tested 5 months after homoionization and Samples Nos. 7 and 8 after 12 months.

Figure 25 shows that the effect of initial cementation is completely destroyed by the time the water diffusion samples have reached their maximum principal effective stress ratio. At this stage they share the same effective stress envelope as the plain water samples which have not been aged ($\bar{\emptyset} = 27°$).

Figure 26 demonstrates the effect of salt in reducing the shear strength of Kaolinite at the maximum principal effective stress ratio. In the salt samples, the new bonds are governed by the existing environment of NaCl. This environment weakens the bond strength as is shown by the result of the Atterberg limits and sediment densities. The friction angle $\bar{\emptyset}$ is 24° compared to $\bar{\emptyset} = 27°$ for the water environment.

Finally the drained envelope of the overconsolidated samples is shown in Figure 27.

5.2.8 Summary of Strength Parameters for Normally Consolidated Samples

Assuming the cohesion intercepts are due to membrane and filter strip restrains, then in all cases:

$$c_u = 0 \quad \text{and} \quad c = 0$$

a) Undrained shear parameters:

At maximum deviator stress

For all samples $S_u = \bar{\sigma}_c \tan 14°$

At maximum principal effective stress ratio

For all water samples $S_u = \bar{\sigma}_c \tan 14°$

For salt diffusion samples $S_u = \bar{\sigma}_c \tan 10°$

b) Drained shear strength parameters:

At maximum deviator stress

For plain water samples $\tau_f = \bar{\sigma}_f \tan 24.5°$

For aged water samples $\tau_f = \bar{\sigma}_f \tan 19.5°$

For salt diffusion samples $\tau_f = \bar{\sigma}_f \tan 16.5°$

At maximum principal effective stress ratio

For all water samples $\tau_{ff} = \bar{\sigma}_{ff} \tan 27°$

For salt diffusion samples $\tau_{ff} = \bar{\sigma}_{ff} \tan 24°$

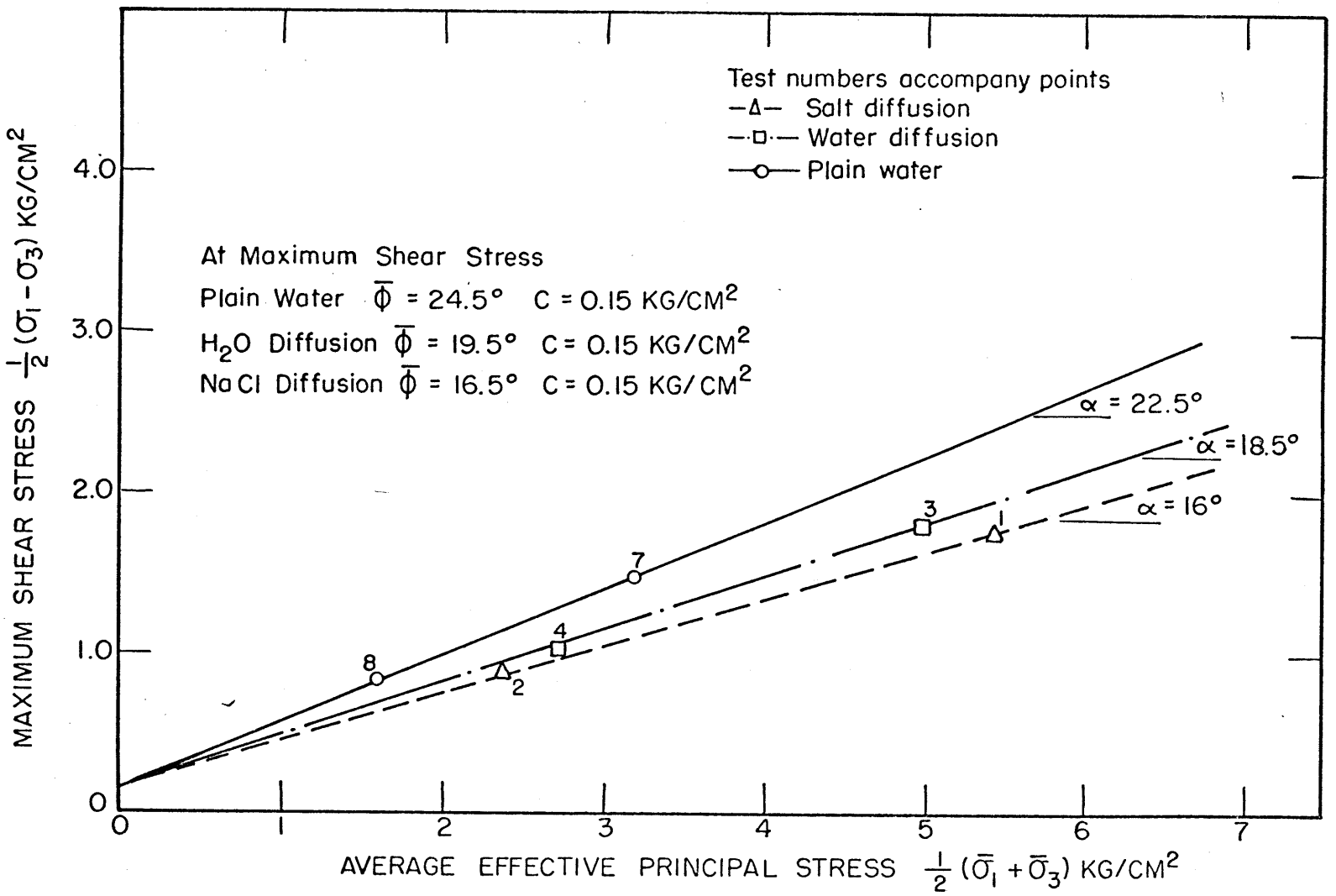

FIGURE 23 EFFECTIVE STRESS ENVELOPE AT MAXIMUM DEVIATOR STRESS

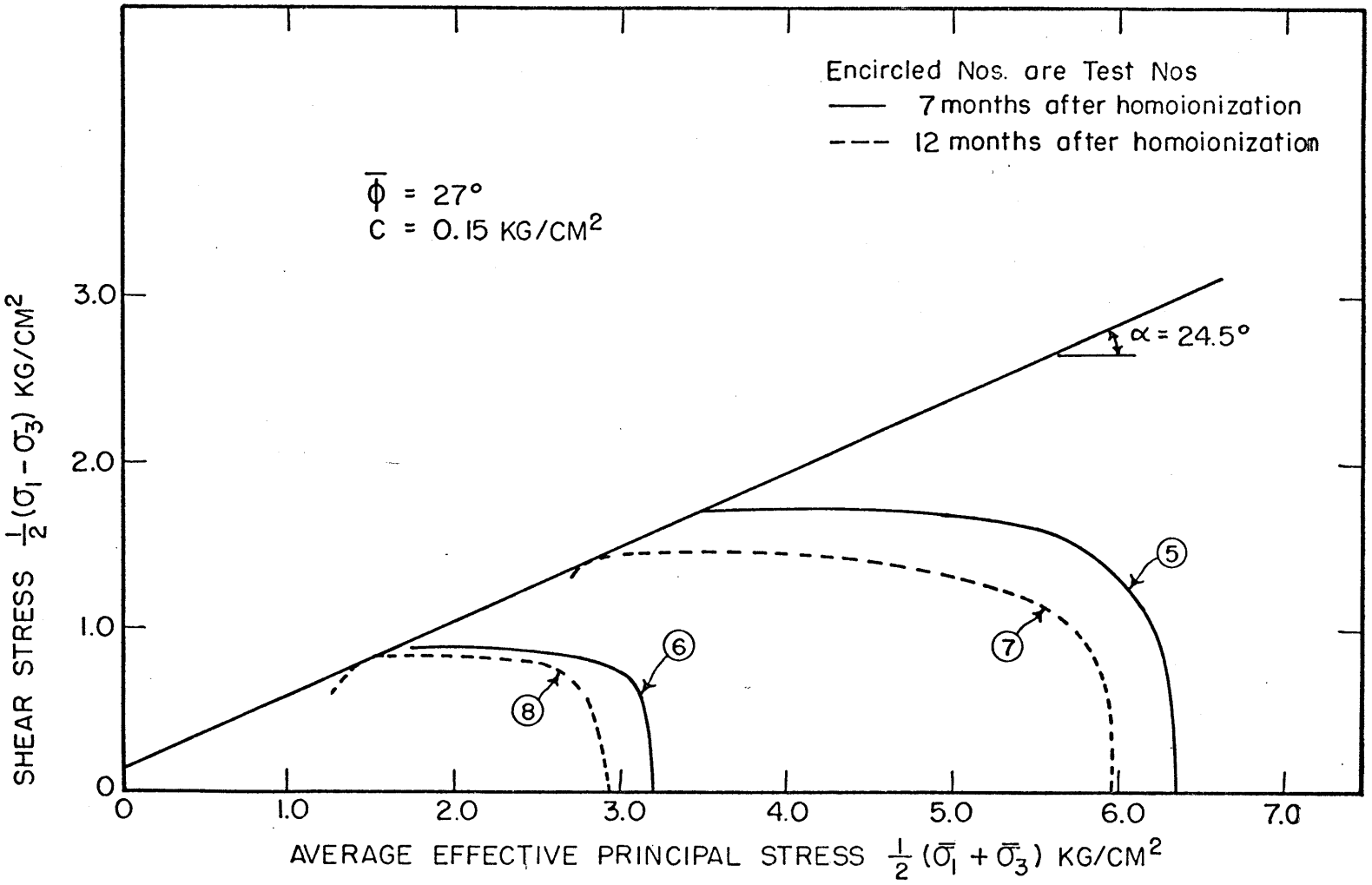

FIGURE 24 EFFECT OF AGING PRIOR TO TRIAXIAL CONSOLIDATION ON THE EFFECTIVE STRESS ENVELOPE

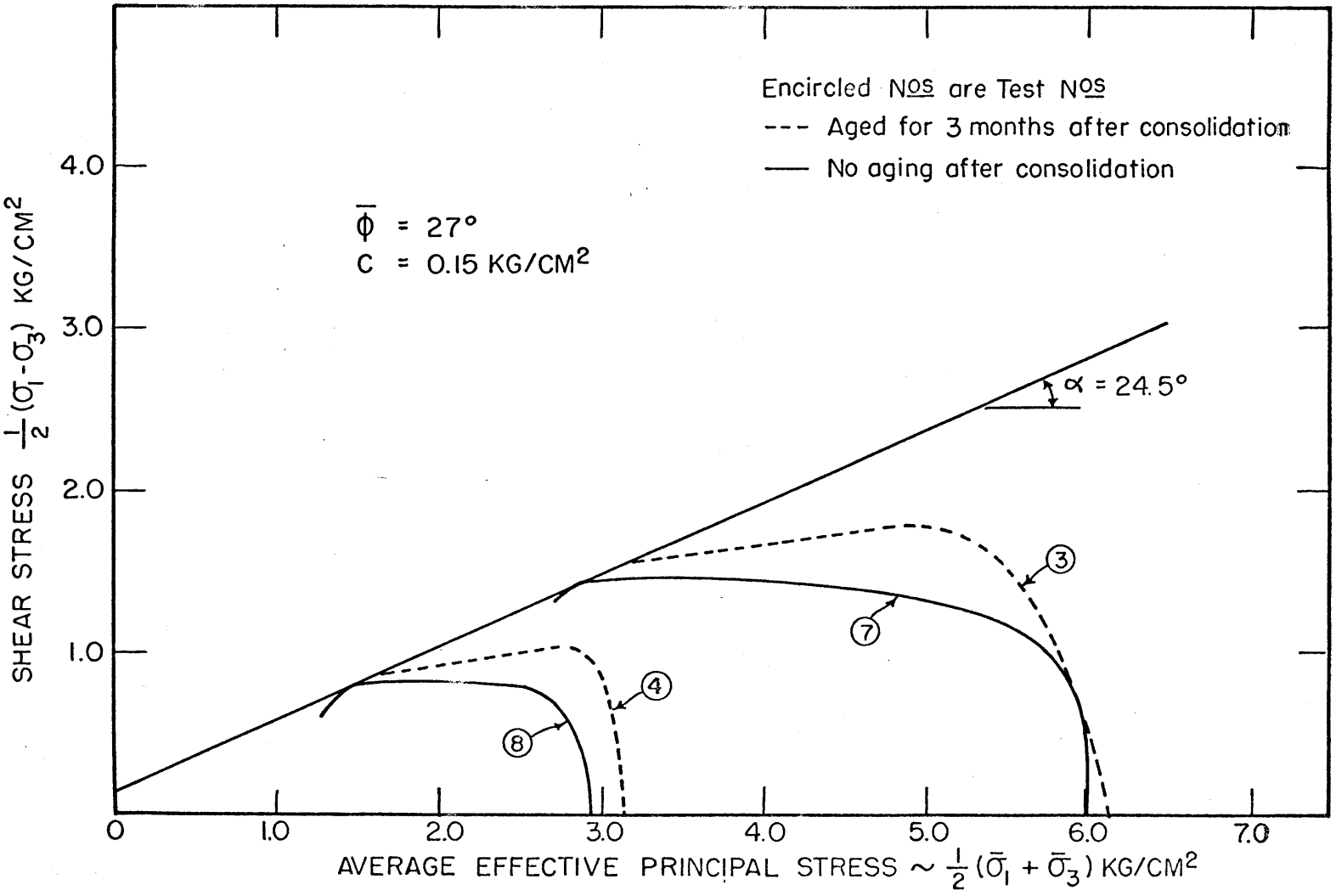

FIGURE 25 EFFECT OF AGING AFTER CONSOLIDATION ON THE EFFECTIVE STRESS ENVELOPE

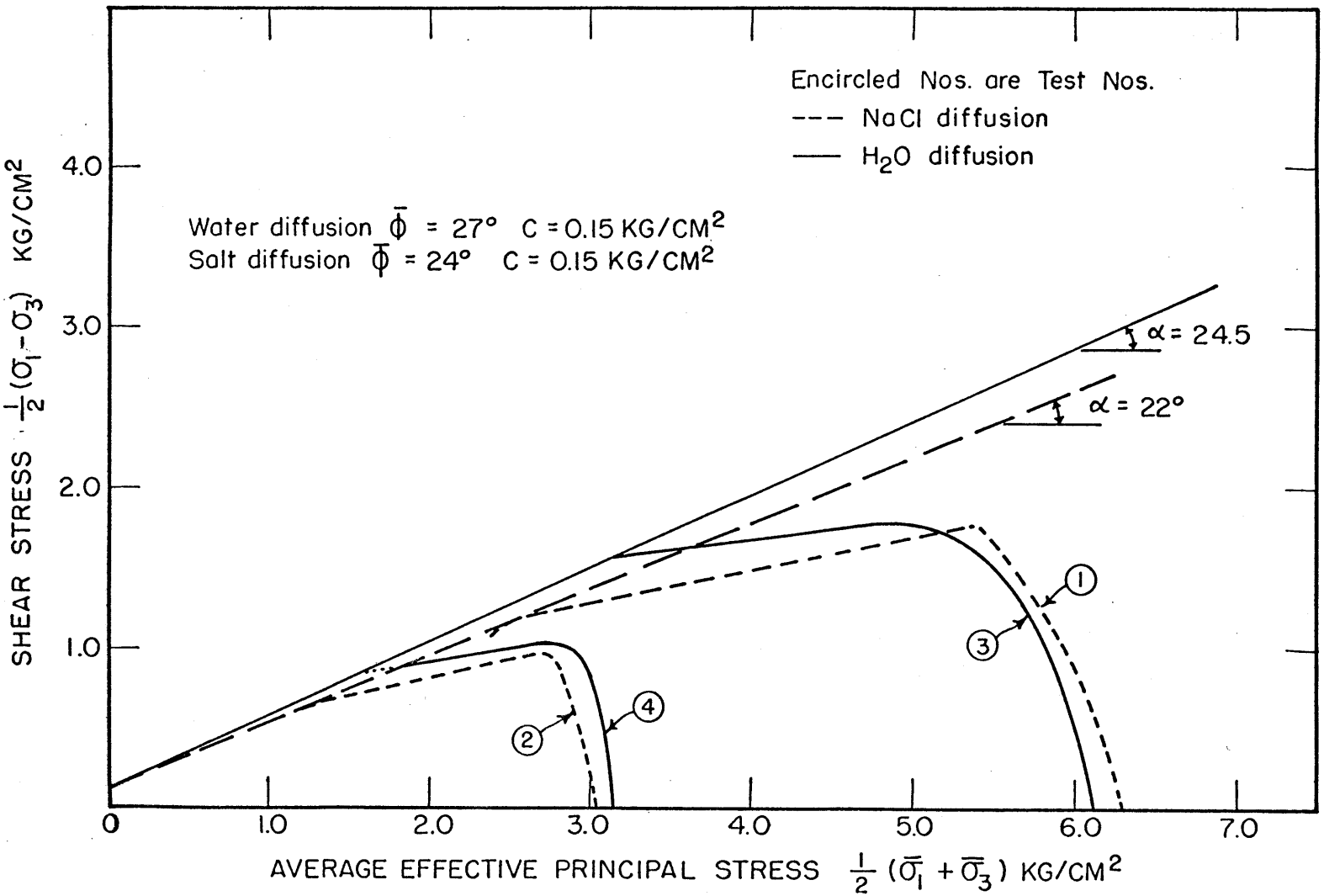

FIGURE 26 EFFECT OF SALT ON THE EFFECTIVE STRESS ENVELOPE

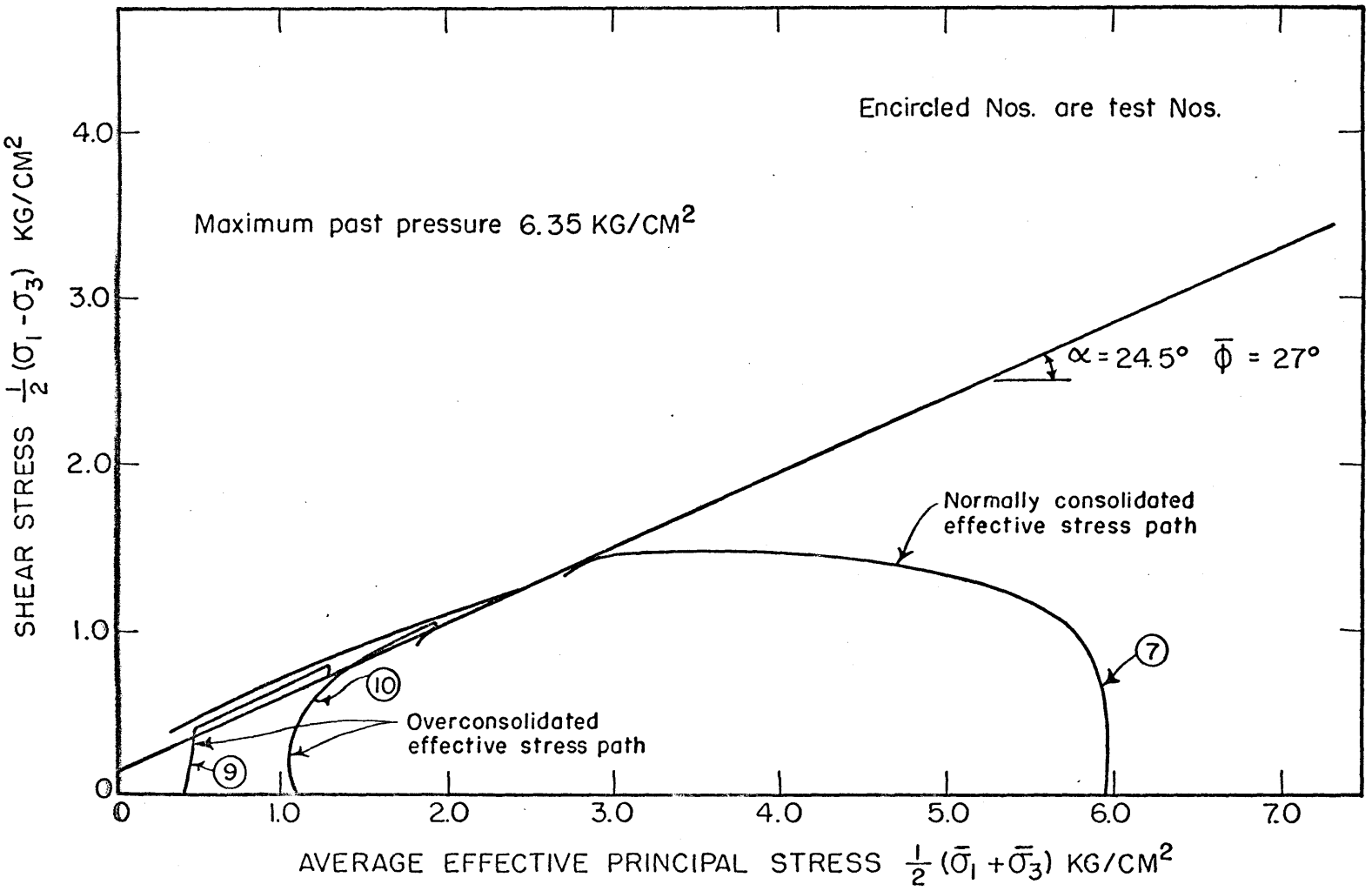

FIGURE 27 EFFECT OF PRECOMPRESSION ON THE EFFECTIVE STRESS ENVELOPE

VI. SUMMARY AND CONCLUSIONS

6.1 Aging Prior to Isotropic Consolidation in the Triaxial Cell

6.1.1 Samples which had been stored for different periods of time prior to isotropic consolidation in the triaxial cell had the same stress-strain characteristics and shared the same strength envelope (Figure 24).

6.1.2 This shows that any differences in structural brittleness ("cementing") which may have occurred during aging are completely destroyed by further consolidation. Therefore, the "cementing" effect which is produced by aging must be very sensitive to the small changes in the soil fabric caused by consolidation.

6.2 Aging After Triaxial Isotropic Consolidation

6.2.1 The effect of aging after isotropic consolidation in the triaxial cell was to produce a stronger and more brittle initial structure, as can be seen from Figures 20 and 21. The maximum deviator stresses were higher than for the corresponding samples which were not aged (Article 6.1.1) and occurred at much lower strains. However, for the same void ratio all samples had the same strength at maximum deviator stress. The aged samples did share the same drained strength envelope* as the

---

* As obtained from undrained compression tests with pore-pressure measurements.

plain water samples at maximum obliquity (Figure 25) but had a lower drained friction angle at maximum deviator stress (Figure 23). The undrained strength envelope* at maximum deviator stress and maximum obliquity was unique for both the aged and plain water samples (Figures 18 and 19).

6.2.2 From the above the following deductions may be drawn:

1. The lower drained friction at maximum deviator stress for the aged samples suggests a more rigid structure since there is more strength per bond.

2. The primary particle has not changed due to aging since at maximum obliquity the aged samples have the same drained and undrained envelopes as the plain water samples.

3. The more rigid structure produced by aging must, therefore, be due to a "cementing" effect which is very likely physical in nature.

4. The "cementing" effect must be very brittle and easily destroyed by small changes in fabric since it shows up only at low strains (at the maximum deviator stress) and is completely destroyed at large strains which accompany conditions of maximum obliquity.

---

* The undrained strength envelope is from plots of S_u versus $\bar{\sigma}_c$.

5. Article 6.1.1 supports this hypothesis on the nature of the "cementing" effect since fabric disturbance must occur during consolidation as well as shear.

6.3 Increase of Pore-Fluid Salinity After Triaxial Consolidation

6.3.1 The stress-strain characteristics of the salt diffusion samples showed a more brittle and less stable structure than the aged water samples. The deviator stress at maximum principal effective stress ratio was lower than for the corresponding aged water sample. At maximum deviator stress the salt samples shared the same undrained strength envelope as all the water samples (Figure 18) but they had a lower drained friction angle (Figure 23). The Skempton A-Factor was much higher for the salt samples at failure ($\bar{\sigma}_1 / \bar{\sigma}_3 \max$). The drained and undrained angles of friction at maximum principal effective stress ratio were lower for the salt samples than for all the water samples (which had the same angles of friction).

The sedimentation tests and Atterberg limits showed that salt in the pore-fluid decreased the electrical attraction between Kaolin particles causing a less flocculated fabric.

The aging period after consolidation was longer for the salt samples than for the aged water samples which

could contribute to the lower drained friction angle at maximum deviator stress (Article 6.2).

6.3.2 The conclusions from the above are:

1. At low strains (i.e. at maximum deviator stress) pore-fluid salinity changes apparently have no effect on the drained and undrained friction angles since there has been only a small change in fabric.

2. Change of pore-fluid salinity after consolidation affects only the drained and undrained shear strength at large strains (i.e. at maximum obliquity) when the initial structure in the failure zone has been completely destroyed.

3. The strength at maximum obliquity will depend on the soil fabric in the shear zone. The more flocculated the fabric at maximum obliquity the stronger the sample.

4. The fabric in the failure zone will be governed by the pore-fluid during shear. The effect of pore-fluid on fabric can be qualitatively obtained from sedimentation tests or liquid limits.

5. The larger the change in fabric during shear, the larger is the A-Factor at failure ($\bar{\sigma}_1 / \bar{\sigma}_3$ max.).

6. In Kaolinite an increase in the pore-fluid salinity causes a decrease in the interparticle electrical

attraction, with a corresponding decrease in degree of flocculation. Therefore, salt decreases the undrained shear strength, and increases the A-Factor at maximum obliquity.

TABLE II - SUMMARY OF TRIAXIAL TEST RESULTS (Normalized)

	Plain Water Samples	Aged Water Samples (Diffusion)	Salt Diffusion Samples (Aged)
$\left(\frac{E}{\bar{\sigma}_c}\right)_{initial}$	170±40	170±?	210±30
$\left(\frac{\bar{\sigma}_1}{\bar{\sigma}_3}\right)_{max.}$	3.16±0.20	2.86±0.10	2.97±0.30
$\left(\frac{\Delta u}{\bar{\sigma}_c}\right)_{max.}$	0.76±0.03	0.73±0.05	0.82±0.40
$\left(\frac{\sigma_1-\sigma_3}{\bar{\sigma}_3}\right)_{max.}$	0.54±0.02	0.62±0.30	0.57±0.01
$\left(\frac{\Delta u}{\Delta\sigma_1-\Delta\sigma_3}\right)_{max.}$	1.47±0.10	1.35±0.10	2.40±0.40

VII. RECOMMENDATIONS FOR FUTURE WORK

The results presented in this thesis lead the author to feel that further work along the following lines is needed to clarify the effects of environment on the shear behaviour of clays:

1. Reliable measurements of the pore-pressures produced during aging if secondary consolidation is not permitted. The mercury jacket described in Appendix C would be useful in preventing membrane leakage.

2. An investigation of the effects of various sedimentation environments on the stress-strain properties of Kaolin.

3. The development of a simple method for determining fabric.

4. A study of the effects of viscosity and dielectric of the pore-fluid on the shear strength of clays. The study should be carried out in a manner similar to that used in this thesis in obtaining the effects of salinity of the pore-fluid on the shear behaviour of Kaolin.

BIBLIOGRAPHY

1. Andresen, A., Bjerrum, L., DiBiago, E. and Kjaernsli, B., "Triaxial Equipment Developed at the Norwegian Geotechnical Institute," Norwegian Geotechnical Institute Publication No. 21, Oslo, 1957.

2. Bishop, Alan W., and Henkel, D. J., "The Measurement of Soil Properties in the Triaxial Test," Edward Arnold Ltd., London, 1957.

3. Bjerrum, L., and Rosenqvist, I. Th., "Some Experiments with Artificially Sedimented Clays," Geotechnique, Vol. 6, September, 1956.

4. Bolger, Justin C., "Rheology of Kaolin Suspension," ScD Thesis, M.I.T., September, 1960.

5. Brindley, G. W., "The Interpretation of Broadened X-Ray Reflections with Special Reference to Clay Minerals," Faraday Society Discussions, No. 11, 1951, pp. 75-82.

6. Casagrande, A., "Research on the Atterberg Limits of Soils," Public Roads, Vol. 13, No. 8, October, 1932.

7. Cashen, G. H., "Electric Charges of Kaolin," Faraday Society Transactions, Vol. 55, 1959, p. 477.

8. Georgia Kaolin Handbook, Georgia Kaolin Company, Elizabeth, N.J.

9. Green, John E., "Effects of Pore Water Salt Concentration on Homoionic Clays," S.M. Thesis, M.I.T., 1956.

10. Grim, Ralph E., Clay Mineralogy, McGraw-Hill, 1953.

11. Hvorslev, M. J., "Uber die Festigkeitseigenschaften Gestorter Bindiger Boden," Ingeniøruidenskabelige Skrifter, A No. 45, Copenhagen, 1937.

12. Kahn, Allan, "Studies on the Size and Shape of Clay Particles in Aqueous Suspension," 6th Clay Minerals, Berkeley, August, 1957, pp. 220-236.

13. Lambe, T. William, Soil Testing for Engineers, Wiley, 1951.

14. Lambe, T. William, "The Structure of Inorganic Soil," ASCE, Separate 315, October, 1953.

15. Lambe, T. William, "The Structure of Compacted Clay" and "The Engineering Behavior of Compacted Clay," Journal of the Soil Mechanics and Foundations Division, Proc. of the ASCE, May, 1958.

16. Lambe, T. William, "A Mechanistic Picture of Shear Strength in Clays," ASCE Research Conference on Shear Strength of Cohesive Soils, Boulder, June, 1960.

17. Martin, R. Torrence, "Water Vapour Sorption on Lithium Kaolinite," 7th National Conference on Clay and Clay Minerals, 1958.

18. Olsen, Harold W., "Hydraulic Flow Through Saturated Clays," ScD Thesis, M.I.T., February, 1961.

19. Peck, R. B., Uyanik, M. E., "Observed and Computed Settlements of Structures in Chicago," Univ. Illinois Eng. Exp. Station Bull. No. 429, 1955.

20. Rutledge, Philip C., "Cooperative Triaxial Shear Research Program of the Corps of Engineers," Progress Report, Waterways Experiment Station, Vicksburg, Mississippi, April, 1947.

21. Schofield, R. K., and Samson, H. R., "Flocculation of Kaolinite Due to the Attraction of Oppositely Charged Crystal Faces," Faraday Society Discussions, No. 18, 1954, pp. 135-145.

22. Skempton, A. W., "The Pore-Pressure Coefficients A and B," Geotechnique, Vol. 4, December, 1954.

23. Taylor, Donald W., Fundamentals of Soil Mechanics, Wiley, 1948.

24. Theissen, P. A., "Wechselseitige Adsorption Von Kaolloiden," Zeitcshrift fur Elektrochemie, Vol. 48, 1942, pp.675-681.

25. Quigley, R. M., "Measurement of Soil Fabric Using X-Ray Diffraction Methods," Internal Report, M.I.T., Soil Engineering Division, February, 1961.

APPENDIX A

PREPARATION OF THE NA KAOLINITE

A-1 Procedure for the Preparation of the Slurry Used in the Large Consolidometer

The dry untreated Kaolinite was placed in 20- and 30-litre pyrex washing jars (six of the former and three of the latter). 450 gms of dry soil was placed in each of the 20-litre jars and 675 gms in each of the 30-litre jars. A 1N NaCl solution was made using $+10^6$ ohms demineralized water. The solution was added to each of the washing jars up to about 10 cm from the top. A high-speed disperser was used to break up the soil lumps and thoroughly mix the slurry. This took about an hour of stirring.

The slurry was then allowed to settle for one day after which time it was possible to syphon off 2/3 of the washing solution free of clay. The jars were then refilled with $+10^6$ ohms of water pH 7.0 ± 0.2 and stirred again with the disperser for half an hour. This was repeated five times. The slurry was then washed with a 0.005N NaCl solution pH 6.7 ± 0.2.

A-2 pH Measurements

The supernatant pH was measured by a Beckman Zeromatic pH meter, using glass electrodes with a recommended range of pH 0 to 11 and -5°C to 80°C. The pH meter was

calibrated using two standard buffer solutions (pH 7 and 10).

A-3 Salt Determinations

The salt content in the supernatant was obtained using a conductivity bridge, Type R.C., using platinum electrodes. The conductivity cell was calibrated using a standard 0.02N KCl solution. To determine the salinity of the pore fluid from the oven-dried samples (as in the case of salt diffusion samples), it was necessary to powder the clay by filling the dried pieces and mixing 1 gm of the powder in 20 cc of $+10^6$ ohms of demineralized water for at least 2 days on a mechanical shaker. The slurry was then centrifuged and the conductivity of the supernatant measured.

A-4 Aluminum Determinations

The extracting solution used in all Al. determinations was 1N NaCl pH 3 obtained with HCl. To compare results the amount of extracting solution must be kept the same. For example in Figure 3 the results were obtained by using 1 gm of dry soil or the equivalent of wet soil and 100 cc of 1N NaCl pH 3. The slurry was mechanically shaken for 24 hours and then centrifuged. 70 cc of the supernatant was removed and stored in small polyethylene bottles for Al. determinations. 70 cc of fresh extracting solution

was added and shaken for another 24 hours. This was repeated for each extraction.

The Aluminum contents of each extraction were determined colorimetrically using a Fisher Electrophotometer as follows:

1) Reagents - Standard Solutions

A. Standard Al solution, stock.
Dissolve 0.1544 gm of $Al_2 (SO_4)_3 \cdot 18 H_2O$ in 100 ml water in a 1-litre volumetric flask. Bring to volume with $NH_4 A_c$ solution.

B. Ammonium Acetate solution (pH 4.8).
(a) Add 700 ml H_2O to a litre volumetric flask.
(b) Add 118 ml acetic acid conc.; mix well.
(c) Add 70 ml NH_4OH conc.; mix well.
(d) When cool, dilute to volume.
(e) Check pH; should be 4.8 ± 0.1.

C. Aluminon Reagent, 0.2%.
Dissolve 0.20 gm Aluminon in 100 ml water. Store in brown glass bottle.

D. Hydroxylamine Hydrochloride solution, 5.0%.

2) Procedure

A. Solution for standard curve, range 0 to 5 Al.
(1) Add 4 ml standard Al solution to 50 ml volumetric flask. Dilute to volume with Ammonium Acetate solution. 1 ml 1 Al.
(2) To test tubes add: (a) 0, 1, 2, 3, 4, 5 ml of diluted Al solution; (b) NH_4A_c to bring total volume of each tube to 5 ml; (c) 1 ml water to each tube. If unknown solutions are in a salt solution then replace the 1 ml water above with 1 ml of proper extracting solution (1N NaCl pH 3). Similarly, if the concentration is low and a larger aliquot of unknown is

used, then increase the volume of water or extracting solution by the same amount.

B. Unknown solutions in test tubes.

(1) Aliquot of unknown, a 1- to 3-ml aliquot may be used directly with proper adjustment of standards as indicated above. For high Al concentrations, the unknown should be diluted with the proper extracting solution before an aliquot is taken for analysis. A one- to ten-dilution embraces the usually encountered concentration range.

(2) Add 5 ml NH_4A_c solution to each unknown.

C. Color development.

(1) To standards unknowns add 4 drops of Hydroxylamine. Mix well.

(2) Aluminon reagent.
Dilute 10 ml of Aluminon reagent to 25 ml with water in a volumetric flask. Add exactly 0.50 ml of diluted Aluminon reagent to each tube. A 10-ml burette works well. Mix well.

(3) Allow to stand 24 hours in dark for full color development. The intensity of color development is very sensitive to temperature and time. Read optical density using a 525-mu filter.

3) Remarks

Unknown solutions must be perfectly clear prior to analysis for Al. If after color development any of the unknown solutions are cloudy, the Al concentration is too high and a new solution must be prepared using a smaller aliquot. The total volume of all standards unknowns should be the same.

A-5 Method of Correcting Void Ratio and Fluid Content

Fluid Content = equivalent weight of water to give same volume of solution divided by weight of soil

$\therefore$ Void Ratio = specific gravity of soil x fluid content

$$\text{Fluid Content} = \frac{(100 + A)\,\omega}{S(100 - A\cdot\omega)} \times 100\%$$

$$\text{Void Ratio } e = \frac{G_s(100 + A)\,\omega}{S(100 - A\cdot\omega)}$$

where ω = water content (not as percentage)

A = weight of NaCl as % weight of water obtained from Graph A-1 where N is gms of NaCl per 100 cc of solution

S = specific gravity of solution for corresponding value of A obtained from Graph A-2.

e.g. Sample No. 1

$\omega = 60.2\%$

$N = 0.7N = 0.7 \times 5.85 = 4.09$

$\therefore\ A = 4.10$

and $S = 1.0265$

$$\therefore\ e_f = \frac{2.62\ (1.041)\ 60.2}{1.0265 \times \left(100 - \frac{4.1 \times 60.2}{100}\right)}$$

$$\frac{2.62 \times 1.041 \times 60.2}{1.0265 \times (100 - 2.47)} = \underline{1.64}$$

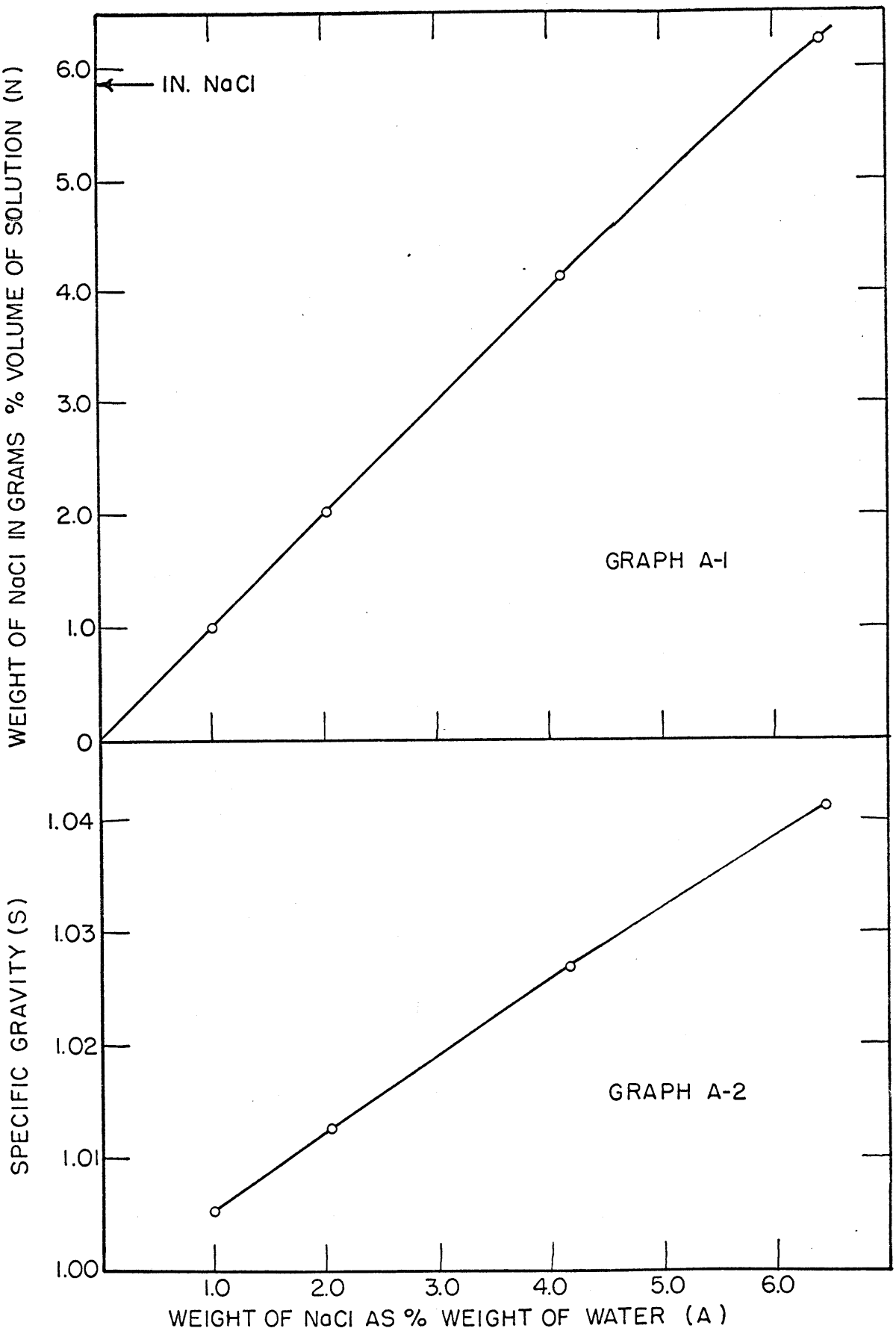

FIGURE A-1 GRAPH FOR DETERMINATION OF FLUID CONTENT
(OBTAINED INDIRECTLY FROM SPECIFIC GRAVITIES OF AQUEOUS SOLUTIONS GIVEN IN LANGE'S BOOK OF CHEMISTRY)

APPENDIX B

B-1 APPARATUS AND PROCEDURE FOR THE PRODUCTION OF LARGE BATCHES OF SATURATED CLAY

Procedure for Sedimentation and Initial Consolidation (Figure B-2)

1. The top cap and piston of the consolidometer are removed and a deaired solution of the required sedimentation environment is poured into the bottom of the consolidometer.

2. The lucite cylinder with funnel as shown in Figure B-2 is placed on top of the consolidometer with a rubber sleeve at the interface covered with silicon grease to produce a vacuum seal.

3. With Valves A and B closed a vacuum is applied through Valve C.

4. When the bottom stone and environment solution is completely deaired, the slurry is fed into the funnel and Valve B is regulated to give a flow into the consolidometer of not more than 100 cc per minute.

5. Valve B is closed once the vacuum chamber is filled. A vacuum is applied at Valve A. The vacuum at C is gradually reduced (but always maintained with a vacuum to hold the vacuum seal) until the level of the slurry is in the consolidometer.

6. Valve A closed and the vacuum released at C, and the lucite cylinder removed.

7. The top cap, piston and consolidometer are assembled, and the top cap bolted to the main holding rods.

Procedure for Final Consolidation (Figure B-3)

1. With the air-release valve open deaired vacuum oil is fed into the top of the consolidometer by means of Valve D. When the space above the piston is filled with oil the air-release valve is closed.

2. The oil-nitrogen interchange is filled with oil and connected to Valve D.

3. A nitrogen tank with a pressure regulator is connected to the top of the oil-nitrogen interchange and with all valves open except the drainage valves and the air-release valve which are kept closed, the pressure is adjusted to one atmosphere by means of the regulator.

4. Top and bottom drainage valves are now open and consolidation proceeds.

5. The pressure is gradually increased to final desired consolidation pressure.

6. If at any time during consolidation it is desired to refill the interchange with oil, Valve D is closed, the nitrogen tank closed and the pressure in the interchange released by opening the oil port. Oil is now poured in through the oil port with the help of a funnel. The oil port is then closed and the pressure re-applied. Valve D is then re-opened.

7. Consolidation is continued until the piston becomes stationary for 48 hours. This is determined by means of the Ames dial which is in contact with the piston rod.

8. All valves are now closed and the oil pressure in the consolidometer released through the air-release valve.

Procedure for Extrusion (Figure B-4)

1. The main holding rods are unbolted and the extrusion rods bolted to the top cap.

2. The consolidometer is inverted and placed on the wooden extrusion stand.

3. The pressure in the oil is now gradually increased until the sample and bottom of the consolidometer start moving. The extrusion is controlled by Valve D.

4. Once the sample is completely extruded Valve D is closed and the top of the consolidometer gently removed.

5. The sample is now cut into small blocks, from which the triaxial samples shall be trimmed.

6. The blocks are completely immersed in water-repellant oil until used.

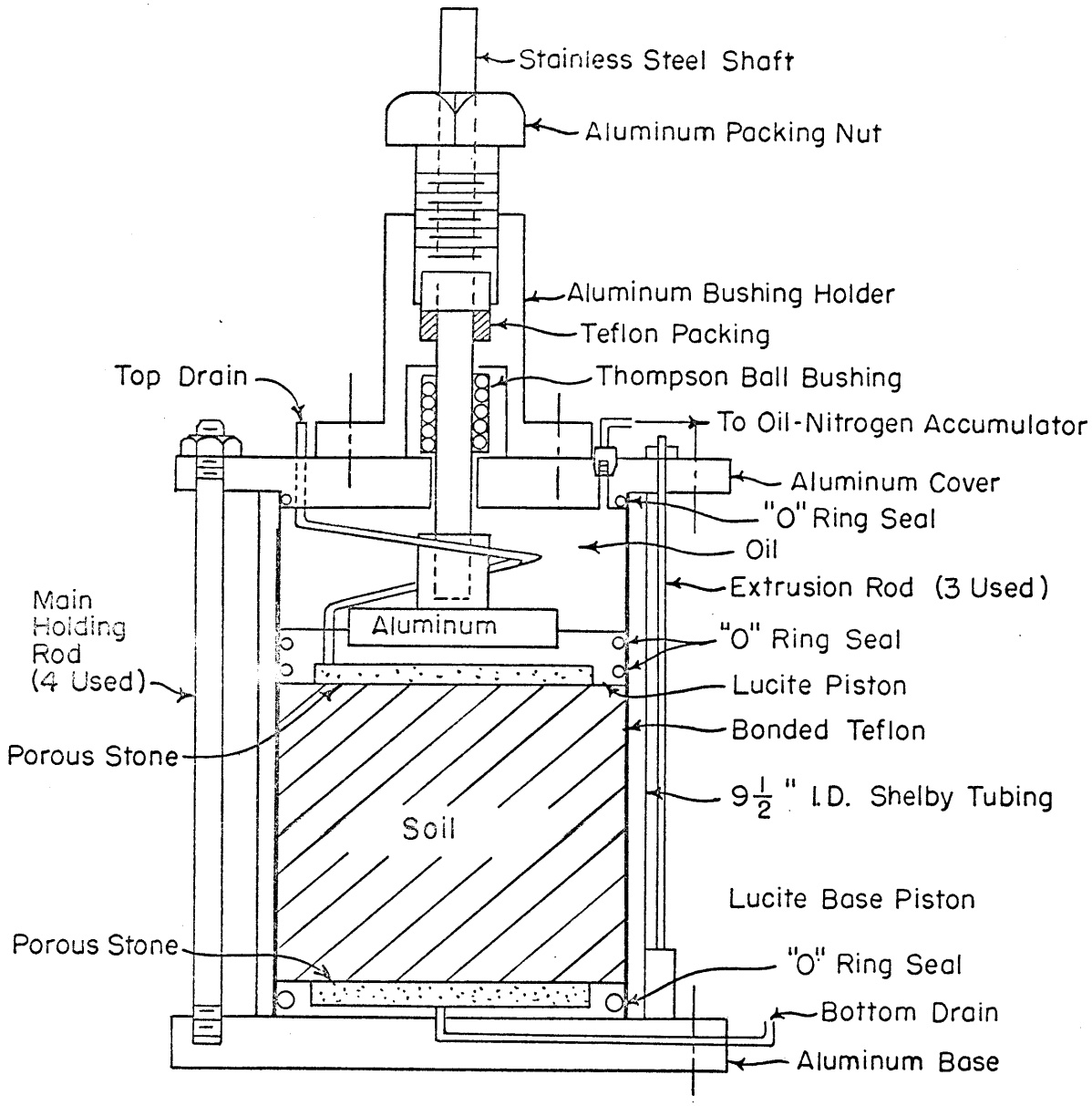

Note: To extrude, relieve pressure, invert consolidometer; remove main holding rods and tighten extrusion rods. Reapply light pressure sufficient to extrude.

FIGURE B-I SELF EXTRUDING CONSOLIDOMETER

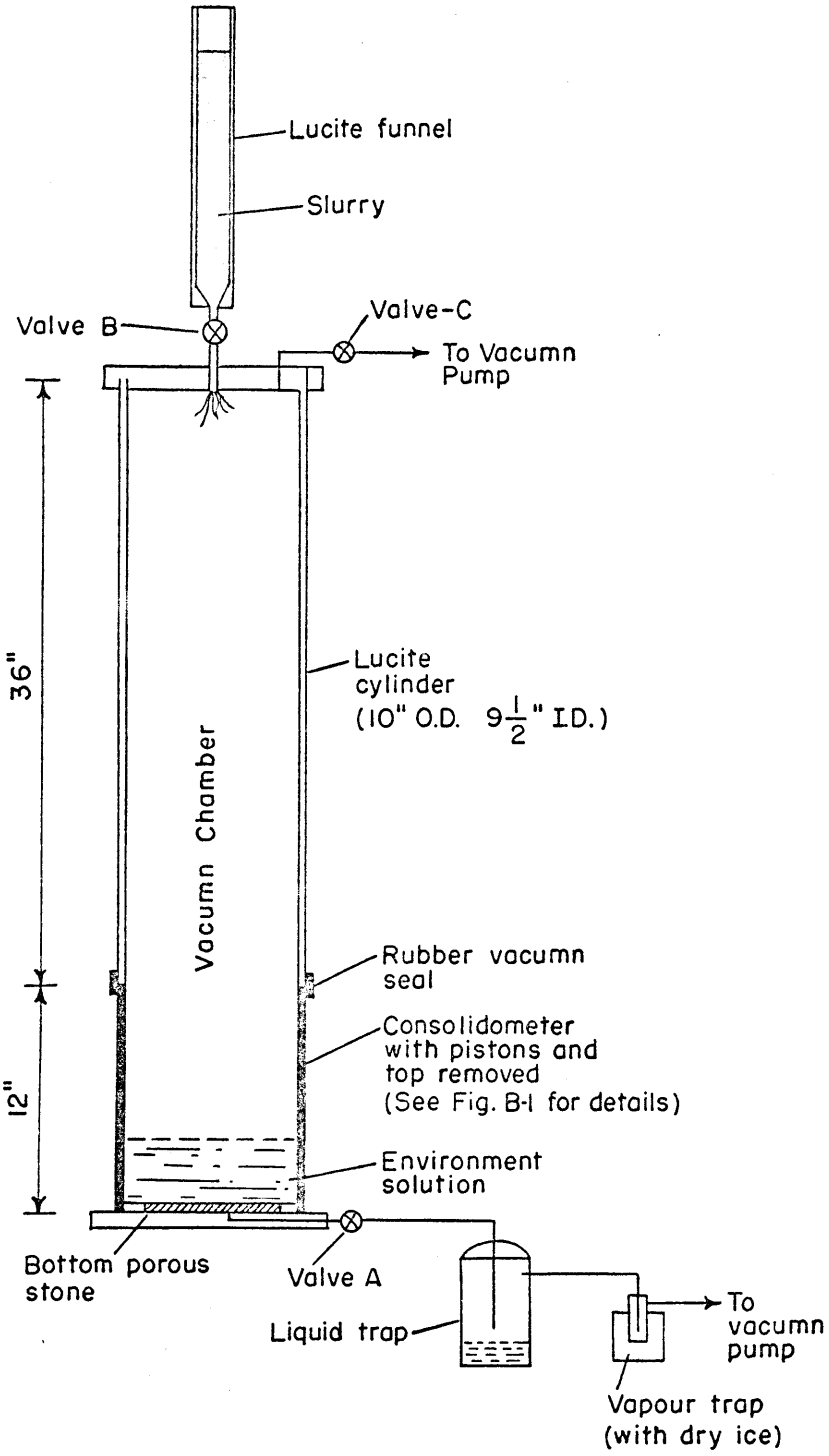

FIGURE B-2 VACUMN SEDIMENTATION AND INITIAL CONSOLIDATION LAYOUT

APPARATUS AND PROCEDURE FOR THE PRODUCTION OF LARGE BATCHES OF SATURATED CLAY (cont'd)

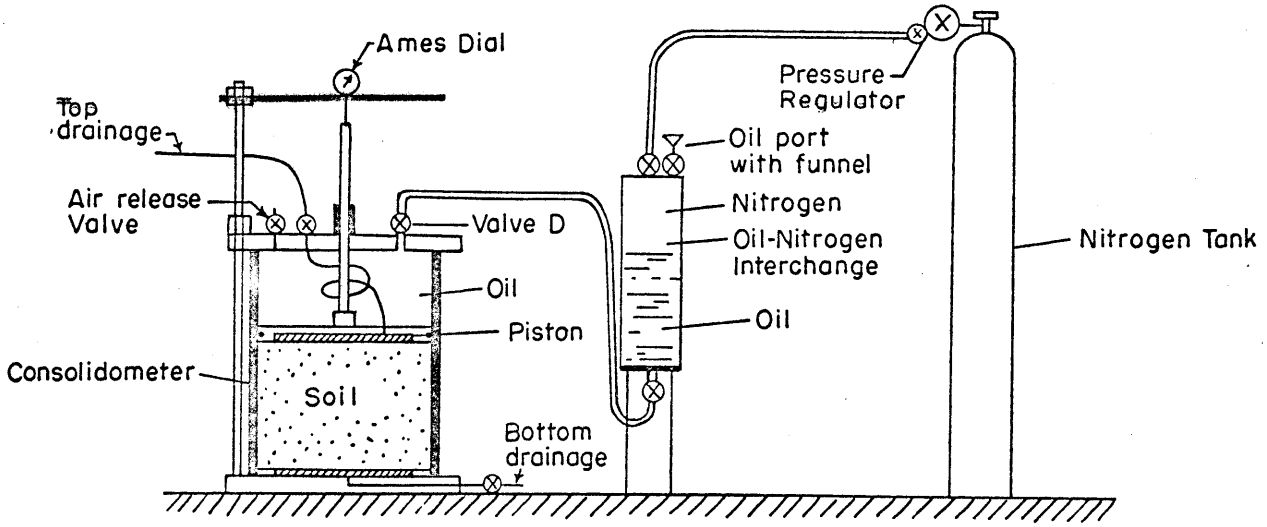

FIGURE B-3 FINAL CONSOLIDATION LAYOUT

APPARATUS AND PROCEDURE FOR THE PRODUCTION OF LARGE BATCHES OF SATURATED CLAY (cont'd)

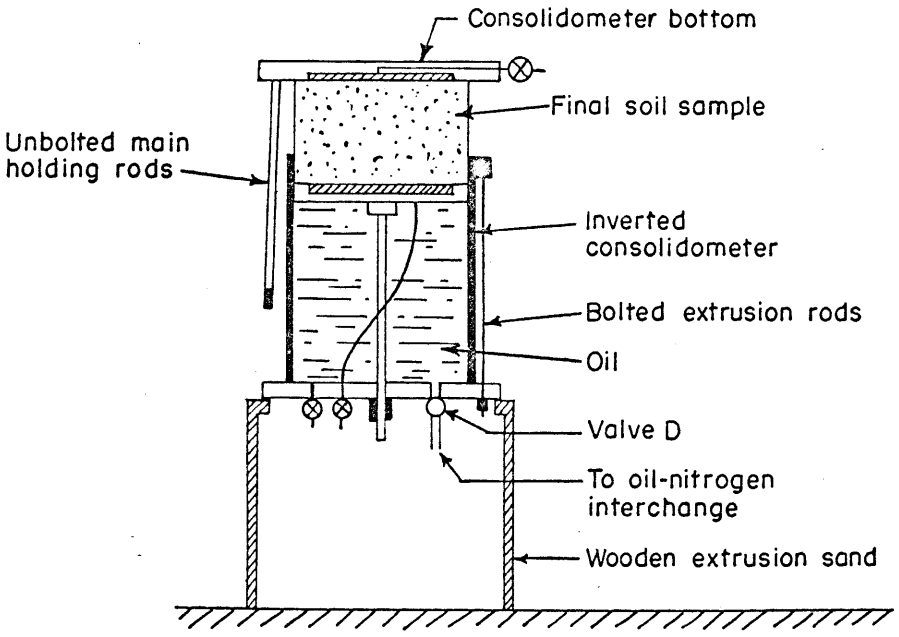

FIGURE B-4 EXTRUSION LAYOUT

B-2 A NEW METHOD FOR PRODUCING SINGLE ISOTROPICALLY CONSOLIDATED SATURATED 1.4" TRIAXIAL SAMPLES

The main features in the new consolidometer (Figure B-5) are:

1. The top drainage cap which consists of a rubber stopper with a hole through it. A 1.3" diameter porous stone is stuck to the bottom of the stopper with rubber cement. The top drainage line is a piece of polyethylene tubing stuck into the hole in the stopper.

2. The bottom drainage cap is a male and female lucite collar with matching taper sealing the membrane by using four 1/4"-20 screws with a recessed porous stone in the male section. The drainage line is spiralled and connected to a central hole in the male section of the hole by a 5/10" brass screw.

3. The screw-on lucite cylinder top is sealed by a rubber gasket.

4. A rubber membrane which is made by immersing a 1 1/2" diameter 8" long test tube in rubber latex (Vultex 1-V-10 supplied by General Latex & Chemical Company, Cambridge, Mass.). The membrane wall thickness is 0.02" and is obtained after six immersions in the latex; each coat is allowed to dry before the next application. Before the last coat has completely dried, four 1/4" wide cotton-elastic strips 5" long are placed down the sides of the membrane and stuck to the still wet latex. These cotton-elastic strips act as filter strips during consolidation.

Procedure

1. One end of the rubber membrane is clamped between the bottom cap and its collar. The other end is rolled over the shoulder of the screw-on lucite chamber top which has already been tightened to the lucite chamber with a rubber gasket forming the seal.

2. The water in the lucite chamber is sucked into the exchanger by means of a vacuum pump until the rubber membrane fills up the chamber as shown in Figure B-5. Valve A is then closed.

3. A couple of inches of the pore-fluid is poured into the extended membrane and the bottom drainage line closed.

4. The slurry which has already been deaired is syphoned into the membrane below the fluid level.

5. With the extended membrane full of slurry the top cap is pulled on and held in place by two 1/4" rods and a cross-bar.

6. The drainage lines are opened and the vacuum in the lucite chamber released.

7. The pressure in the chamber is gradually raised to the required consolidation pressure by means of a nitrogen tank.

8. After consolidation is complete Valve A is closed and the lucite chamber top is unscrewed. The top and bottom drainage caps are removed and the membrane peeled off the sample. The sample is then trimmed or stored in oil.

A NEW METHOD FOR PRODUCING SINGLE ISOTROPICALLY CONSOLIDATED SATURATED 1.4" TRIAXIAL SAMPLES

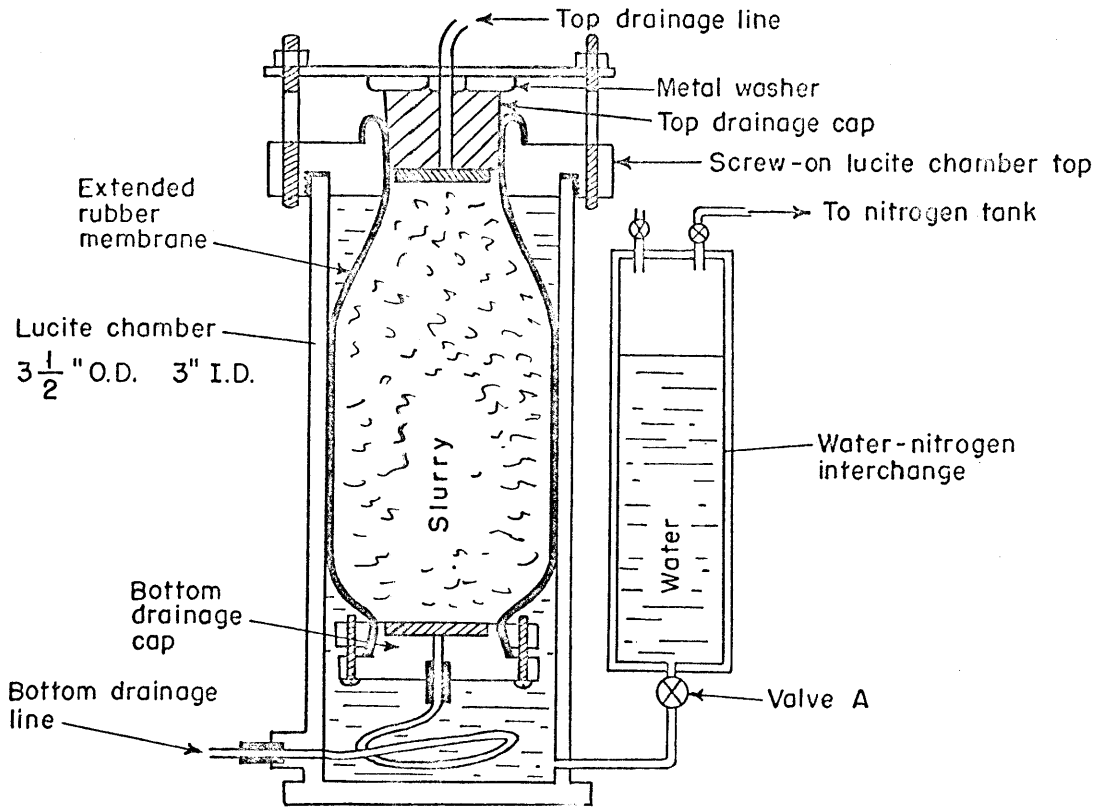

FIGURE B-5 THE NEW SMALL CONSOLIDOMETER FOR ISOTROPIC CONSOLIDATION

APPENDIX C

A NEW INNER MERCURY JACKET FOR THE STANDARD TRIAXIAL CELL

An assembled 1.4" triaxial sample with the mercury jacket is shown in Figure C-1.

The main advantages of this apparatus are:

1. No alterations to the standard triaxial cell are needed when using the Hg jacket.
2. The mercury surrounding the sample eliminates any diffusion of air through the rubber membrane.
3. Small volume changes can be measured without calibrating the cell since there are no pressure gradients across the walls of the inner Hg. jacket.

The main features of the mercury jacket are:

1. A thin-walled jacket with coarse female threads at the bottom. The top of the jacket has a neck 2 cm long, 0.667" I.D. and is graduated in millimeters. With the 1/2" diameter loading ram in position this gives 0.1 cc volume change per millimeter.
2. A lucite jacket-base collar with an O-ring on the inside, forming a seal between the collar and the cell pedestal. The outside has a male thread and is milled square to take a wrench.
3. A top drainage line at least 12" in length which is spiralled inside the mercury chamber. The line must be of sufficient length so as to have the top cap outside the jacket while assembling the sample.
4. A seal between the jacket and collar, provided by screwing the latter into the jacket which is not allowed to rotate.
5. An external lucite container with mercury under the cell pressure. To refill the jacket, the container is inverted and mercury is gravity fed into the jacket.

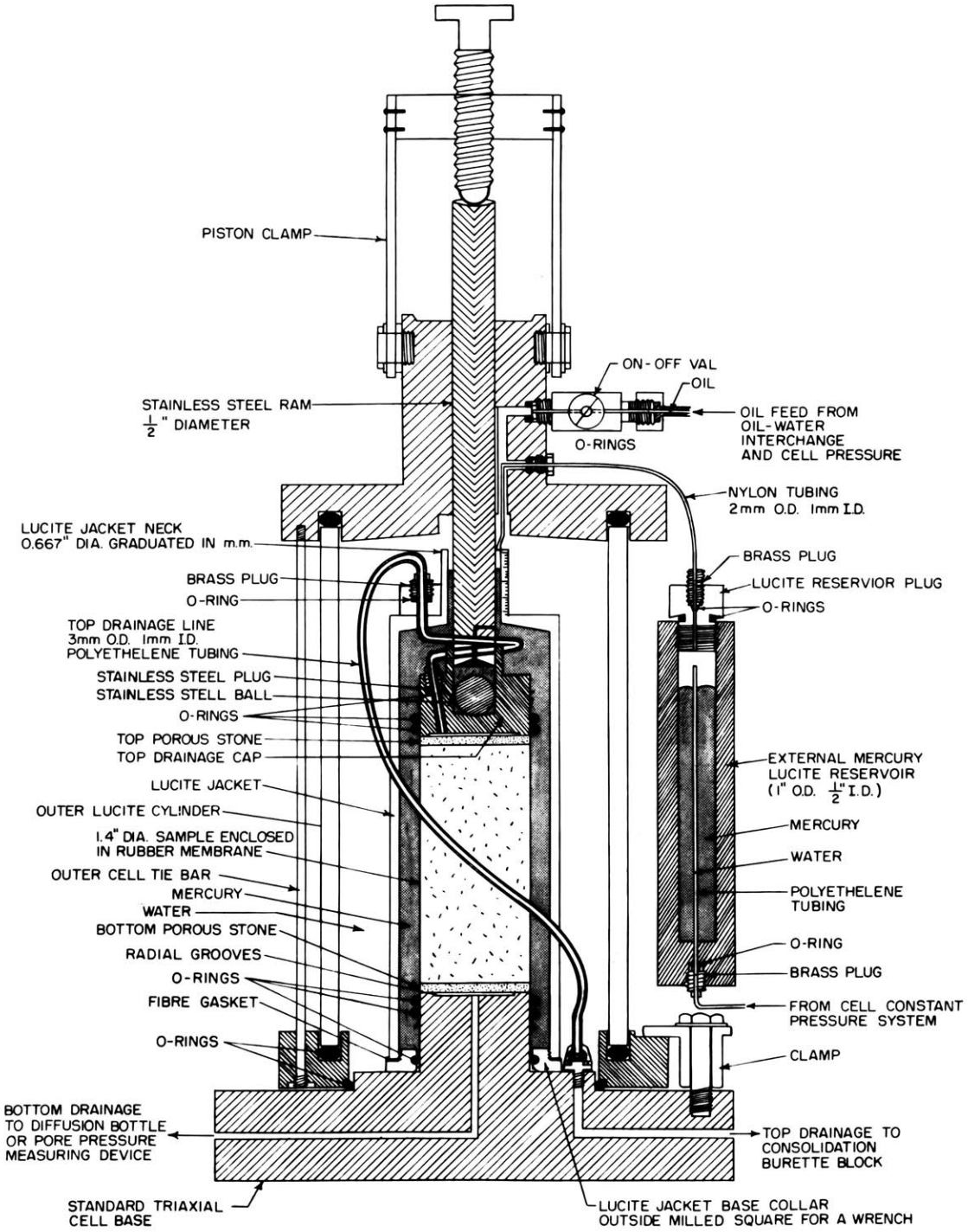

FIGURE C-I STANDARD TRIAXIAL CELL WITH NEW INNER MERCURY JACKET FOR MEASURING SMALL VOLUME CHANGES DURING SECONDARY CONSOLIDATION AND DIFFUSION

APPENDIX D

MISCELLANEOUS TEST RESULTS

RESULTS OF SEDIMENTATION TESTS NOT MENTIONED IN THE TEXT

NaCl Normality	50°C		27°C		4°C	
	pH	γ_d gm/cc	pH	γ_d gm/cc	pH	γ_d gm/cc
0	10.13	0.57	7.48	0.39	7.82	0.40
0.001	10.01	0.33	-	-	9.33	0.39
0.003	10.11	0.22	7.82	0.23	9.61	0.28
0.010	7.70	0.09	7.20	0.09	7.40	0.11
0.030	9.22	0.08	7.40	0.09	9.78	0.11
0.100	9.70	0.08	7.20	0.09	9.90	0.11
0.300	-	-	9.90	0.10	8.43	0.12
1.000	-	-	9.22	0.10	9.75	0.11

The above tests were run with untreated soil in 100-cc graduates. Two grams of the untreated Kaolinite was used with 2 cc of 0.1N NaOH. The volumes were then brought up to 100 cc with the various NaCl solutions. The slurries were mixed in a Waring Blender at the temperatures stated. During the first four months of sedimentation the temperatures were kept constant at those of mixing. By this time the sediments had reached constant density. The samples were then stored at room temperature for eight months during which time no appreciable change in volume occurred. The pH was measured at the end of one year. No explanation can be given at this time for the variation in pH.

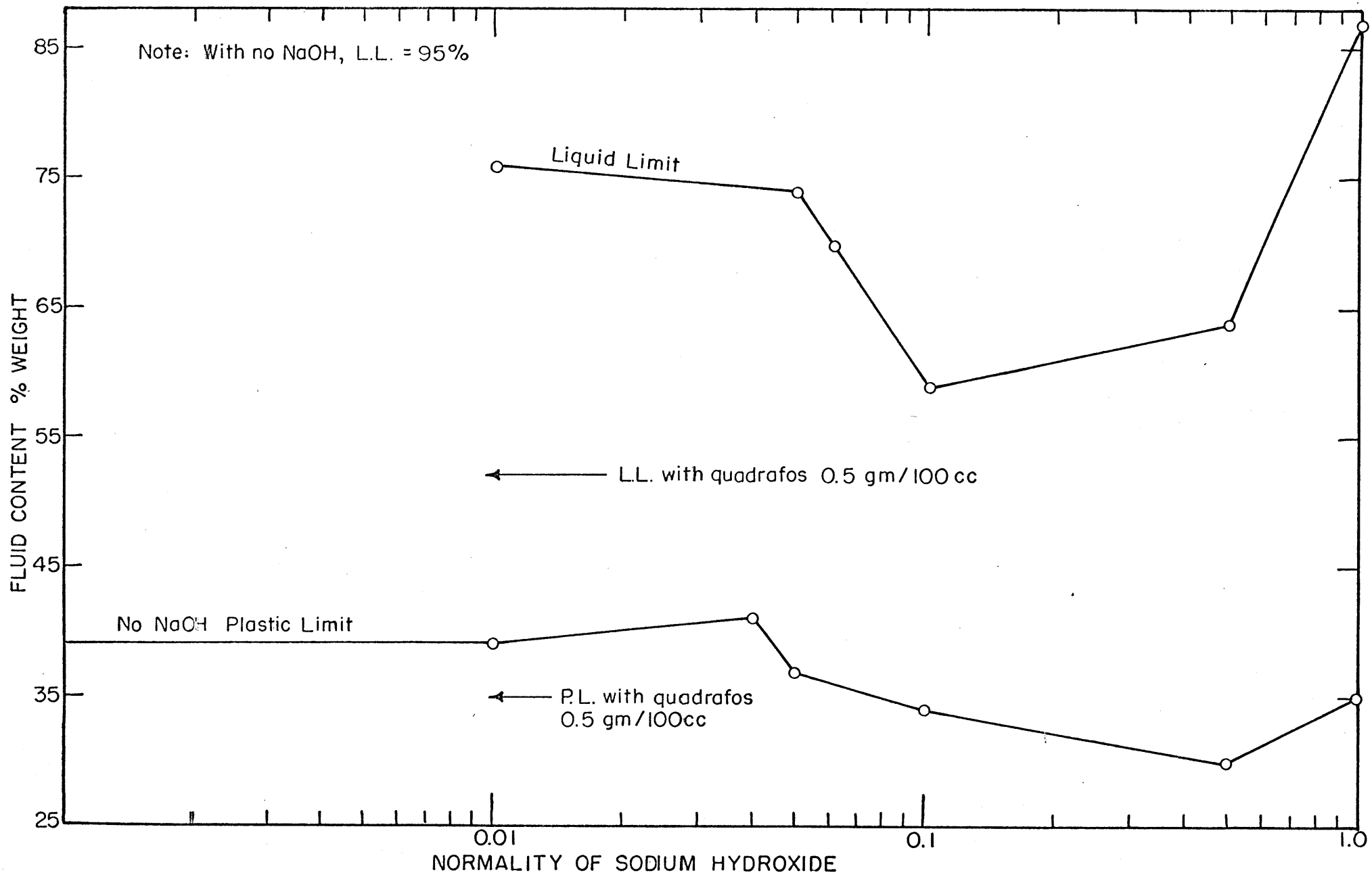

FIGURE D-1 EFFECT OF SODIUM HYDROXIDE ON THE ATTERBERG LIMITS OF KAOLIN

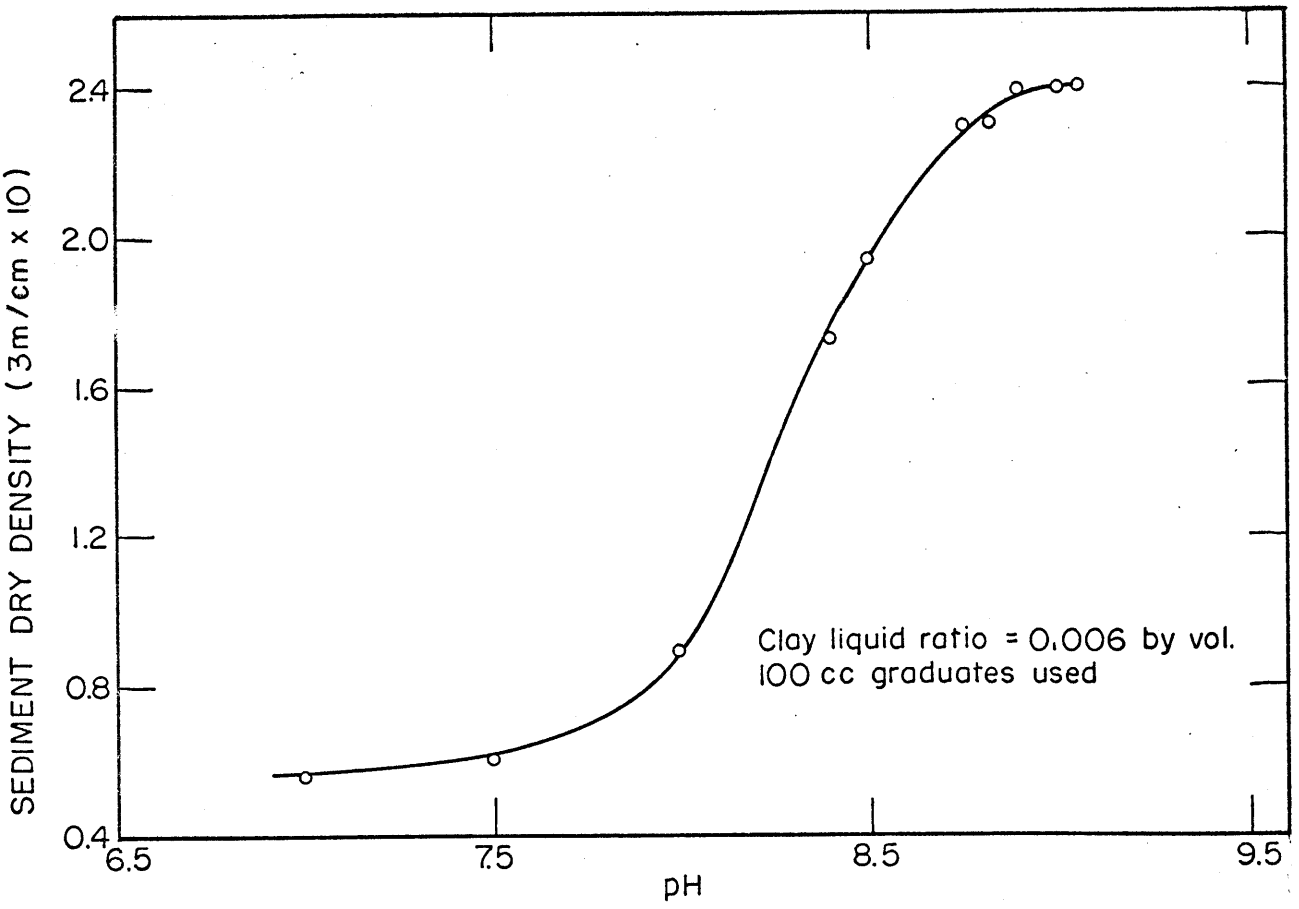

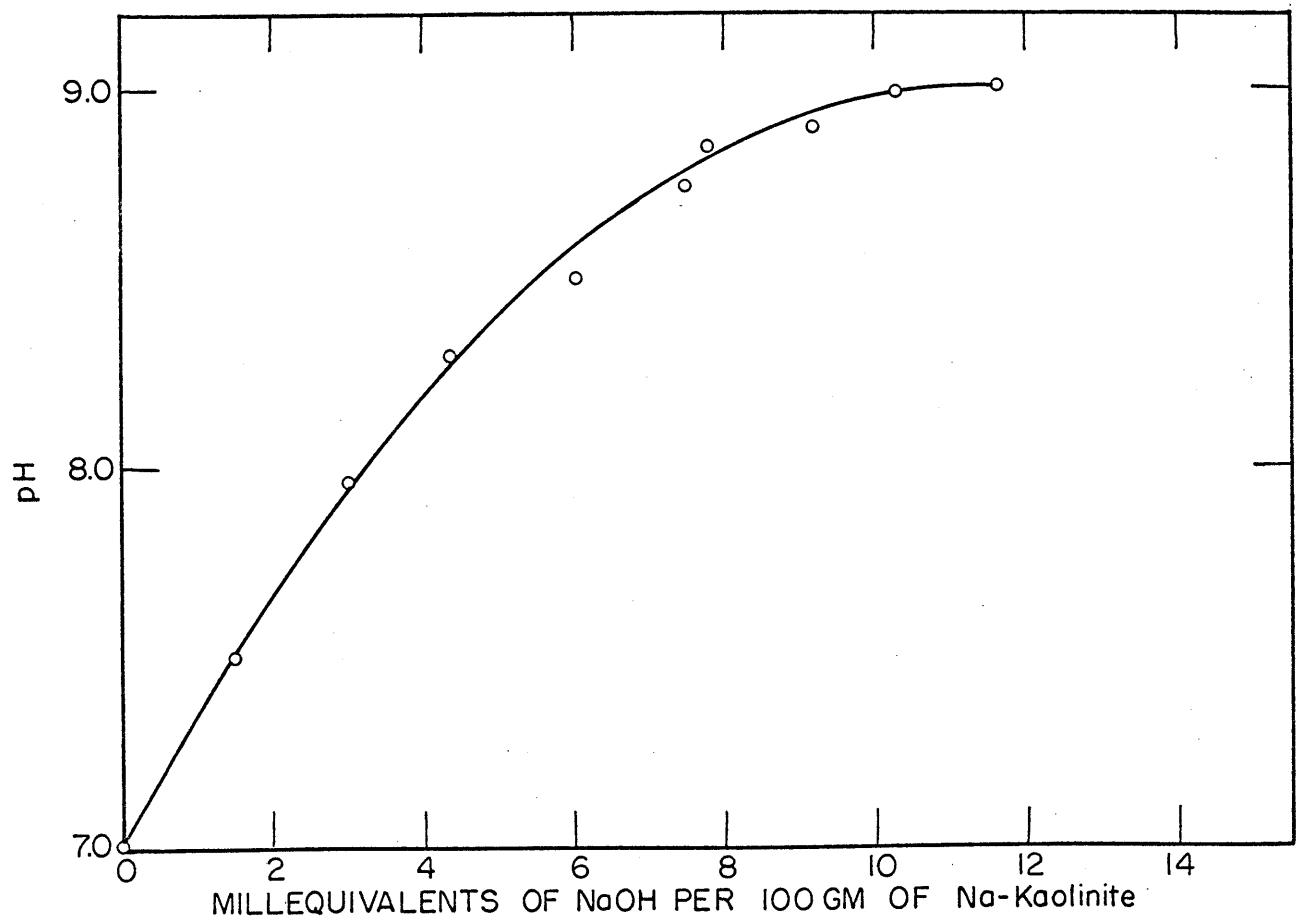

FIGURE D-2 EFFECT OF NaOH ON HOMOIONIC Na-KAOLINITE

APPENDIX E

NORMALIZED STRESS-STRAIN RELATIONSHIPS FOR THE TRIAXIAL TESTS

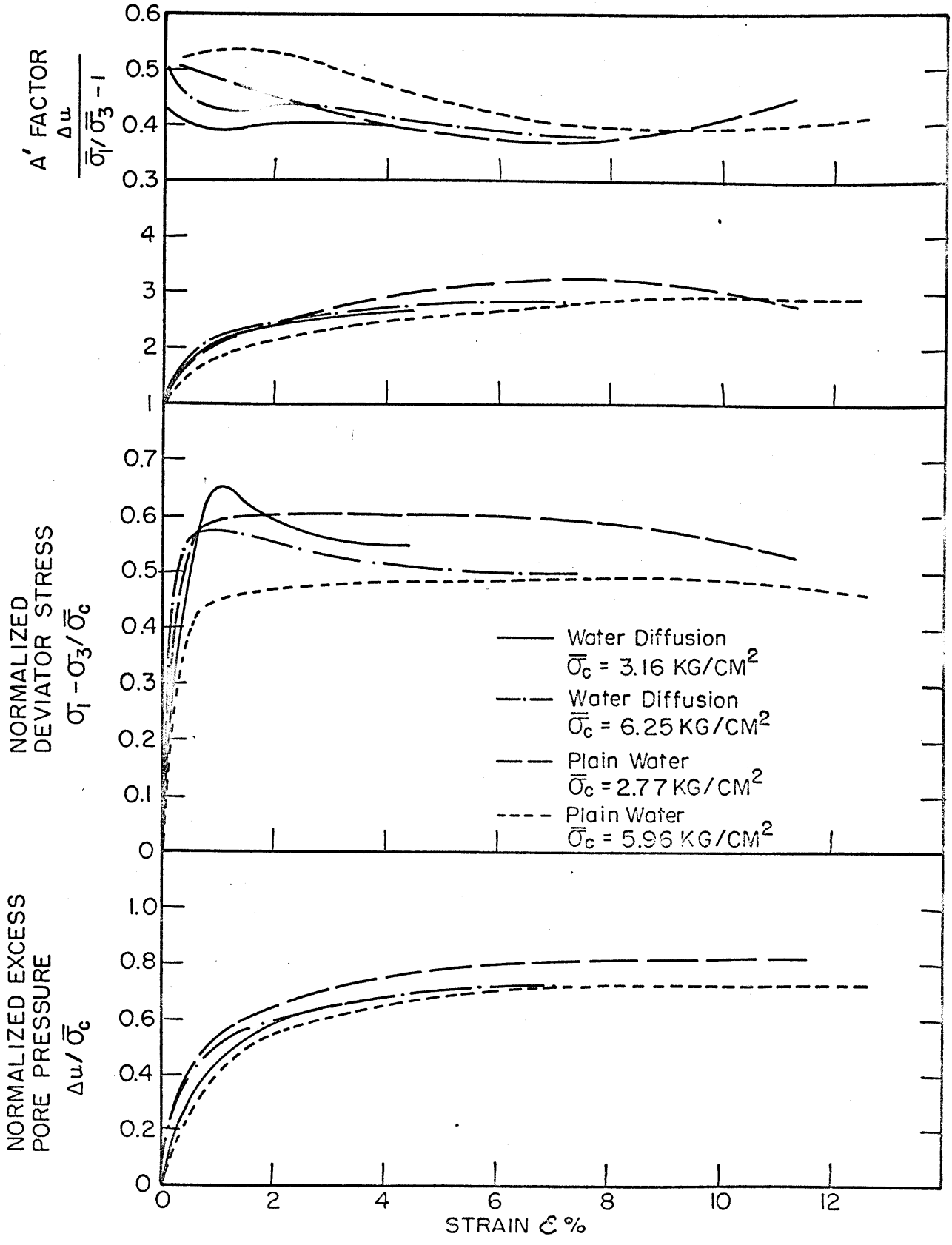

FIGURE E-1 EFFECT OF AGING ON THE NORMALIZED STRESS-STRAIN CURVES

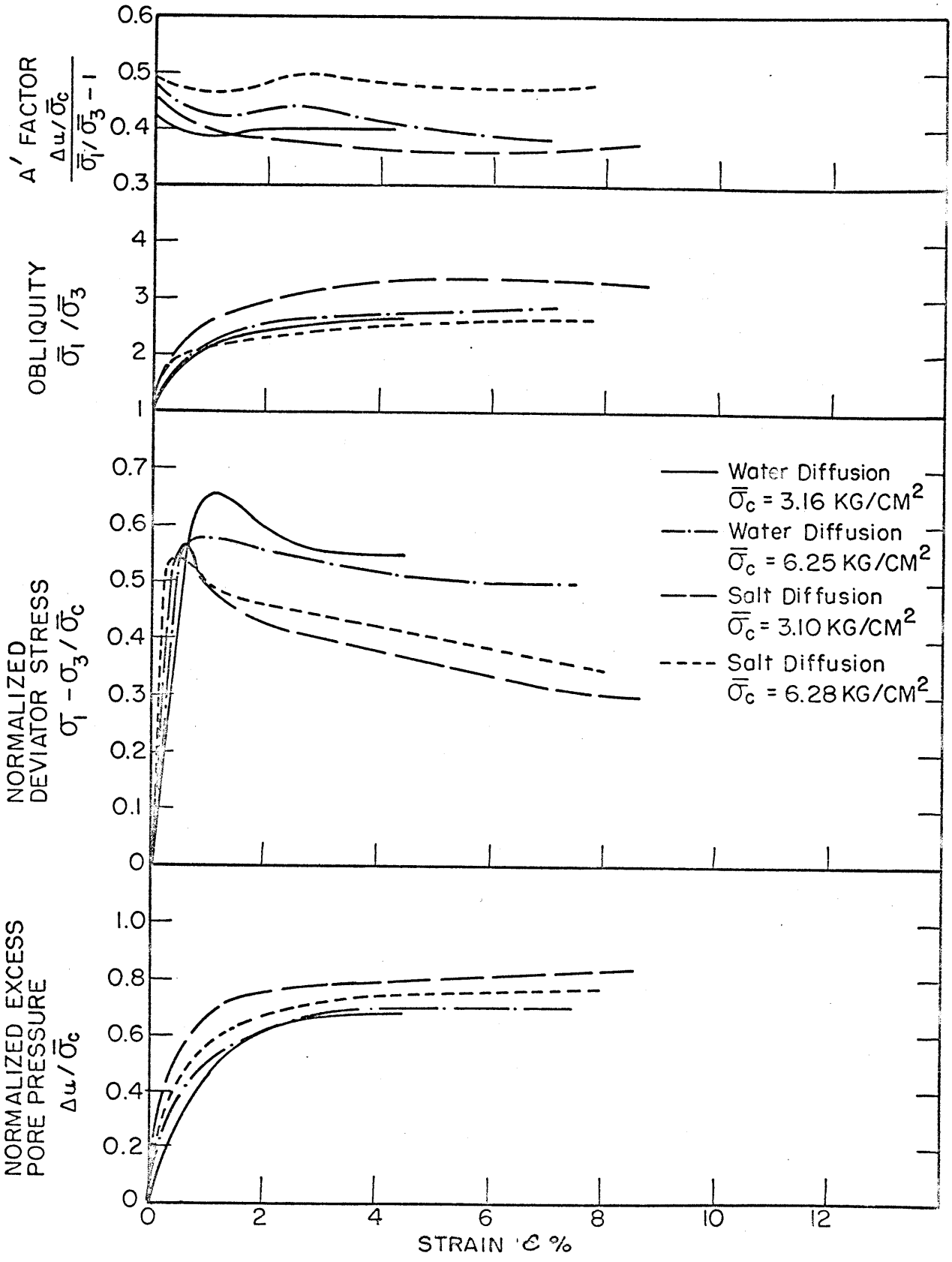

FIGURE E-2 EFFECT OF SALT ON THE NORMALIZED STRES-STRAIN CURVES